

**Numerical Model and Analysis on Performance of a  
Straight-Through Swirl Tube Cyclone (Inertial Gas-Solid  
Separator)**

Soroush Saberi

A Thesis  
in  
The Department  
of  
Mechanical and Industrial Engineering

Presented in Partial Fulfillment of the Requirements  
For the Degree of Master of Applied Science (Mechanical Engineering) at  
Concordia University  
Montreal, Quebec, Canada

August 2014

© Soroush Saberi, 2014

CONCORDIA UNIVERSITY

School of Graduate Studies

This is to certify that the thesis prepared

By: **SOROUSH SABERI**

Entitled: **Numerical Model and Analysis on Performance of a Straight-Through Swirl  
Tube Cyclone (Inertial Gas-Solid Separator)**

and submitted in partial fulfillment of the requirements for the degree of

**Master of Applied Science (Mechanical Engineering)**

Complies with the regulations of the University and meets the accepted standards with respect to originality and quality.

Signed by the final examining committee:

\_\_\_\_\_ Chair

**Dr. Ramin Sedaghati** Examiner

**Dr. Radu Zmeureanu** Examiner

**Dr. Wahid Ghaly** Supervisor

**Dr. Ion Stiharu** Supervisor

Approved by \_\_\_\_\_

Chair of Department or Graduate Program Director

\_\_\_\_\_  
Dean of Faculty

Date \_\_\_\_\_

# ABSTRACT

Numerical Model and analysis on performance of a straight-through swirl tube cyclone

Soroush Saberi

A numerical simulation for the rotational flow inside a special configuration of inertial gas-solid separators is performed. The inertial gas-solid separator of the present work can be fit in category of straight-through swirl tube cyclones. Using the results of parametric studies a modified geometry configuration for the inertial gas-solid separator is achieved which shows considerable performance improvement in comparison with the original model. In this approach, the CAD model for the original geometry of the dust separator was generated and the turbulent flow field was solved using time-independent solver and Reynolds stress turbulence model. The solution approach demonstrates consistency with the a

vailable experimental data proving the accuracy of the solution method. The highly rotational flow pattern and its features are described by analyzing the different flow variables. The main contributors of the pressure loss production in the flow field are identified and the most effective geometry parameters are recognized in order to perform the parametric analysis. The modifications are implemented on the original geometry and flow simulation is performed for each new configuration with the same solution method as used for the original model. The flow field changes are evaluated by comparing the contours of flow variables and the generated pressure loss for each case are compared with original configuration. Considering the results of parametric studies, a final model was made and solved numerically. The results show that the final modifications will result in considerable improvements in the amount of pressure loss while preserves the same dust collection efficiency.

## **ACKNOWLEDGMENT**

I would like to thank all the great people who helped me so much throughout this research work.

I express my deepest appreciation to my supervisors Dr. Wahid Ghaly and Dr. Ion Stiharu who trusted me and offered me this great opportunity, motivated me, supported me continuously and provided me with their guidance during the course of this work.

I sincerely thank my wonderful parents, without whom it was impossible for me to complete this journey, for their financial and mental support, sympathy and care.

I would like to express my heartfelt appreciation to all my friends, Milad Mousavi, Alfin Leo Matin Komeili, Araz Arbabi, Shayesteh Mohammadbeigi, Raja Ramamurthy and others in the CFD lab who were always helpful and kind to me. Thank you very much all.

## Table of Contents

List of Figures .....	viii
List of Tables.....	xi
Nomenclature .....	xiii
Chapter 1 .....	1
Introduction.....	1
1.1. Application of inertial gas-solid separator.....	1
1.2. Physical description.....	1
1.3. Performance of inertial gas-solid separator .....	2
1.4. Objectives of the present study.....	3
1.5. Thesis outline.....	3
Chapter 2.....	5
Literature review .....	5
2.1. Cyclone history of development and applications.....	5
2.2. Experimental investigations & empirical models.....	8
2.3. Cyclones and computational fluid dynamics.....	11
2.4. Optimization of the cyclones.....	15
2.5. Previous works on swirl tubes .....	16
Chapter 3.....	18
Numerical implementation.....	18
3.1. Components of computational fluid dynamics.....	18
3.2. Governing equations (Navier-Stokes equation).....	19
3.2.1. Conservation of mass (continuity).....	19
3.2.2. Conservation of momentum.....	20
3.2.3. General scalar transport equation.....	21

3.2.4.	Reynolds Averaged Navier Stokes equations (RANS).....	21
3.3.	Solving the RANS Equation .....	22
3.3.1.	Mathematical Modeling and Simplification .....	22
3.3.2.	Discretization approach (finite volume method) .....	24
3.3.3.	Deriving system of algebraic equations.....	28
3.3.4.	Linearizing the algebraic equations and solution of system.....	29
3.3.5.	Pressure based and density based solvers .....	29
3.4.	Turbulence modeling.....	31
3.4.1.	Near Wall Treatment and Grid Considerations .....	32
3.4.2.	Wall Yplus ( $y^+$ ) .....	34
3.5.	Boundary Conditions (BC).....	36
3.5.1.	Mass Flow Inlet.....	36
3.5.2.	Wall Boundaries.....	36
3.5.3.	Outflow .....	36
3.6.	Finalized Proposed CFD Setup .....	37
3.6.1.	Computational Grid (Mesh).....	37
3.6.2.	Solver settings.....	39
3.6.3.	Discussion on the numerical model and settings .....	40
Chapter 4.....		43
4.1.	Geometry and model dimensions.....	44
4.2.	CFD analysis of inertial gas-solid separator .....	47
4.2.1.	Available experimental data and considerations.....	47
4.2.2.	Boundary layer resolution & time independency .....	48
4.3.	Inertial gas-solid separator finalized model validation.....	53
4.4.	Parametric study of the inertial gas-solid separator .....	62

4.4.1.	Selection of geometrical parameters .....	62
4.4.2.	Results of parametric studies .....	64
4.4.3.	Conclusion of the findings in parametric studies.....	85
Chapter 5.....		87
5.1.	Geometry of the optimized model.....	87
5.2.	Simulation settings and results.....	88
Chapter 6.....		98
Conclusion.....		98
6.1.	Summary.....	98
6.2.	Future work.....	100
Bibliography .....		101

## List of Figures

Figure 1- Geometry of the inertial gas-solid separator .....	2
Figure 2- Schematic geometry of a tangential inlet cyclone.....	6
Figure 3- Schematic geometry of a straight-through swirl tube .....	6
Figure 4- First cyclone patent by John M.Finch, 1885 (US patent 325,521) .....	7
Figure 5- Examples of industrial cyclones, from left to right, Oneida wood shop cyclone; two-stage LSR core separator Butcher; Dyson vacuum cleaner [10] .....	9
Figure 6- Schematic of a tangential cyclone with dimension names [10] .....	10
Figure 7- Comparison between the results of mathematical models, experiment, and the numerical simulation [10, 19] .....	14
Figure 8- Shell TSS with swirl tube[30] .....	16
Figure 9- Schematic of a fluid element (control volume).....	20
Figure 10- Graphical illustration of a CV in finite volume method .....	26
Figure 11- Comparison between boundary layer mesh required for wall function method vs. enhanced wall treatment .....	34
Figure 12- Schematic of definition of wall $Y_{plus}$ .....	35
Figure 13- Surface mesh on the static vanes.....	38
Figure 14- Overall view of the mesh, 672,000 cells .....	38
Figure 15- Contours of velocity magnitude at $x=0$ plane obtained from standard WF method illustrating a large separation zone.....	41
Figure 16- Schematic of CFD domain of the Mnoclone.....	43
Figure 17- Schematic of inertial gas-solid separator static vanes and outlets configuration.....	44
Figure 18- 2D drawing of the original configuration of inertial gas-solid separator .....	45
Figure 19- Configuration of extension tubes .....	46
Figure 20- Experimental data of inlet to Outlet total pressure drop at 10% bleed [54].....	48
Figure 21- Boundary layer mesh compatible with wall functions ( $y^+ > 11.225$ ).....	49
Figure 22- Boundary layer compatible with enhanced wall treatment ( $y^+ < 1$ ).....	50
Figure 23- Static pressure value vs. time- right: enhanced wall treatment left: wall function .....	52
Figure 24- Scaled residuals for steady state solution of original model at 20cfm .....	55

Figure 25- Contours of static pressure for original model at symmetry cut-plane ( $x=0$ ), 20 cfm flow rate .....	56
Figure 26-Contours of total pressure for original model at symmetry cut plane ( $x=0$ ), 20 cfm flow rate .....	57
Figure 27-Contours of velocity magnitude for original model at symmetry cut-plane ( $x=0$ ) at 20 cfm flow rate .....	57
Figure 28-Contours of tangential velocity for original model at symmetry cut-plane ( $x=0$ ) at 20cfm flow rate .....	58
Figure 29- Contours of radial velocity for original model at symmetry cut-plane ( $x=0$ ) at 20 cfm .....	59
Figure 30- Comparison between numerical and experimental results of total pressure loss, original model .....	60
Figure 31- Comparison between results of different core mesh resolutions .....	62
Figure 32- Illustration of name of geometrical dimesnions.....	64
Figure 33- Graphical illustration of diffuser straight length and divergence angle variation.....	66
Figure 34-Comparison of pressure contours for different diffuser angles, top left: (org+1°); right : original; bottom left: (org-2.5°) ; right : (org-5°) .....	67
Figure 35- Comparison of velocity magnitude contours for different diffuser angles, top left: (org+1°); right : original; bottom left: (org-2.5°) ; right : (org-5°).....	68
Figure 36- Comparison of tangential velocity contours for different diffuser angles, top left: (org+1°); right : original; bottom left: (org-2.5°) ; right : (org-5°).....	69
Figure 37-Comparison between results of total pressure loss for different diffuser modifications at 40cfm flow rate .....	71
Figure 38- Graphical illustration of diffuser inlet diameter (thickness) variation .....	73
Figure 39-Comparison of pressure contours for different diffuser diamaters, top left: org-10% ; right : original; bottom left: org+10% ; right : org+20%.....	74
Figure 40- Comparison of velocity magnitude contours for different diffuser diamaters, top left: org-10% ; right : original; bottom left: org+10% ; right : org+20%.....	75
Figure 41-Comparison of tangential velocity contours for different diffuser diameters, top left: org-10% ; right : original; bottom left: org+10% ; right : org+20%.....	76
Figure 42-Comparison of pressure loss for diffuser diameter modifications at 20 cfm flow rate	78

Figure 43- Graphical illustration of vanes axial length modifications .....	80
Figure 44-Comparison of pressure contours for different vanes lengths, top: original ; bottom left : org-20% vanes ; right: org+20%.....	81
Figure 45- Comparison of velocity magnitude contours for different vanes lengths, top: original ; bottom left : org-20% vanes ; right: org+20%.....	82
Figure 46-Comparison of tangential velocity contours for different vane lengths, top: original ; bottom left : org-20% vanes ; right: org+20%.....	83
Figure 47- Comparison of total pressure loss changes for different vane lengths at 20cfm flow rate.....	85
Figure 48- Geometry of the proposed inertial gas-solid separator model (units: inches).....	87
Figure 49-Comparisin between static ressure contours of original and optimized model, top: original model ; bottom: optimized model.....	90
Figure 50-Comparisin between total pressure contours of original and optimized model, top: original model ; bottom: optimized model.....	91
Figure 51-Comparison velocity magnitude contours of original and optimized model, top: original model ; bottom: optimized model.....	92
Figure 52-Comparison of tangential velocity contours of original and optimized model, top: original model; bottom: optimized model.....	93
Figure 53- locations of extracting the radial distribution of tangential velocity.....	94
Figure 54- Comparison between radial distributions of tangential velocity at line 1 .....	95
Figure 55- Comparison between radial distribution of tangential velocity at line 2 .....	95
Figure 56-Comparison of pressure loss between experiment, original model and optimized model .....	97

## List of Tables

Table 1- Empirical models geometrical correlations ( $\beta$ ).....	11
Table 2- Solver settings used to simulate the flow inside the Inertial gas-solid separator .....	39
Table 3- Comparison of the results of FIRST order and SECOND order solutions at 20cfm .....	42
Table 4- Extension tubes lengths (L=overall length of the original model) .....	46
Table 5- Thickness of first grid layer , EWT vs. WF .....	50
Table 6- Total number of grids, EWT vs. WF .....	50
Table 7- Initial setting of solver, steady state and time-dependant calculations .....	51
Table 8- Comarison between static pressures obtained from steady-state calculations, EWT vs. WF.....	52
Table 9-Comarison between static pressures obtained from time-dependent calculations at 0.2 seconds, EWT vs. WF.....	52
Table 10- Properties of working fluid.....	53
Table 11- Wall $y^+$ values of the original model at 20cfm .....	54
Table 12- Comparison between numerical vs. exp results of total pressure loss for original model .....	60
Table 13- Comparison between experimental and numerical total pressure loss at 20 cfm (units: inches w.g.) .....	61
Table 14- Comparison between results of total pressure loss obtained from different mesh resolutions at all operating flow rates (units: inches w.g.) .....	61
Table 15-Selected paramters and range of modification (org=original).....	64
Table 16-Initial solver settings for modification of diffuser divergence angle .....	65
Table 17- Comparion between the results of total pressure loss for different diffuser divergence angles .....	70
Table 18-Percentage of pressure loss change relative to original model for different diffuser divergence angles.....	70
Table 19- Initial solver settings for cases of diffuser inlet diameter modification .....	72
Table 20-Comparion between the results of total pressure loss for different diffuser inlet diameters .....	77
Table 21-Percentage of total pressure loss change relative to original model for different modifications of diffuser inlet diameters .....	77

Table 22- Initial settings of solver for cases of vane length modification.....	80
Table 23- Comparison between results of total pressure loss for different vane lengths (units: inches water).....	84
Table 24- Comparison between total pressure loss change for vane length modifications relative to original model.....	84
Table 25-Initial settings of solver for calculations of optimized model vs. original model .....	89
Table 26- Wall Yplus values obtained from simulations of optimized model .....	89
Table 27-Comparison between the results of total pressure loss for original and optimized model .....	96
Table 28-Percentage of total pressure loss change of optimized model relative to original model .....	96

## Nomenclature

$a$	Length of vortex finder of tangential cyclone
$B$	Dust outlet diameter
$b$	Width of vortex finder of tangential cyclone
$b$	Body forces
CAD	Computer aided design
CFD	Computational fluid dynamics
CV	Control volume
$D$	Overall diameter of tangential cyclone
$D_e$	Diameter of gas outlet tangential cyclone
$D_H$	Hydraulic diameter
$ds$	Surface of a fluid element
$dv$	Volume of a fluid element
EWT	Enhanced wall treatment
$F$	Force
$H$	Overall height of tangential cyclone
$h$	Height of vortex finder of tangential cyclone
$i, j$	Counters
$n$	Normal vector
$P$	Static pressure

Pa	Pascal, pressure unit
$P_o$	Total pressure
$P'$	Pressure correction
$Q$	Source matrix
RSM	Reynolds stress turbulence model
$s$	Length of gas outlet of tangential cyclone
$T$	Stresses tensor
$u, v, w$	Velocity components
$V$	Velocity
$v_i$	Inlet velocity
WF	Wall functions
$\mu$	Viscosity
$\beta$	Geometry correlation of empirical models for pressure loss
$\rho_g$	Gas density
$\rho$	Density
$\overline{u'_i u'_j}$	Reynolds stress terms
$\phi$	Flow scalar variable
$\frac{\partial}{\partial x}, \frac{\partial}{\partial y}$	Gradients in x and y directions
$\delta^n$	Solution residuals
$\alpha_p$	Relaxation factor

# Chapter 1

## Introduction

### 1.1. Application of inertial gas-solid separator

Inertial gas-solid separator is a permanent inertial air-filter which is a special format of the cyclones and fits in the category of straight-through swirl tube cyclones (in the next chapter different categories of the cyclones are discussed). The application of inertial gas-solid separator is significant in the large diesel engines where its main objective is to collect the dust particles from the air. The inertial gas-solid separator is a pre-cleaner which filters out larger dust particles after which there will be a battery of secondary filters for fine filtration. A set of inertial gas-solid separator will be installed as a primary filtration system upstream of a diesel engine to increase the life time of the secondary filters which are expensive to replace. However, as in case of any internal flow, there will be energy losses associated with the advancement of the flow through the inertial gas-solid separator duct.

### 1.2. Physical description

Structure of the inertial gas-solid separator is consisting of a main straight tube with one axial inlet, a set of static vanes downstream of the inlet and two axial outlets one for dust particles and one for clean air. The contaminated flow enters the inertial gas-solid separator and starts to spin by passing through the static vanes. Centrifugal forces drive the dust particles towards the periphery and then the particles leave the flow through a slot which is designed to collect them. The filtered air then enters a diffuser in order to be decelerated as it moves towards the engines. The flow leaves the inertial gas-solid separator from both outlets with same direction as it enters hence; this configuration is known as straight-through configuration. Figure 1 shows the overall geometry of a inertial gas-solid separator where the inlet is located at right hand side and the static vanes can be seen right after the inlet.

### 1.3. Performance of inertial gas-solid separator

Basically in cyclonic flows there are two parameters determining the performance; particle collection efficiency and total pressure loss [1, 2]. inertial gas-solid separators can be employed for different applications to meet different requirements. However, in some applications the main objective is to collect the maximum particles, in some others the fuel consumption which is a function of total pressure loss is of higher importance. The application of current configuration of the inertial gas-solid separator is mostly in diesel engines of transporting vehicles which implies the importance of total pressure loss in the system. The working fluid of inertial gas-solid separator is air and considering the range of operating velocities (Mach number below 0.3) the air can be considered as incompressible. The assumption of adiabatic flow would be reasonable and the flow inside the inertial gas-solid separator is turbulent according to the range of flow Reynolds number.

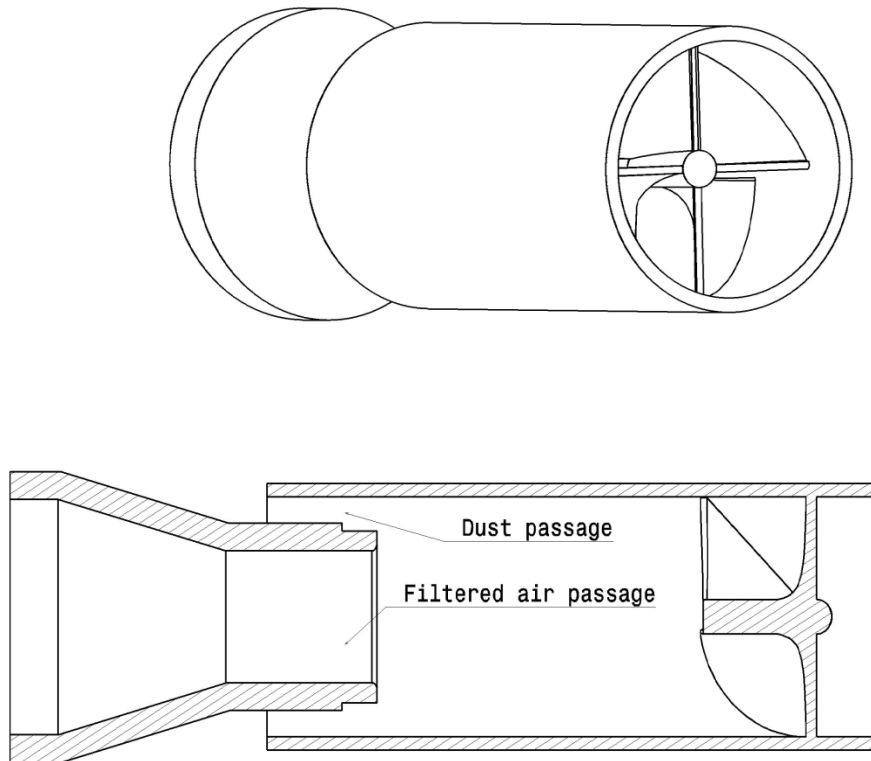


Figure 1- Geometry of the inertial gas-solid separator

## **1.4. Objectives of the present study**

The aim of this study is to investigate the flow inside the inertial gas-solid separator while there has not been any numerical models developed for these gas-solid separators. The overall total pressure loss generated by the inertial gas-solid separator will be obtained by simulating the flow using computational fluid dynamics (CFD). The achievements of this work can also be used for a general category of cyclones called “straight-through swirl tubes” which have not been under the focus of cyclone flow investigations. The results of this project will lead to understanding of the complex flow pattern inside these gas-solid separators. Furthermore, one would be able to understand the relation between the geometrical parameters of the inertial gas-solid separator and its performance. In order to accomplish the above mentioned goals the following steps were completed:

- Dimensions of the inertial gas-solid separator were measured and the first CAD model for the original configuration was built using the CATIA software.
- Different numerical settings and models have been tested in order to find the most efficient and accurate ones suitable for inertial gas-solid separator flow simulation.
- After achieving stable and accurate CFD solutions, the values of total pressure loss were compared to available experimental data. The flow field variables such as pressure and velocity have been evaluated in order to understand the inertial gas-solid separator flow physics and features.
- After evaluation of the performance of the original model, the effect of different geometrical parameters has been assessed. CAD models of each new geometry configuration have been made and flow simulation was performed with the proposed CFD settings. The results led to understanding the effect of each geometry parameter on the performance of the inertial gas-solid separator. Based on these assessments a new geometry is proposed which shows considerable performance improvement.

## **1.5. Thesis outline**

The memoire consist of 6 chapters including the introduction. The second chapter is the literature review and the history of the development of the cyclones. Different categories of the cyclones are introduced and the history of experiments, mathematical models, and CFD simulations in this field is discussed.

Chapter three gives a detailed overview of the flow equations and the fundamentals behind the commercial CFD softwares. The flow equations are presented and followed by the description of different solution methods and algorithms. Non-responsive or weak solution methods for the present application are discussed and the possible deviations from the accurate results are presented. At the end of this chapter the optimum CFD setup including computational grid and solution method is presented. This CFD model is found to be applicable for the original configuration of the inertial gas-solid separator as well as the models with modified geometries.

Chapter four presents the validation analysis of the inertial gas-solid separator's numerical model using the available experimental data. Boundary layer mesh resolution as well as the core mesh resolution is validated and the results are presented. In addition, the results of comparisons between the steady-state and time-dependent analysis are presented in order to prove that the time-dependent phenomena in the flow field are negligible. Further in this chapter the effects of different geometry parameters on the performance of inertial gas-solid separator are evaluated. The effect of three geometry parameters on the performance of the inertial gas-solid separator is evaluated by analyzing the flow variable contours as well as the amount of total pressure loss. The conclusion of the findings from these studies is presented at the end of this chapter and most effective geometrical parameters are discussed. During the discussions, comments are made on the possible effects of each parameter on the collection efficiency as well. These comments are based on the distribution of tangential velocity in the flow field.

An optimized model for the inertial gas-solid separator is presented in detail in chapter five. The CAD drawings as well as the CFD results showing the performance improvements are presented in this chapter. The proposed final model is shown to be highly effective in reducing the amount of total pressure loss in comparison to the inertial gas-solid separator's original configuration where a reduction of total pressure loss up to 35% is achieved. Also by evaluating the tangential velocity distribution in the flow field, it is proved that the collection efficiency of the proposed configuration will have minimal deviation from the original case.

Chapter six summarizes the main achievements of the present research including the discussion on the inertial gas-solid separator flow features and effect of geometry parameters on its performance.

# Chapter 2

## Literature review

### 2.1.Cyclone history of development and applications

Among the different particle separators such as settling chambers, liquid scrubbers, fiber or cloth filters and electrostatic precipitators, cyclones or centrifugal collectors are known by their structural simplicity, high efficiency and low operating and maintenance costs. There are no rotary parts in their structure and they can be built by different type of materials to operate in various working conditions [3]. All these reasons have made them the most popularly used gas-solid and liquid-solid separators [4]. Today cyclones can separate the particles as small as 2 microns with minimal energy consumption. Cyclones are generally categorized in two groups:

- Tangential inlet cyclones
- Axial inlet cyclones or swirl tubes

Tangential inlet cyclones also can be categorized according to their geometrical configurations. Circular, slot type and wrap-around inlets are the forms of tangential inlet cyclones which all work with reversed flow concept. As it can be seen in Figure 2, in a tangential inlet cyclone, flow starts to spin by moving tangent to the cyclone's body. Rotational movement of the flow separates the particles from the flow. The particles get collected from the dust outlet designed at the bottom of the body and the filtered flow moves upward towards the gas outlet or vortex finder. That is where the reversed flow exists in the cyclones flow pattern. Despite the tangential inlet cyclones, the sub-categories of swirl tubes are not conceptually identical. Reversed-flow and Straight-through swirl tubes both have axial inlets but the "straight-through" cyclone doesn't work with the reversed flow phenomenon. The flow exits the swirl tube with the same direction as it enters and there is no change in the flow direction from downward to upward. As it is shown in figure 3, in the structure of swirl tubes, stationary guide vanes are installed in a duct in order to generate rotational swirling flow. In the tangential inlet cyclones, flow rotates by passing tangent to the curved inlet configuration. Centrifugal force of swirling flow drives the particles towards the periphery of the duct and separates them from the main

stream. Presence of the static guide vanes in the structure of swirl tubes generates challenges in modelling their geometry whereas the geometry of tangential inlet cyclones is less complex and easier to model due to absence of the static vanes. Inertial gas-solid separator is also an axial dust collector which can be fit in category of straight-through swirl tubes.

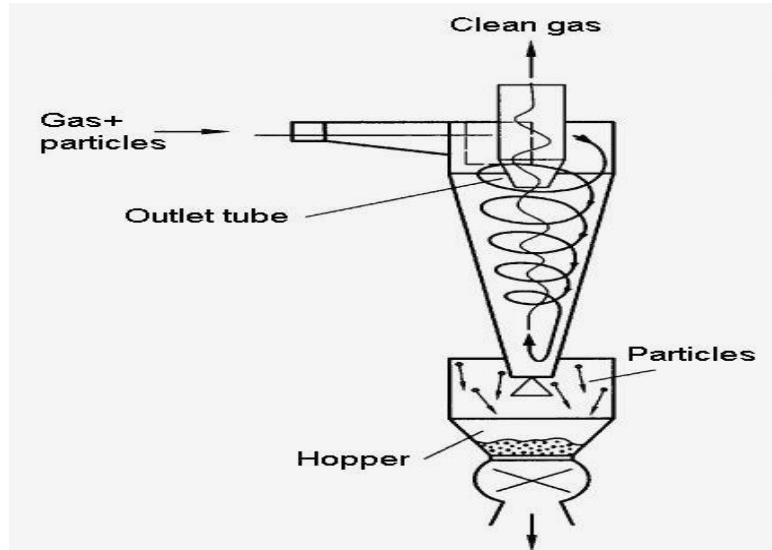


Figure 2- Schematic geometry of a tangential inlet cyclone

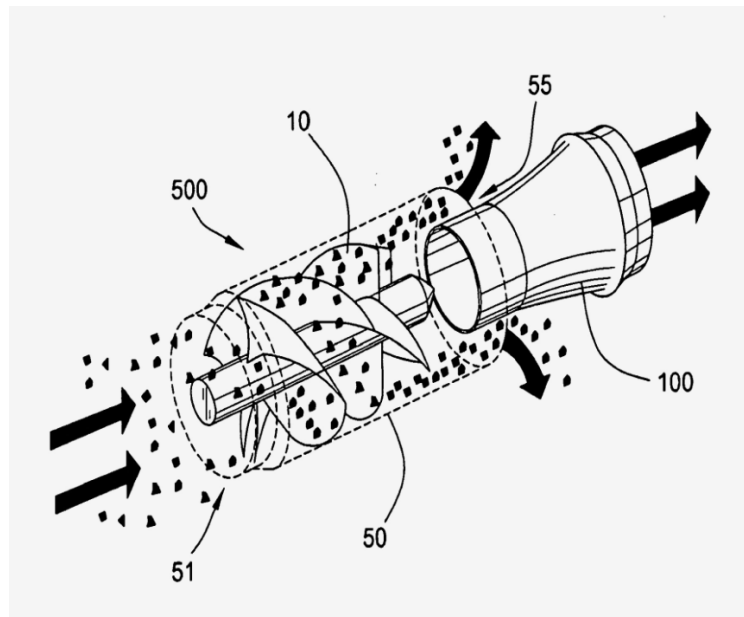


Figure 3- Schematic geometry of a straight-through swirl tube

The first official cyclone invention which is recorded in the US patent office backs to 1885 by John M. Finch (see figure 4) however the history of the idea to use such concept for the purpose of particle collection from the flow was back to early 1800s. During the time researchers from different countries such as United States, UK, Japan and Germany contributed in this growing research area. According to an article published in 1939, cyclones at that time were efficient enough to collect the dust particles as small as 10 microns [5].

Application of cyclones was enormous due to their adoptability with different pressure and temperature levels as well as different particle loadings. At the beginning cyclones were mostly employed to collect the dust and particles from exhausts of the factories. Industries of coal, flour and wood were the early utilizers of the cyclones. Cyclones gradually found their place in more applications wherever the particle or fluid droplet separation was required. Today, cyclones have variety of applications and can be found in food industries, transportation, petrochemical, dust sampling, vacuum cleaning and gas turbine industries [6].

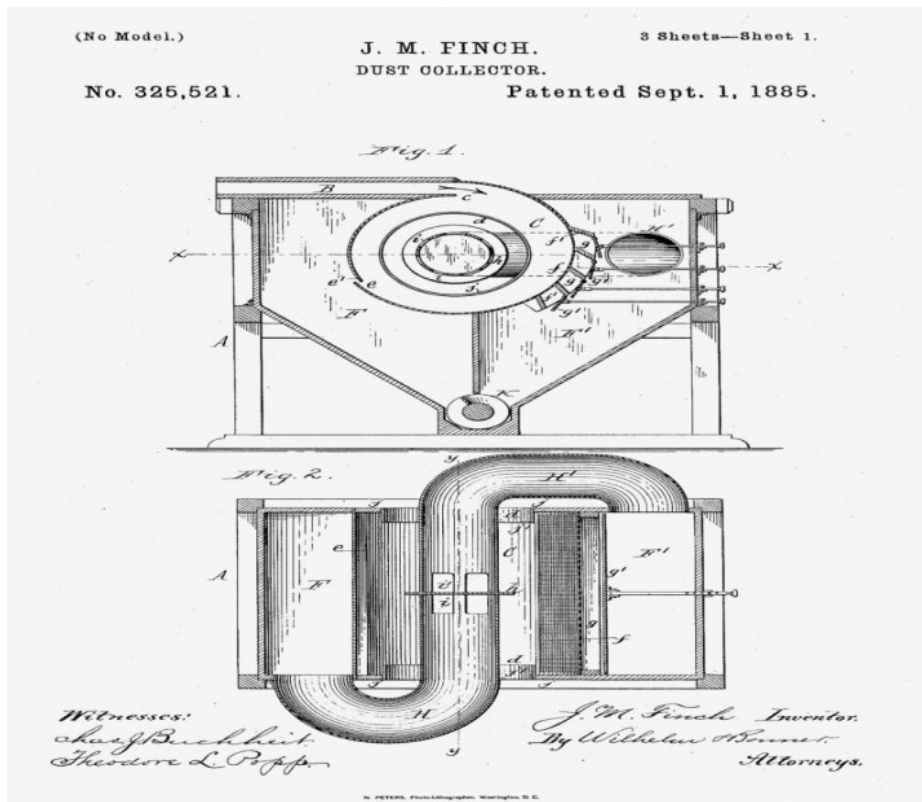


Figure 4- First cyclone patent by John M.Finch, 1885 (US patent 325,521)

The environmental impacts of the industrial particle pollution became a critical concern such that the governmental regulations came into effect for this type of pollution. Cyclones could be placed downstream of a production line where the purpose is to reduce the exhaust dust. They can also be installed upstream of a sensitive mechanism and work as a pre-filter preventing particles to enter that specific mechanism such as a turbine stage (the turbine blades work in high temperature conditions and the effect of erosion can be highly destructive). Cyclones could also work as an initial diluter where by decreasing the particle loading, the life-time of a row of expensive and sensitive filters installed next to them increases.

Cyclones are designed in different geometries and shapes. From the recent configuration we can mention Oneida wood shop cyclone, two-stage LSR Core Separator-Butcher and Dyson vacuum cleaner multiclone, see figure 5 [7-9]. In addition to the particle removal applications cyclones can be used to collect the fluid droplets from the flow.

Due to its structural simplicity and low operational costs, the flow inside the cyclone was believed to be simple therefore cyclones were not under focus of performance analysis at the beginning. As the industrial application of cyclones became numerous and they became one of the important members of production lines, their associated pressure loss as well as their collection efficiency became an important subject of interest for the investigators. Starting around 1930 the researches had more close attention to the performance characteristics of the cyclones such as flow path inside the cyclones, velocity distribution, pressure loss and the capability of the cyclones in terms of collection efficiency. Experimental measurements and mathematical models have been evolved for cyclone applications but there was minor success and result confidence until the invention of measurement methods which enabled the investigators to make more progress.

## **2.2. Experimental investigations & empirical models**

As it is mentioned above, researchers became more interested in flow pattern inside the cyclones as of early 1900. The first efforts were focused on designing appropriate experiments and try to generate empirical models. The main focus of these investigations was the parameters such as pressure drop and collection efficiency.

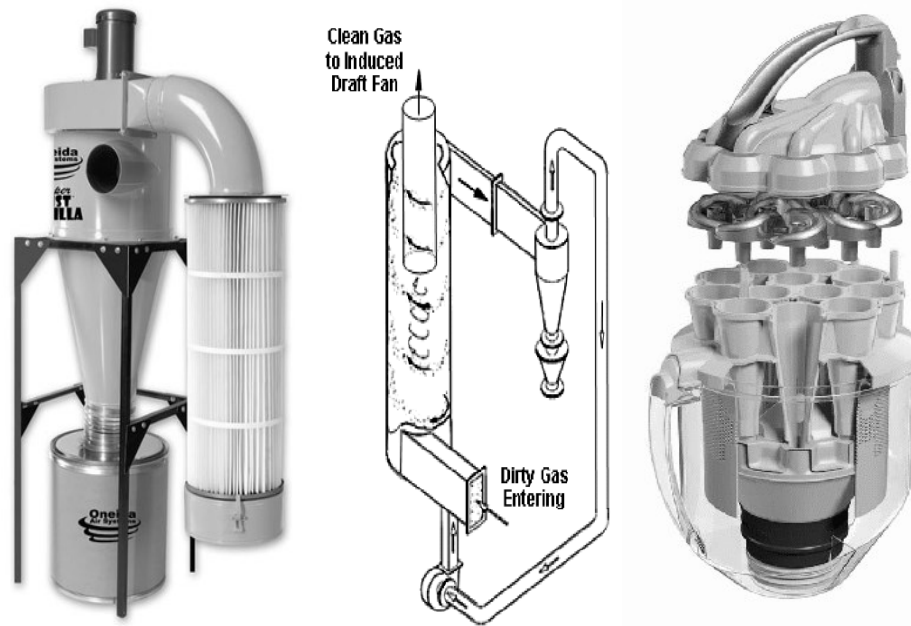


**Figure 5- Examples of industrial cyclones, from left to right, Oneida wood shop cyclone; two-stage LSR core separator Butcher; Dyson vacuum cleaner [10]**

Among the early works we may mention the work of Shepherd and Lapple in 1939. They believed that understanding the flow pattern is highly important in coordinating the theoretical predictions. They published a paper in which they have reported an experimental investigation on a 12 inch glass cyclone. They obtained velocity distribution graphs for the flow inside the cyclone and expressed an empirical formulation to relate the performance parameters to the geometric parameters such as inlet diameter and height. Since then a large variety of mathematical models have been developed and reported where some of them deal with the velocity distribution and the rest with pressure drop and collection efficiency [11]. Invention of new measurement tools such as Laser-Doppler anemometry (LDA) and particle image velocimetry (PIV) helped the investigators to make much more progress in analyzing the flow inside the cyclones and to validate their mathematical models [12]. In most of the cases the models predict the axial and radial velocity in a simple and straightforward manner however more close attention is on the tangential velocity inside the cyclone which is more challenging to predict and therefore has been the subject of different mathematical models. Varieties of models have been presented in order to predict the tangential velocity. Among them we can mention *n-*

**Type model** proposed by Alexander in 1949 which proved to be applicable for all of the cyclones and **Barth's model** back to 1956 which was more suitable for the swirl tubes.

Pressure loss is an important performance parameter which was always subject of plenty of researches and mathematical models. It is believed that in cyclone flow 80% of pressure loss is generated by energy dissipation of viscous stresses of the turbulent rotational flow. Among the pressure loss models we can mention **Stairmand model** back to 1949. This model was suitable for tangential inlet cyclones; **Barth's pressure loss model** which was applicable to all cyclones and swirl tubes and is a simple and useful model for the cyclones as reported by the researchers. There are also few empirical models such as the ones presented by **Shepherd-Lapple**, **Casal-Martinez** and **Dirgo** which their applicability is mostly for the tangential inlet cyclones with low loading of the solids [11, 13, 14]. In 2007, Cortes and Gil published a comprehensive report summarizing the traditional algebraic models including the models for tangential velocity and pressure drop. They concluded despite the current achievements still the lack of advanced ideas can be sensed. They have reported the **Muschelknautz pressure loss model** and **Trefz and Muschelknautz collection efficiency model** as the most accurate models according to comparisons made with the experimental data [12].

### 2.2.1. Discussion on three empirical models

In this section the formulations of three empirical models Shepherd-Lapple, Casal-Martinez and Dirgo are brought. Figure 6 shows draft of a tangential inlet cyclone demonstrating the different dimension and the names assigned to them.

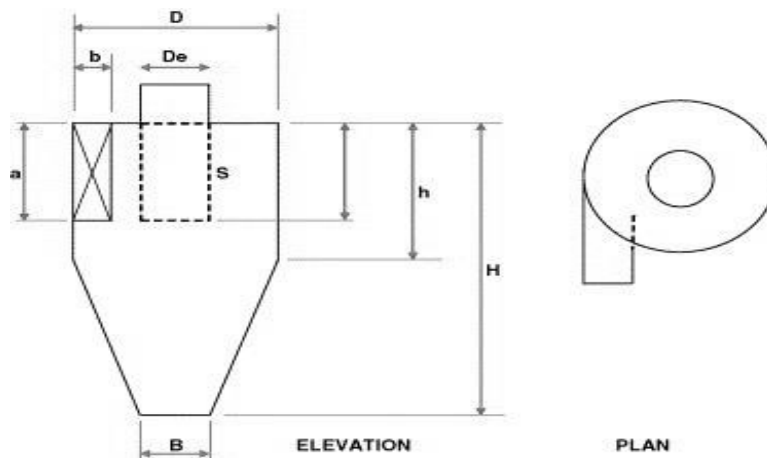


Figure 6- Schematic of a tangential cyclone with dimension names [10]

The amount of pressure loss in these three models is related to geometrical parameters as well as working flow density and inlet velocity. In all these models the general equation for pressure loss can be written as:

$$\Delta P = \beta \frac{\rho_g v_i^2}{2} \quad (2-1)$$

In equation (2-1),  $\rho_g$  represents gas density and  $v_i$  is the inlet velocity. The difference between the models is the definition of  $\beta$  as presented in the table 1 where H represents the overall height of the tangential cyclone, D represents the overall diameter,  $D_e$  is the inlet diameter, and B is the dust outlet diameter. Comparison between the results of these mathematical models and the results achieved from numerical simulations will be presented at the end of this chapter where we can see the result of Dirgo model shows more consistency when compared with numerical results achieved from CFD softwares [10].

**Table 1- Empirical models geometrical correlations ( $\beta$ )**

<i>Name of the Model</i>	$\beta$
Shepherd and Lapple	$\beta = 16 \frac{ab}{D_e^2}$
Casal and Martinez	$\beta = 11.3 \left( \frac{ab}{D_e^2} \right)^2 + 3.33$
Dirgo	$\beta = 20 \left( \frac{ab}{D_e^2} \right) \left[ \frac{\frac{S}{D}}{\left( \frac{H}{D} \right) \left( \frac{h}{D} \right) \left( \frac{B}{D} \right)} \right]^{\frac{1}{3}}$

## 2.3. Cyclones and computational fluid dynamics

### 2.3.1. History and advantages

As the computational fluid dynamics has been emerged and developed, considerable progress has been achieved by the investigators. CFD is shown to be highly capable of predicting and

simulating the flows inside the cyclones beside the fact that it is faster and less costly relative to the experiments. There are lots of research articles in the literature which employed the CFD as a strong tool in order to simulate the flow inside the cyclones and to validate the old and new experiments and mathematical models. Swithenbank and Boysan [15, 16] were the pioneers of using the computational fluid dynamics for purpose of modeling the swirled flow inside the cyclones. Evolution of CFD revealed that the flow inside the cyclones is not simple and need higher technology, time and focus. Highly turbulent flow and near wall phenomenon make strong challenges in predicting the behavior of the flow inside the cyclones [4]. Variety of in-house codes and softwares emerged in order to facilitate the flow simulations. The simulation using CFD became faster and more reliable following the increase and progresses in the computational resources. The machines were able to solve for higher number of computational grids which was a requirement for turbulent flows such as the ones inside the cyclones. The computational resources became capable of solving more complex mathematical equations such as Reynolds Averaged Navier-Stokes equations (RANS). Griffiths and Boysan [17] published one of the first and most comprehensive researches on the capability of the CFD in modelling the flow inside the cyclones. Their articles have been referred in numerous CFD publications. They employed commercial packages such as FLUENT® in order simulate the flow inside the cyclones and to achieve the performance parameters. They were able to accomplish their parametric studies using the CFD softwares and compare them with the experiment. They were able to generate the performance curves using CFD and compare it with semi-empirical theories such as Barth's theory. They have concluded that the CFD was capable to predict even small details of the flow field such that in their report, graphs of particle trajectories, velocity vectors and collection efficiency is presented. Numerous articles exist in the literature each of them evaluating the effect of specific geometrical parameters (inlet dimensions and shapes, vortex finder dimensions, cyclone body diameter) on the performance of the cyclones [18-21]. Raoufi et al [22] have conducted a set of CFD simulations on 4 different cylinder-shaped and 6 cone-shaped vortex finders (cyclones outlet). They have varied the angle convergence and divergence of vortex finders and assessed the effects of these geometrical changes on pressure loss and collection efficiency. They achieved acceptable consistency with the experimental result. Elsayed and Lacor also published few articles introducing optimized geometrical configurations to achieve the minimum pressure drop and maximum collection efficiency. They used the CFD

as a tool to validate their results and compared them to mathematical models such as Muschelknautz method of modeling (MM). They introduced a new design with considerable improvement in the pressure drop relative to the Stairmand design [23]. Beside the geometrical parameters, fluid properties temperature, density and viscosity were also subjects of different researches. Gimbun and Chuah et al have evaluated the effect of temperature and inlet velocity on the pressure drop of the gas cyclones. They used the commercial CFD software FLUENT to assess their results. They announced the CFD as the best method for purpose of cyclone flow simulation by means of which they were able to get the numerical results as close as 3% to the experimental results [10]. Figure 7 shows a sample result achieved by Gimbun and Chuah et al [10, 19] which indicates the variation of pressure loss vs. velocity inlet. The results of different CFD models of RNG  $k-\epsilon$  and Reynolds stress model are compared to mathematical models of Dirgo, Shepherd & Lapple, Coker & Casal and Martinez. Great consistency between the Dirgo semi-empirical model and Reynolds stress numerical model was observed.

Highly swirled flow inside the cyclones could be accompanied by unstable and non-steady phenomena such as separations and vortices. Prediction of such unstable flow needs more complex formulation and computational grid evaluation. This complexity has attracted the researchers to investigate these phenomena more carefully and to develop more robust and reliable methods in order to capture and analyze the details of flow inside the cyclones. Researchers published their conclusions introducing appropriate combinations of computational grid and turbulence models. Hoekstra and Derksen [24] have conducted a comprehensive analysis both numerically and experimentally (LDV) and compared them in their publications. They have evaluated different turbulence closure models and their capability to capture the vortices and the fluctuating velocity components in the swirled flow inside the cyclones. Their reports are accompanied with distribution of tangential and axial velocities along the radial and axial directions. They have reported the Reynolds Stress Transport model as a reliable model to predict the turbulent stresses in the flow.

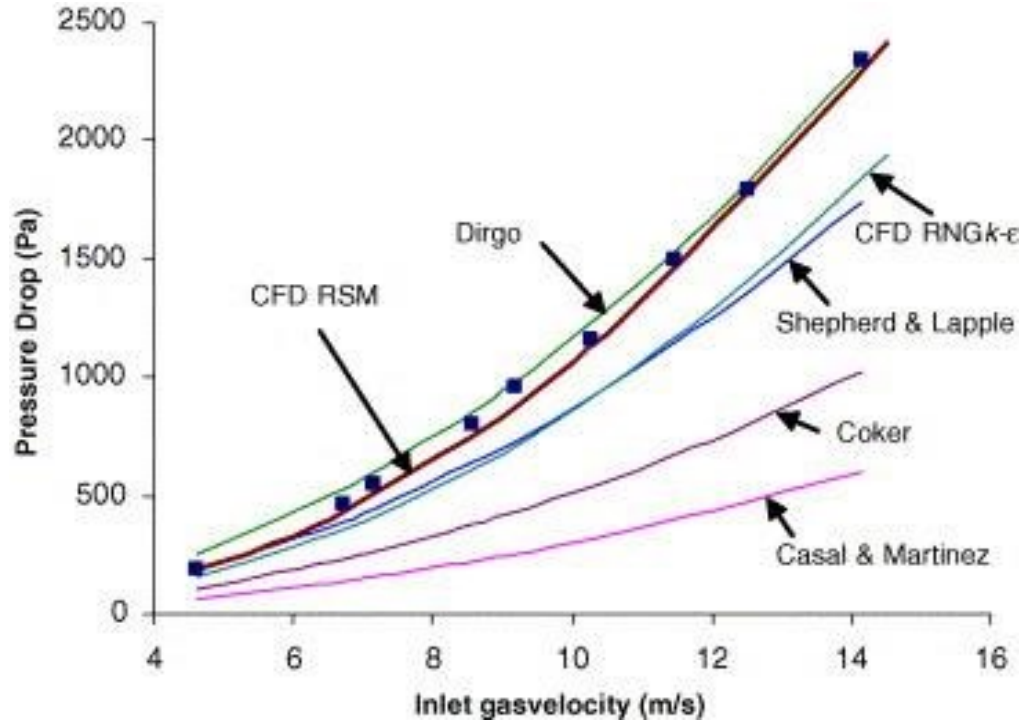


Figure 7- Comparison between the results of mathematical models, experiment, and the numerical simulation [10, 19]

### 2.3.2.Challenges in CFD simulations

Despite the capabilities of computational fluid dynamics, there are some aspects of it which requires careful attention. Generating a sufficiently fine computational grid with high quality is of high importance in CFD. This matter becomes quite challenging when one deals with complex geometries such as cyclones and swirl tubes. Even few highly skewed or corrupted grids can cause the simulation to fail. Besides, recently a fair number of turbulent models and solution algorithms have been developed and applied in the commercial softwares each having specific requirements of computational grids. Applying each model could end to some results which can be completely wrong and misleading. In conclusion before starting a CFD simulation, one should have a fair knowledge of the possible flow characteristics to set up the simulation specially when using the commercial packages. In order to start the CFD simulations, an initial guess for the flow properties such, pressure, density, velocity and viscosity is required. The initial values will be distributed over all the computational nodes and the calculation will be started from those values. Realistic initialization of the flow field before starting the solution is another important challenge which needs expertise. Ill or non-accurate initial values distributed

over the computational grids, can cause the failure of the solution, long computational time or weakly converged and non-reliable results. In addition, once the solution of the CFD calculation has converged, carefully post-processing is required in order to recognize the non-realistic and misleading results. During the recent years, varieties of models with different complexity and number of equations have been developed. Solution algorithms are also developed in order to make the flow solvers more accurate and logical. The higher the accuracy of simulation is higher allocated memory and CPU time would be required. A complex model which solves 7 transport equations at the same time (for example RSTM) will take much more time to converge and needs finer computational grid but it produces more accurate results in case of convergence. However a simpler model can solve fewer equations and work with coarser grids. Therefore there should be a compromise between computational time and cost vs. the accuracy and preciseness.

## 2.4. Optimization of the cyclones

In addition to the parametric studies, optimization algorithms are also widely used in order to find an optimized configuration for the cyclones [25, 26]. As it was mentioned before decreasing the pressure loss and increasing collection efficiency are the main objectives of optimization investigations for cyclones. Ravi et al [27] have done a multiobjective optimization using *nondominated sorting genetic algorithm (NSGA)*. Their objective functions for this optimization were maximization of the overall collection efficiency and the minimization of the pressure drop. They have reported NSGA as a capable algorithm for the purpose of cyclones and mentioned the diameter of the cyclone and vortex finder as important decision variable defining the cyclone performance. Referring back to Figure 6 and considering the dimensions names, results of their research showed the optimal variables are the ones on the highest or lowest possible limits. For example optimal value for the collection efficiency achieved by maximum value of decision variable  $\frac{H}{D}$  and minimum value of  $\frac{B}{D}$ . It means if the ratio of cyclone's height to diameter increases, the collection efficiency increases accordingly but on the other hand it is necessary to choose a low value for ratio of dust outlet to cyclone diameter. They have also observed a good consistency between their predictions and the optimal value of decision variable  $\frac{D_e}{D}$  predicted by Dirgo and Leith models. Safikhani et al also have published a paper in 2010, optimizing the cyclones for minimum pressure drop using GMDH-type algorithm. Their decision

variables were also geometrical parameters of cyclones ( $\frac{D_e}{D}, \frac{H}{D}$ ) mostly same as other researches with difference in the optimization algorithm. They achieved and reported acceptable tradeoffs between collection efficiency and pressure drop and verified their results using CFD [28].

## 2.5. Previous works on swirl tubes

Despite all the comprehensive experimental works, empirical models and CFD simulations focused on tangential inlet cyclones, few researches have been performed on the swirl tubes [29]. Weiming et al have done one of the few researches aiming to relate the performance parameters of the swirl tubes to tangential inlet cyclones. They performed their research on the Shell TSS® swirl tube which is a type of reversed flow swirl tube. As it can be seen (see Figure 8), the difference between tangential inlet cyclone and swirl tube is the direction of the inlet. Swirl tubes will generate the required rotation in the flow but still the reversed flow exists in the flow pattern. Weiming et al have published the experimental results for overall efficiency and pressure drop of a swirl tube and compared them with experimental results and empirical models for the tangential inlet cyclones. They concluded that the performance of a swirl tubes is acceptable as a well-designed cyclone and is comparable to tangential inlet family of cyclones despite the differences in the overall sizes and shapes [30].

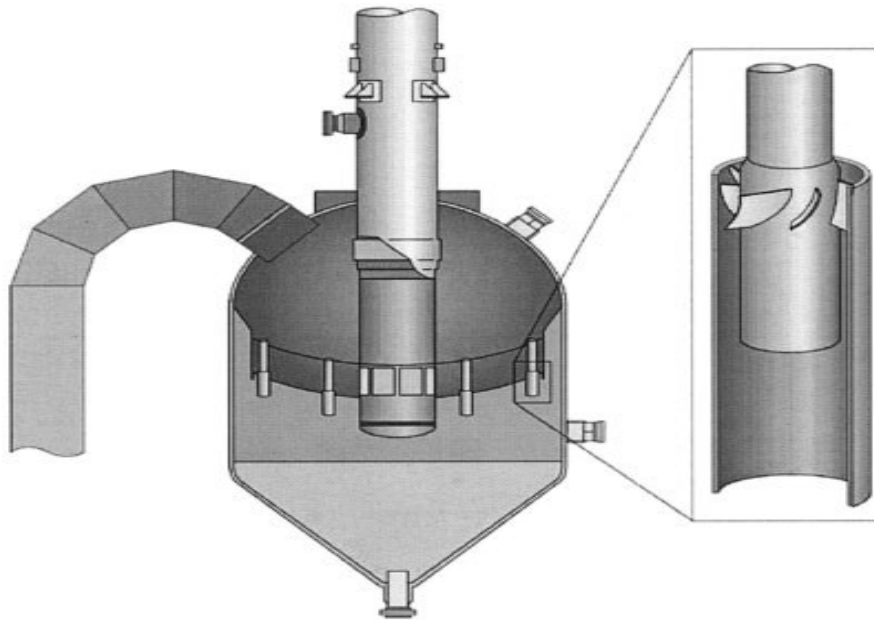


Figure 8- Shell TSS with swirl tube[30]

In addition of the above configuration, the swirl tube can be designed with both inlet and outlets in the same direction and without reversed flow (see Figure 2). Related work to this configuration is even rarer than the one with reversed flow.

Among the few works in the field of swirl tubes most of them are more focused on the experiments and empirical models and to the author's knowledge there are very few CFD simulations and optimization works reported in the literature for application of swirl tubes especially for the straight-through swirl tubes (without reversed flow).

# Chapter 3

## Numerical implementation

Computational fluid dynamics (CFD) is a largely employed tool for solving and simulating the fluid flows in variety of applications. In CFD since the flow equations of motion are not analytically solvable; they will be expressed in terms of partial differential equations and then will be solved by use of numerical methods [31]. In the field of cyclonic flows, computational fluid dynamics is been mostly used and shown to be a reliable tool for simulating the flow and predicting its features. Numerous researches have taken advantage from CFD as a tool to validate and/or investigate experimental measurements or mathematical models predictions. In this way some of the researchers developed in-house CFD codes [32-34] whereas others have used the commercial packages such as ANSYS CFD® [24, 35]. Recently, the industries are more interested in the results achieved by CFD tools due to their reliability, low cost and time consumption.

### 3.1. Components of computational fluid dynamics

Computational fluid dynamics consists of few fundamental elements:

- **Mathematical model:** The first component of a numerical simulation is the mathematical model. These mathematical models contain flow equations; conservation equations and equations of motion. Depending on the case and application, realistic assumptions along with empirical or semi-empirical relations will be employed in order to simplify and solve the flow equations.
- **Computational grid and discretization of flow equations:** Computational grid (mesh) and discretization approach are important elements of CFD. The system of flow equations (mathematical model) needs to be discretized and solved numerically, because so far there are no unique analytical solutions found for them. The discretized equations will then be solved over the computational grid using numerical techniques. The results quality is highly dependent on the computational grid, discretization approach and the numerical technique used to derive them.

- **Solution convergence:** A numerical simulation is converged when the boundary conditions of the flow field are achieved and stabilized by the process of solution. It doesn't necessarily imply the accuracy of the results since a numerical solution can converge to non-realistic results due to different reasons. Convergence criteria of a solution have to be accompanied by post-processing of the data in order to prevent any misleading and wrong conclusions. The convergence criteria are achieved from the conservation laws, i.e. mass conservation, momentum conservation and energy conservation.

Commercial CFD codes have been developed during the past years enabling the researchers to generate and modify the computational grids, employ different numerical methods and adjust the configuration of simulations much faster and more convenient. However, using the commercial softwares without having deep knowledge of fluid mechanics will lead to inevitable errors and misinterpretation of the results. Understanding the flow equations and fundamentals of numerical solutions which are the basics behind the CFD software is necessary to obtain accurate and reliable results. In computational fluid dynamics the user's input including computational grid, solution methods and algorithms, initial values, and boundary conditions have considerable effects on the outcome of calculations.

## **3.2. Governing equations (Navier-Stokes equation)**

In the process of simulating the flow, Navier-Stokes equations including mass conservation and momentum conservation equations, along with conservation equations of other scalars such as energy will be solved. In this section the fundamental flow equations are briefly discussed.

### **3.2.1. Conservation of mass (continuity)**

The mass conservation law simply implies that the mass inside a control volume, as well as the overall flow domain, would not be created nor destroyed. Figure 9 shows a fluid element, control volume, for which the flow equations will be written. Equation (3-1) is the mathematical expression of the mass conservation law in integral form.

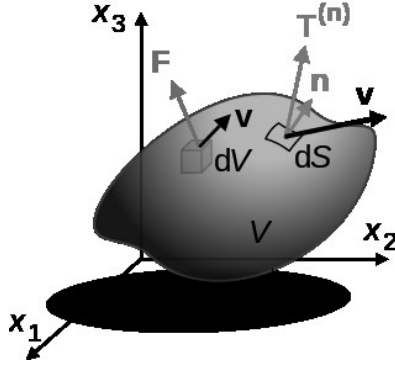


Figure 9- Schematic of a fluid element (control volume)

$$\frac{\partial}{\partial t} \int \rho dv + \int \rho V \cdot n ds = 0 \quad (3- 1)$$

In the above equation,  $dv$  represents the volume of fluid element. This equation expresses that the time rate of change of mass inside a control volume equals to summation of the mass entering and exiting the control volume. In case of a steady state flow, the time rate of change is equal to zero so the incoming mass flow rate should be balanced with all the mass flow rates leaving the flow domain. The mass balance of inlet and outlet boundaries in the flow domain has to be checked in post-processing of CFD results.

### 3.2.2. Conservation of momentum

The concept of conservation of momentum is Newton's second law. The summation of forces acting on the fluid elements is in relation with their acceleration. There are two sources of forces ( $F$ ) in the momentum equation: **surface forces** such as forces created by pressure and shear stresses and **body forces** such as gravity and centrifugal forces. The mathematical expression of the conservation of momentum in integral form is:

$$\frac{\partial}{\partial t} \int \rho V dv + \int \rho V V \cdot n ds = \sum F \quad (3- 2)$$

The right hand side of the equation (3-2) can be split and rewritten as follows:

$$\frac{\partial}{\partial t} \int \rho V dv + \int \rho V V \cdot n ds = \int T \cdot n ds + \int \rho b dv \quad (3- 3)$$

In equation (3-3),  $T$  is the stresses tensor which contains the terms of static pressure and viscosity forces imposed on the fluid element, and  $b$  represents the body forces.

### 3.2.3. General scalar transport equation

The integral form of the generic conservation equation for a scalar quantity ( $\phi$ ) is as follows:

$$\frac{\partial}{\partial t} \int \rho \phi dV + \oint \rho \phi V \cdot n dS = \oint \Gamma \nabla \phi \cdot n dS + \int q_\phi dV \quad (3-4)$$

In equation (3-4) the  $q_\phi$  is the source or sink of  $\phi$  per unit volume, where  $\Gamma$  represents the diffusion coefficient of scalar  $\phi$ . The terms on the right hand side of the above equation represent the transport of scalar  $\phi$  whereas the left hand side terms are the convection terms. The conservation equation can be written for any scalar in the flow field such as energy and temperature. For instance if the heat transfer needs to be considered in the flow field, conservation of energy equation will be solved along with other flow equations. Turbulence phenomenon also requires additional unknown scalars to be solved, such as Reynolds stresses and turbulence dissipation rate. Therefore additional conservation equations need to be added to the system of flow equations. The number of turbulent scalars and their corresponding conservation equations depends on the turbulent behavior of the flow, required precision of the solution, and the employed turbulence closure model.

### 3.2.4. Reynolds Averaged Navier Stokes equations (RANS)

Turbulent flow motion is described by Reynolds-averaged Navier-Stokes (RANS) equations. In order to obtain the flow's system of equations, Reynolds averaging method splits the flow variables into two parts; mean value, either ensemble-averaged or time-averaged, and the fluctuating values. This method can be implemented for all flow scalars and conservation equations.

$$\phi = \bar{\phi} + \phi' \quad (3-5)$$

Substituting equation (3-5) in the continuity and momentum equations, taking a time or ensemble average and showing the mean values without the over bar, the Navier-Stokes equations will have the following Cartesian tensor form:

Continuity Eq

$$\frac{\partial \rho}{\partial t} + \frac{\partial}{\partial x_i} (\rho u_i) = 0 \quad (3-6)$$

Momentum Eq

$$\frac{\partial}{\partial t} (\rho u_i) + \frac{\partial}{\partial x_j} (\rho u_i u_j) + \frac{\partial}{\partial x_j} (-\overline{\rho u'_i u'_j}) = -\frac{\partial P}{\partial x_i} + \frac{\partial}{\partial x_j} \left[ \mu \left( \frac{\partial u_i}{\partial x_j} + \frac{\partial u_j}{\partial x_i} - \frac{2}{3} \delta_{ij} \frac{\partial u_l}{\partial x_l} \right) \right] \quad (3-7)$$

By substituting 1, 2, 3 for indices  $i$  and  $j$ , 6 equations for momentum conservation would be achieved. The term  $\overline{\rho u'_i u'_j}$  is called **Reynolds Stress** which in general has the form of  $\overline{\rho u'_i \phi'}$  and is known as **turbulent scalar flux term**.

Reynolds averaging adds some unknowns to the system of flow equations. **Turbulence Models** or closure models contain additional equations (empirical and semi empirical) by means of which additional unknowns of the system would be solved.

### 3.3. Solving the RANS Equation

#### 3.3.1. Mathematical Modeling and Simplification

Defining a mathematical model is the first step of every numerical simulation. Mathematical equations will be accompanied by simplifying assumptions, where the conservation equations will be rewritten in simpler forms. Any flow category can fit in a specific mathematical model and consequently a particular numerical simulation method would be required to solve it. An example of simplification can be the assumption of a two-dimensional (2D) flow instead of 3D flow wherever the variation of flow in the third dimension is not of interest or is negligible (for example the flow over an infinite wing which can be simplified to its 2-D section). This assumption cancels the third component of all flow equations; therefore 2 equations out of 6 momentum equations will be cancelled. Below, two examples of mathematical simplifications most widely used in CFD simulations are discussed.

- **Steady, Incompressible Flow**

Flows without major complexities in their path, which produces large instabilities, flows without any rotating part in their domain, and flows with time-independent boundary conditions can be considered as steady state flows. On the other hand, flows with Mach number below the value of 0.3 are basically considered as incompressible. That implies the fact that throughout the domain the flow's density wouldn't experience any changes. Flow moves with a velocity well below the speed of sound and would be aware of the upcoming geometrical changes or other phenomena. Therefore, the flow would have enough time to adopt itself while it proceeds in the domain. The differential form of continuity equation considering three dimensional, steady ( $\frac{\partial}{\partial t} = 0$ ), and incompressible flow ( $\rho = \text{constant}$ ) will be simplified to:

$$\nabla \cdot \mathbf{V} = 0 \quad (3-8)$$

Considering the same conditions the momentum equation will have the following form

$$\mathbf{v} \cdot \nabla \mathbf{v} = -\frac{1}{\rho} \nabla P + \frac{\mu}{\rho} \nabla^2 \mathbf{v} + \mathbf{F}_b \quad (3-9)$$

In equation (3-9),  $F_b$  represents the body forces.

In the next chapters, it will be shown that the flow inside the inertial gas-solid separator can be considered as steady state. The boundary conditions are time-independent and the flow instabilities were found to be detectable in the steady state solution.

- **Boundary layers**

When a viscous flow passes over a solid surface a boundary layer will be shaped in the vicinity of the surface. In case of turbulent flow, the flow inside the boundary layer is of high importance because of the presence of large gradients of scalars in that region. Flows along predominant direction are good examples of boundary layer flow i.e. shear flow. The pressure in these flows is considered to be function of x and z directions only, therefore “y” will be omitted from the pressure formulation. Considering this assumption, the continuity equation would not be changed but the momentum equations in y direction will not be considered in the system of flow equations. Below the simplified momentum equations are presented:

$$\rho \frac{Du}{Dt} = -\frac{\partial p}{\partial x} + \mu \frac{\partial^2 u}{\partial y^2} - \rho \frac{\partial}{\partial y} (\overline{u'v'}) + \rho F_x \quad (3-10)$$

$$\rho \frac{Dw}{Dt} = -\frac{\partial p}{\partial z} + \mu \frac{\partial^2 w}{\partial y^2} - \rho \frac{\partial}{\partial y} (\overline{w'v'}) + \rho F_z \quad (3-11)$$

The original RANS equations will be replaced by the equations (3-10) and (3-11) in the vicinity of the walls. In the future sections, the methods and algorithms to solve the flow equations over the computational grid (mesh) will be discussed.

### 3.3.2. Discretization approach (finite volume method)

After defining the mathematical model which includes the simplified equations as well as the nominal boundary conditions, a suitable discretization method is necessary in order to proceed with numerical calculations. Discretization is actually the method of estimating the above discussed differential equations by the appropriate system of algebraic equations. Three types of mostly used methods of discretization are: *finite element method (FE)*, *finite difference method (FD)* and *finite volume method (FV)*. Among these methods the most compatible one for the complex geometries is the finite volume method.

The finite volume method is known as simplest and the most understandable discretization method because every term of the differential equations in this method has a physical interpretation and sensibility for the analyzers. A computational grid will divide the solution domain into a number of control volumes (CV). The control volumes in this method are independent of coordinate systems and the computational grid just defines the control volumes boundaries. That makes the FV a suitable one for the complex geometries. Each control volume has a computational node located at its center and the values on the surfaces of that control volumes are related to the central nodes of neighboring cells using interpolation. For each computational node an algebraic equation will be derived in which the values of neighbor nodes are visible [36]. As it was discussed in the flow equations section, the aim of flow simulation is to solve the system of conservation equations. The finite volume method for a steady state flow starts with the generic form of conservation equation as follow:

$$\oint \rho \phi V \cdot n dS = \oint \Gamma \nabla \phi \cdot n dS + \int q_{\phi} dv \quad (3-12)$$

This equation contains two integrals over the surface of the control volumes and one term over the volume. Equation (3-12) will be applied to each control volume as well as the overall computational domain. The next step is to obtain an algebraic equation for each and every CV by

approximating the surface integrals as well as volume integral by a quadrature formulae. Approximating the integral terms has two consecutive steps:

- Each integral term (surface or volume) will be approximated by the product of central node value and area or volume of that computational cell (CV).
- Unknown nodal values will be estimated using different interpolation methods from neighboring nodes.

The order of approximation in the above steps should be matching. So far different integral approximation methods as well as interpolation methods have been developed. *Midpoint rule* and the famous *Trapezoid rule* are examples of second order methods and *Simpson's rule* is a fourth order method for approximation of the surface integrals. For the volume integrals the simplest method is to replace the integral by product of center node value and the volume of the CV which is a second order approximation as well. If the order of integral approximations is higher, the resolution and precision of the solution would be higher but with the expense of additional computational time and resource.

### **Interpolation schemes**

As it is mentioned above, after estimation of surface and volume integrals by the product of nodal value and its consistent area or volume, an interpolation scheme would be required in order to estimate the value of scalars at the surfaces of the CV. The interpolation methods are widely developed and variety of them have been used in the literature such as *upwinding interpolation (UDS)*, *linear interpolation (CDS)*, *Quadratic upwind interpolation (QUICK)*, *higher order schemes*, extrapolation methods such as *linear upwind scheme (LUDS)* and also some methods were developed by blending one or more of the above mentioned methods. Among these methods *upwinding method* is highly used for the application of cyclonic flows. Upwinding means that the value of  $\phi$  at a face of a CV is derived from the CV's upstream (upwind) neighbor cell. Depending on the number of terms of the Taylor series being used to extract the required value at the control surface (one of the surfaces of the control volume), this method can be first order upwinding or higher orders upwinding. Higher orders of interpolation will end up with more accurate results but with the expense of higher computational resource and time. Figure 10 is a 2D schematic of the computational grid. The center points "P, N, E and S"

are the computational nodes. In order to solve the integrals in the generic conservation equations, the values of  $\phi$  at p, n, e and s need to be found by interpolating the values at neighboring cells.

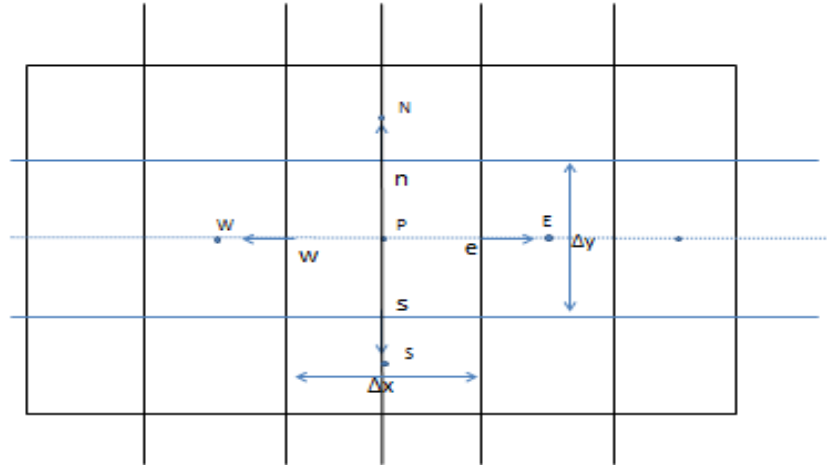


Figure 10- Graphical illustration of a CV in finite volume method

Conservation equations for the control volume (around node P) will be written. In order to find the surface integrals on the surface “e” in the above sketch, the value of  $\phi$  at the surface “e” has to be estimated. Interpolation methods will be used to estimate a unique value of  $\phi$  which represents the whole surface. The upwinding simply approximates the  $\phi$  value at “e” by its value at the upstream cell as follow:

$$\phi_e = \begin{cases} \phi_P & \text{if } (\mathbf{v} \cdot \mathbf{n})_e > 0 \\ \phi_E & \text{if } (\mathbf{v} \cdot \mathbf{n})_e < 0 \end{cases} \quad (3-13)$$

The above equation is derived from only the first term of Taylor series therefore it is a first order upwinding discretization. This method is the only one which is known to give non-oscillatory results [36]. Considering the Taylor series expansion, different degrees of upwinding can be obtained. The first term of the Taylor series will give a first order approximation while picking the second term will have the second order approximation accuracy.

$$\phi_e = \phi_p + (x_e - x_p) \left( \frac{\partial \phi}{\partial x} \right)_p + \text{Higher orders} \quad (3-14)$$

Other interpolation methods use different combinations of neighbor values to get the value at point “e”. For example the **linear interpolation method** which is the simplest second order method has the following form:

$$\phi_e = \phi_E \alpha_e + \phi_P(1 - \alpha_e) \quad (3-15)$$

Where the  $\alpha_e$  is the linear interpolation coefficient derived by:  $\frac{\Delta x_{eP}}{\Delta x_{EP}}$ . The above interpolation schemes are available in the CFD commercial packages in order to be applied according to the case. For the current inertial gas-solid separator which is modeled in this research (category of straight-through swirl tube), the first order interpolation methods were non-reliable and inaccurate. Hence, a second order upwinding scheme was used to solve the flow equations.

### **Special pressure interpolation methods (ANSYS-FLUENT)**

In addition to the upwinding schemes which are described above, there are some special interpolation schemes for pressure which are different than previous mentioned methods and are introduced in the ANSYS-FLUENT v14.57 commercial package. Choosing the pressure based solver, few pressure interpolation methods including the *Standard*, *PRESTO*, *Linear*, *Second Order* and *Body Force Weighted* would be available. Depending on the case one of these interpolation schemes can be used. For the cyclonic flows (rotational reversed flows), the standard and PRESTO schemes are judiciously used since they have shown better convergence and accuracy. In case of inertial gas-solid separator the standard pressure interpolation showed satisfactory precision and stability of the results.

### **Gradient interpolation methods**

In addition to the value of  $\phi$  itself, the diffusive term of conservation equations ( $\phi \Gamma \nabla \phi . n dS$ ) requires the gradient of  $\phi$  between center points P and E ( $\frac{\partial \phi}{\partial x}$  or  $\frac{\partial \phi}{\partial y}$ ) to be calculated. Estimations of gradient are always of second order. There are several methods for gradient evaluation which are also available in commercial packages. *Green Gauss Cell based*, *Green Gauss Node based* and *Least Square Cell based* gradient estimation methods are the mostly used ones. The least square cell based method is a suitable method for the cases with complex geometry with unstructured mesh. This method is also popularly used for the cyclonic flow simulations. The

accuracy and required computational resource was verified to be satisfactory for the present analysis. This method estimates the gradients simply by the following equation.

$$\nabla\phi_P = \frac{\phi_E - \phi_P}{\Delta r_{EP}} \quad (3-16)$$

In this equation  $\Delta r_{EP}$  is the distance between center points P and E. This method will be finalized by a matrix equation  $[J](\nabla\phi)_P = \Delta\phi$  in which [J] is only dependent on geometry and computational grid and the solution would be the values of  $\nabla\phi$  at CV center points.

### 3.3.3. Deriving system of algebraic equations

After estimating the surface and volume integrals (Flux and Source integrals) and using the interpolation to get the surface values, the system of algebraic equations will be created. This equation for an arbitrary computational node “P” system can be written as follow:

$$\mathbf{A}_P\phi_P + \sum_I \mathbf{A}_I\phi_I = \mathbf{Q}_P \quad (3-17)$$

In the above equation P is the control point itself and I points are the other points in the domain. For each control volume a line of algebraic equation (3-17) will be written which includes the terms from the rest of the nodes in computational domain. The linearity of the algebraic equation depends upon the method of estimation for integrals as well as the interpolation methods. Finally a matrix equation can be derived as follow:

$$\mathbf{A}\phi = \mathbf{Q} \quad (3-18)$$

Equation (3-18) represents the system of flow equations in terms of algebraic equations. Matrices A (interpolation coefficients) and Q (source matrix) are the known matrices in this equation and matrix  $\phi$  is the matrix of unknowns which its members are the  $\phi$  values at computational nodes. An initial guess will be provided for  $\phi$  matrix (initialization of the solution). Using this initial guess the software starts to solve the flow until reaching a solution for  $\phi$  for the first iteration. The results of first iteration will have a deviation from the values that satisfy the equation (3-18). In each of the next iterations solver tries to decrease the amount of error in previous iteration. This method is the iterative method for solving the matrix equations. In the next section linearizing approaches will be briefly discussed.

### 3.3.4. Linearizing the algebraic equations and solution of system

Different methods exist in order to solve the equation (3-18) for the  $\phi$ . Depending on the linearity or non-linearity of governing equations there are two general categories of methods which are appropriate. *Direct methods* such as *Gauss Elimination* which is mostly suitable for linear system whereas *Iterative methods* which is more suitable for non-linear equations systems. Basically second order discretization methods are accompanied by non-linearity. Using direct methods for these systems (non-linear) will be highly time consuming, expensive and sometimes not necessary. Therefore iterative methods will be used in most of the cases. An initial guess will be given to the equations and after the first iteration the matrix  $\phi^n$  will be obtained. Considering the equation  $A\phi=Q$ , at the iteration number "n" the equation (3-19) can be written:

$$A\phi^n = Q - \delta^n \quad (3-19)$$

In this equation  $\delta^n$  is the value of residual at iteration number n. The objective of the iterations would be driving the  $\delta^n$  (residual) to zero.

### 3.3.5. Pressure based and density based solvers

Pressure based and density based methods are both algorithms of solving the flow and can be used for a wide variety of flows. They both use the finite volume discretization algorithm but they linearize and solve the equations with different algorithms. In some cases the quality of solution is better, convergence is faster and flow features are better captured by using one of them. These methods also differ in the way and sequence that they solve the flow equations. Pressure based solver is originally developed for incompressible flows whereas the density based solver which is designed for high-speed compressible flows. Recently both solvers can be employed to simulate both the incompressible and compressible flows however basically density-based formulation is more advantageous and accurate in modeling the high-speed compressible flows in comparison with pressure based solver [37]. The pressure based solver is more popular for the cyclonic flows and we will employ this solver for our simulations. There are two algorithms for pressure based solver which will be discussed here.

#### Coupled solver vs. segregated solver

Pressure based solver has two algorithms to solve the flow, segregated algorithms and coupled algorithm. Coupled algorithm solver is much faster in convergence but since it solves

the continuity and momentum equations at the same time it need much more computational resource and memory than the segregated solver [38]. In case of cyclonic flows, the segregated solver was effective and accurate.

### **Pressure correction methods**

There are four segregated methods which are in the same family but with slight changes in the way they correct the pressure values including *SIMPLE*, *SIMPLEC*, *PISO*, and *FSM (fractional step method)*. For steady state flows *SIMPLE* or *SIMPLEC* methods are recommended and used in the cyclonic flow simulations. In some cases *SIMPLE* correction method might be advantageous in convergence speed and stability but in some others *SIMPLEC* would be more appropriate [39].

The *SIMPLE* algorithm follows the following steps in order to solve the discretized flow equations.

-An initial guess will be given to the numerical domain solving the momentum equation for u, v and w the components of velocity field consecutively.

-The updated velocity values and mass fluxes will be used to calculate the pressure correction ( $P'$ ) using a formula.

-The pressure correction will be added to the initial value of pressure ( $P^n$ ) using an under relaxation factor ( $\alpha_p$ ) to get the next iteration's pressure ( $P^{n+1}$ ). Momentum equation will be solved again to find the updated velocities and then examining the continuity satisfaction.

$$P^{n+1} = P^n + \alpha_p P' \quad (3- 20)$$

- This process continues until the convergence is achieved and continuity satisfied.

### **Under Relaxation ( $\alpha_p$ )**

Under relaxation factor is a constant which determines the corrected value of the variables ( $P^{n+1}$ ) in each solution iteration. In some cases in order to stabilize the solution residuals it is necessary to set lower under relaxation factors. In this case the smaller change in the initial value of the next iteration would enable the solution stability. The under relaxation factors can be varied and set for each and every flow equations such as pressure and momentum

### 3.4. Turbulence modeling

As it is discussed in previous sections, turbulence models provide some additional equations in order to close the system of flow equations (RANS) by solving for turbulent scalars such as Reynolds stresses and turbulence dissipation rate. It is of high importance to have a preliminary knowledge of the turbulence phenomena and boundary layer in the flow field before proceeding with the simulation. In internal flow simulations inside the tubes, turbulent flow is expected if the Reynolds number exceeds the value of 2,300 [38]. Therefore it would be necessary to find an initial value for the Reynolds number to see whether the flow is turbulent or laminar.

The characteristic dimension for computing Reynolds number in internal flows is hydraulic diameter (HD). In case of pipe and tube flows the HD is identical to pipe or tube diameter.

$$\mathbf{Reynolds\ no} = \frac{\rho \times V \times D_H}{\mu} \quad (3- 21)$$

In case of swirl tubes similar to the other cyclones, the accuracy of results strongly depends on the chosen turbulence model. Due to complexity of rotational flow inside the cyclones, it's been observed that some of the turbulence models are inadequate for the cyclone flow simulations. Different turbulence models along with their modifications exist but not all of them are capable of adequately predict the turbulent flows behavior. Still the lack of a robust turbulence model in order to solve the complex flows can be sensed. According to Cortes and Gil, an appropriate turbulence model is the one that account for curvature of averaged streamlines, high swirl intensity and radial shear and adverse pressure gradients and recirculating zones [3]. In ANSYS-FLUENT commercial CFD code, different turbulence models are provided for the users where choosing the one which is more consistent with an specific application and considering the requirements of each turbulence model is necessary to obtain stable and accurate results. One of the most trusted turbulence models is the standard k-ε. This model and k-ω turbulence model are known as two-equation turbulence models since they solve only two additional equations in order to solve the Reynolds stresses while for 3D flow the Reynolds stress tensor has 6 terms. Therefore these models are shown to be not capable in case of highly swirled flows and flows with boundary layer separation. Since the flow in inertial gas-solid separator is in the category of highly swirled and boundary layer separation in the diverging part of the diffuser is expected due to high angle of divergence, two equation turbulence models led to non-reliable and not

convergent results [15]. A modification for the k- $\epsilon$  model was developed and introduced by Yakhot and Orszag [40] called renormalization-group analysis (RNG k- $\epsilon$ ). This model is modified somehow to better capture the swirled flows features. Comprehensive studies have been done by different researchers such as the one published by Griffiths and Boysan as well as the one by Papageorgakis and Assanis [17, 41]. The focus of Griffiths and Boysan was mostly on the cyclonic flows. They have evaluated fair number of turbulent flows for different cases and have done a comprehensive literature investigation which indicates that for highly swirled flows the *Reynolds Stress Model (RSM)* shows considerable improved performance when compared to other models such as k- $\epsilon$ , RNG k- $\epsilon$  and k- $\omega$ . The RSM model solves the transport equations for all the 6 terms of Reynolds stress tensor along with an equation for turbulence dissipation rate ( $\epsilon$ ). This model results in high precision of the solution but with higher computational cost. However, Reynolds stress model is the mostly employed model in cyclonic flows. In the FLUENT software, the Reynolds stress model is introduced as the most elaborate and complex model which solves 5 additional equations in comparison to two equation models [38]. In conclusion, for the case of swirl-tube filters the most accurate and reliable model would be the one which considers all the terms of Reynolds stresses (RSM). For the current research different turbulence models were tested to verify their performance. The two equation turbulence models (k- $\epsilon$  and k- $\omega$ ) as well as their modifications were observed to be non-reliable and sometimes they led to divergence of the solution. The Reynolds stress turbulence model was found to produce satisfactory results however it is slower in the convergence and is more time consuming.

### **3.4.1. Near Wall Treatment and Grid Considerations**

The main issue in simulating a turbulent flow is the near wall flow since flow variables experience large gradients in the near wall region (boundary layer). Consequently a computational grid should be consistent and capable of solving the flow in this region. Therefore accuracy of the flow solution is highly dependent on the near wall modelling method. It is been proved by variety of experimental works that the near wall region of turbulent flows consists of three consecutive layers starting from the wall called viscous sublayer, buffer layer and fully turbulent region. There are two methods accounting for the near wall region provided by FLUENT. One is the **wall function method** and the other is **near wall modelling** [42]. Wall functions are semi-empirical formulae (containing the scalars conservation and turbulent

quantities) which relate the cells adjacent to the wall to the fully turbulent region without solving for the viscous region of the boundary layer. Among the pioneers of proposing the wall functions one can name the Spalding and Wolfshtein [43, 44]. Since the wall function method replaces the boundary layer with some empirical coefficients, there is no need to have a fine computational grid at the wall vicinity and in some cases having a fine grid near the wall and using the wall functions will result in wrong or inaccurate solution.

In ANSYS FLUENT four types of wall treatments are provided to be used with RSM turbulence model where the users can select the most appropriate one according to their requirements. Standard wall functions, scalable wall functions and non-equilibrium wall functions are the mostly used wall functions for turbulent flows which are also available in FLUENT. Among the wall functions, standard wall function is the default in FLUENT are mentioned to be useful for most cases with high Reynolds number however their reliability for the relatively low Reynolds number flows with curvature and rotation is an issue. The non-equilibrium wall functions method is another alternative for near wall treatment which accounts for pressure gradients inside the boundary layer. In non-equilibrium wall functions, a pressure term is added to the mean velocity formula which enables the model to account for the pressure gradients inside the boundary layer such as those in swirling flows and separated boundary layers. The accuracy of this model in comparison with the standard wall functions was investigated by Jae -Yong Kim et al. The results proposed that the non-equilibrium wall functions are suitable for the cyclonic flow simulations [45, 46]. In addition to the wall functions, near wall modelling option is available in FLUENT software which solves the flow in each and every cell from the wall all along the boundary layer until the fully turbulent region. It is clear that the near wall modelling requires quiet fine computational grid near the wall. This matter results in considerably large number of grids and consequently higher required computational time and resource. Since this method solves for every small turbulence features in the boundary layer, it is also slower in convergence in comparison with wall functions.

Choosing a near wall model depends on the required accuracy and resolution of the boundary layer. If the effects of walls on the wall-bounded flow are considerable, gradients of different variables inside the boundary layer are required to be considered (for example heat transfer phenomenon) or the separation phenomenon to a large extent is predicted in the boundary layer

region, having a fine mesh and using a near wall model would be required otherwise the computational expense of the near wall modelling is not justifiable. In the current research, it was observed that using both these models results in a unique solution which shows the capability of the wall functions in predicting and resolving the boundary layer. Figure 11 is a graphical demonstration of the two near wall modelling methods. On the left hand side a coarse near wall cell can be seen where the distance of first computational node from the wall is much higher than the right hand side model. The value of this first node will be calculated directly from the wall functions whereas in the case of near wall modelling the flow inside the boundary layer is solved with more than twenty computational nodes. It is clear that the distance of first computational node from the wall is highly important in CFD simulations. A non-dimensional distance “ $y^+$ ” (also function of fluid velocity) is used to compare the resolution of different computational grids and judge their sufficiency according to different turbulence model requirements.

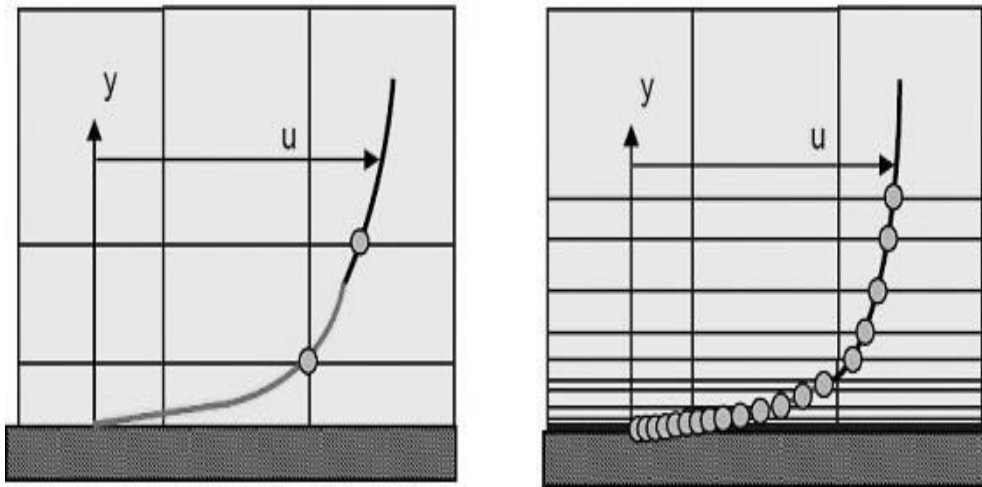


**Figure 11- Comparison between boundary layer mesh required for wall function method vs. enhanced wall treatment**

### 3.4.2. Wall Yplus ( $y^+$ )

As it was mentioned in the previous section, wall Yplus is an important non-dimensional parameter which depends on the distance of first computational node from the wall as well as the flow Reynolds number [47]. It is necessary to check the value of the  $y^+$  on all wall boundaries before proceeding with post-processing of the results. The requirement of each turbulence model and near wall modelling for  $y^+$  should be respected and checked after the solution convergence.

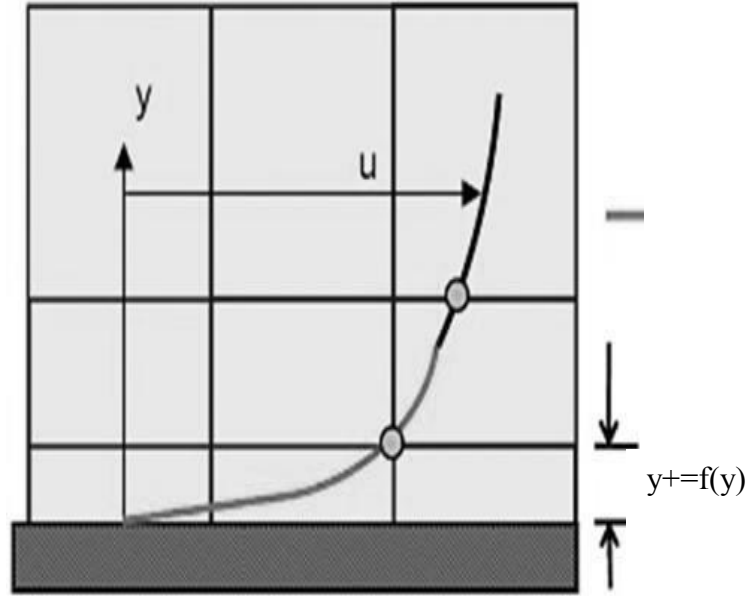


Figure 12- Schematic of definition of wall Yplus

$$y^+ = \frac{\rho u_t y}{\mu} \quad (3-22)$$

In the above equation  $u_t$  is the friction velocity related to the wall shear coefficient and flow density

$$u_t = \sqrt{\frac{\tau_w}{\rho}} \quad (3-23)$$

It is clear from the definition of  $y^+$  for an incompressible flow that  $y^+$  is a function of distance and velocity (Reynolds number). As the first computational grid gets far from the wall, or the flow velocity increases, the value of  $y^+$  becomes larger. In the ANSYS-FLUENT software the suggested minimum value of  $y^+$  for the wall functions method is around 11.225 ( $y^+ \geq 11.225$ ) depending on the chosen wall functions. This means a quite large first layer thickness is required to solve the flow. It is also recommended to prevent  $y^+$  below the limits because it results in deteriorative and inaccurate results. For enhanced wall treatment  $y^+ \sim 1$  is recommended since a highly fine mesh is required in vicinity of the wall.

## **3.5. Boundary Conditions (BC)**

Flow equations derived in this chapter are applicable for different types of flow but boundary conditions as well as initial values limit them to a specific flow field such as flow inside a cyclone or swirl tube. Boundary conditions are actually the values that solver tries to reach them at the end of the solution iterations. A brief discussion of possible boundary conditions with more focus on the cyclones is brought in the following material.

### **3.5.1. Mass Flow Inlet**

The required mass flow rate at the inlet will be imposed normal to the boundary. This mass flow rate input results in a velocity distribution at the inlet boundary. It is also necessary to define the turbulence intensity and hydraulic diameter of the flow at the inlet.

### **3.5.2. Wall Boundaries**

This boundary condition imposes “no slip” condition which implies that the fluid particle is either stationary immediately at the wall or moving with the same velocity as the moving wall which for a stationary wall would be zero.

### **3.5.3. Outflow**

Outflow boundary condition is a suitable consideration where the flow information (such as pressure) at the outlet is not available. Therefore this boundary condition does not require the values of pressure, velocity and other flow quantities at the outlet. Extrapolation will be used to achieve the required values at the outlet zone from the inside cells. One of the features of this boundary condition is that it is possible to divide the mass flow between the outlets. In cases where the flow domain has more than one outlet, the mass flow can be divided in desired portions between them and this is possible by specifying a weighting ratio for mass flow rate.

There are some limitations associated with this boundary condition which is listed below.

- Outflow is not applicable for compressible flows.
- Using the outflow with velocity inlet boundary condition, pressure inlet or outlet boundaries in the same flow domain is not possible.
- Outflow is not applicable for multiphase flow solvers.

One of the assumptions of this boundary condition is zero diffusive flux at the outlet. If there is an area change in the flow pattern or strong flow instability is expected near the outlet boundary, using the outflow boundary condition is not recommended due to presence of large gradients normal to the outlet surface. In such cases, it is proposed to move the outlet surface downstream by using an extension duct which is also considered in current research.

### **3.6. Finalized Proposed CFD Setup**

Following the discussion in this chapter about different solution algorithms, turbulence models and computational grid criterions, we will now finalize a CFD setup for the subject of the current project which is a swirl tube cyclone. Varieties of suggested algorithms and models have been tested in this research and it is observed some of them result in inaccurate or weak solutions. Some of them also would not change the accuracy and quality of the convergence as it was reported in the literature. The following paragraphs contain the detail of the finalized model which observed to have enough accuracy and require acceptable computational resources and time.

#### **3.6.1. Computational Grid (Mesh)**

As it is discussed in this chapter, generating a computational grid which satisfies the requirements of the turbulence model and obtains the required resolution is targeted. In addition, due to presence of static guide vanes in the structure of swirl tubes, their geometry is complex in comparison to the other cyclone categories. The number of cells in the flow domain is another parameter which should match the available computational resources. There are only few researches on the swirl tubes and especially the straight-through category but for the complex geometries it is recommended to use unstructured mesh since generating a structured mesh (HEXA) for complex geometries would not increase the accuracy such that to compensate the required computational resources and time.

ANSYS ICEM CFD is used to generate the unstructured computational grid. This commercial code is already evaluated and used by the researchers for the application of cyclones simulations but as it was mentioned not for the application of swirl tubes [48-50]. Figure 13 shows the generated computational grid on the static vanes and Figure 14 shows the overall computational domain including the body and the diffuser as well as the generated boundary layer mesh.

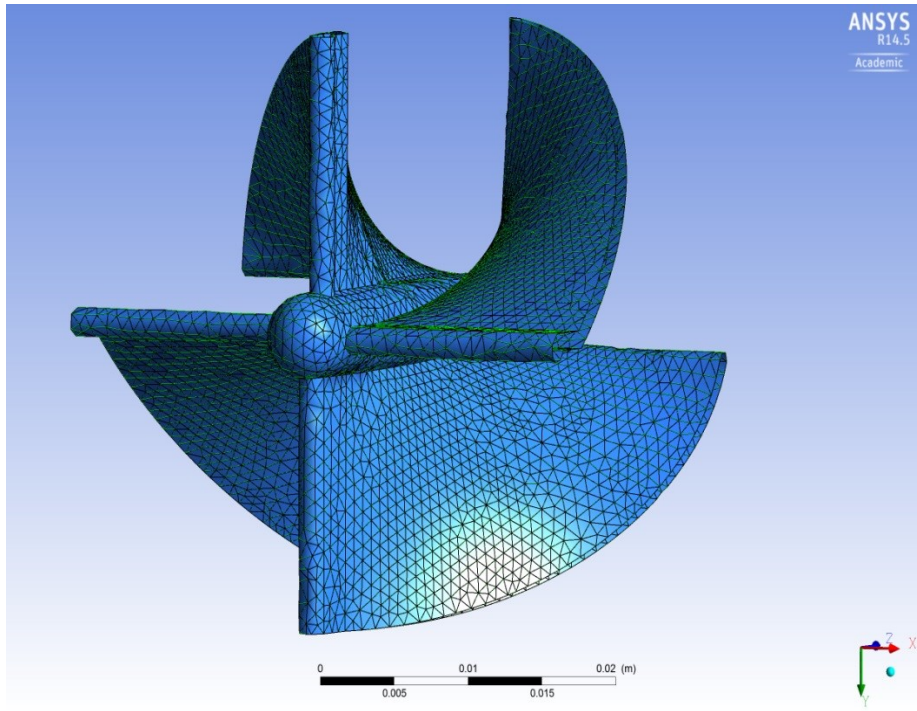


**Figure 13- Surface mesh on the static vanes**

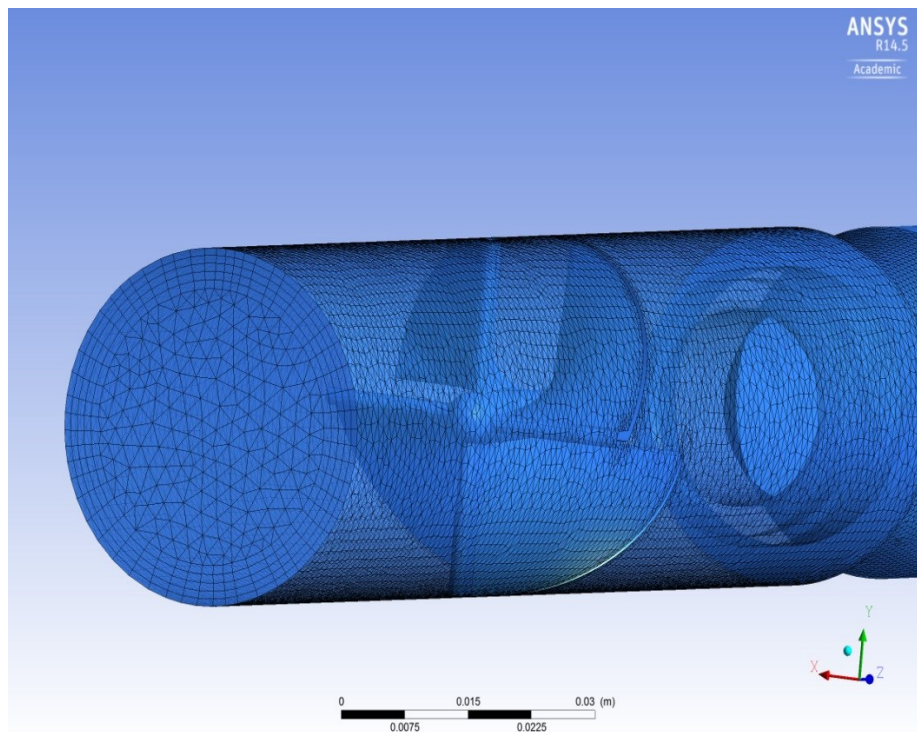


**Figure 14-Overall view of the mesh, 672,000 cells**

As one can see in the Figure 14, the boundary layer in the simulations is captured using the prism layers near to the wall. The thickness of the first layer is of high importance in order to capture the turbulent features inside the boundary layer. The resolution of the first layer is therefore adjusted in order to satisfy the requirements of Reynolds stress turbulence model as well as the non-equilibrium wall functions ( $y^+ > 11.225$ ). Different first layer resolutions have been tested and simulated until the point the confidence on the results has been achieved. After importing the generated mesh in the FLUENT software the first step in setting up the simulations is to scale the mesh which is generated in the ICEM. The dimensions and directions of the model have to be checked and set to the desired ones (millimeters or inches).

### 3.6.2. Solver settings

Table 2 summarizes the chosen solver settings. Numerous simulations were performed and tested. After evaluating the results, the following solver settings were used for the application of straight-through swirl tube (inertial gas-solid separator)

**Table 2- Solver settings used to simulate the flow inside the inertial gas-solid separator**

<b>Solver</b>	Pressure Based
<b>Time dependency</b>	Steady State
<b>Turbulence model</b>	Reynolds Stress (RSTM)
<b>Near-Wall Treatment</b>	Non-Equilibrium Wall Function
<b>Boundary Conditions</b>	Inlet: Mass Flow Inlet Outlets : Outflow Geometry surfaces : Wall (no slip)
<b>Pressure-Velocity Coupling</b>	Segregated- SIMPLE
<b>Spatial Discretization</b>	Gradients : Least Squares Cell Based Pressure: Standard Momentum : Second order Turbulent kinetic energy: Second order Turbulent dissipation rate: Second order

### 3.6.3. Discussion on the numerical model and settings

Various models and algorithms have been tried and evaluated for the application of cyclonic flows but there are very few works which can be related to the straight-through swirl tubes and inertial gas-solid separator. It was necessary to validate the compatibility of the suggested methods for the inertial gas-solid separator flow. Use of SIMPLEC pressure velocity coupling instead of SIMPLE method was suggested by few researchers in order to obtain faster convergence but the improvement was not observed in case of current swirl tube. Therefore the SIMPLE method which is the default method was chosen for the flow simulations [51, 52].

The steady state solution was observed to give satisfactory results and the time dependent analysis did not show important differences. The results of this analysis will be presented in the next chapter showing the acceptable consistency between the solution obtained by the steady-state and the ones from time dependent solution after a certain flow time.

Reynolds stress turbulence model is the most sophisticated and largely used model in the literature for the application of cyclonic flows [38]. In the present project the accuracy of this model was verified by comparing the experimental and CFD results as well as comparison with other turbulence models. Choosing other turbulence models led to divergence of the solution or weak convergence. One of the proposed turbulence models in the previous works was k- $\epsilon$  RNG model which was introduced as a capable model for rotating and complex flows but for the case of inertial gas-solid separator the result was not satisfactory. The use of k- $\epsilon$  RNG resulted in large non-realistic vortices and separations in the diverging part of the diffuser which considerably affects the accuracy of the pressure loss measurements. Non-realistic vortices were also observed in case of using the standard wall functions (SWF) for the near wall modelling. Figure 15 shows the contours of velocity magnitude obtained at symmetry cut-plane of the inertial gas-solid separator. The inlet is located on the left hand side and the static vanes can be seen downstream of the inlet. The large separation region is visible in the diverging part of the

diffuser. Consequent of this non-realistic vortex is up to 30% error in the obtained values for inlet to outlet pressure loss.

Due to complexity of the flow inside the inertial gas-solid separator, second order discretization approaches were used to solve for the flow equations of motion. However it was observed that the solution should be started by first order discretization in order to acquire better solution convergence. Starting the solution directly from the second order discretization resulted in either divergence or poor convergence of the final solutions. Table 3 shows values achieved by using first order and second order approaches proving that in order to achieve sufficient resolution of the solution second order discretization has to be employed. This table also contains inlet to outlet total pressure drop for the inertial gas-solid separator at the volume flow rate of 20 cfm.

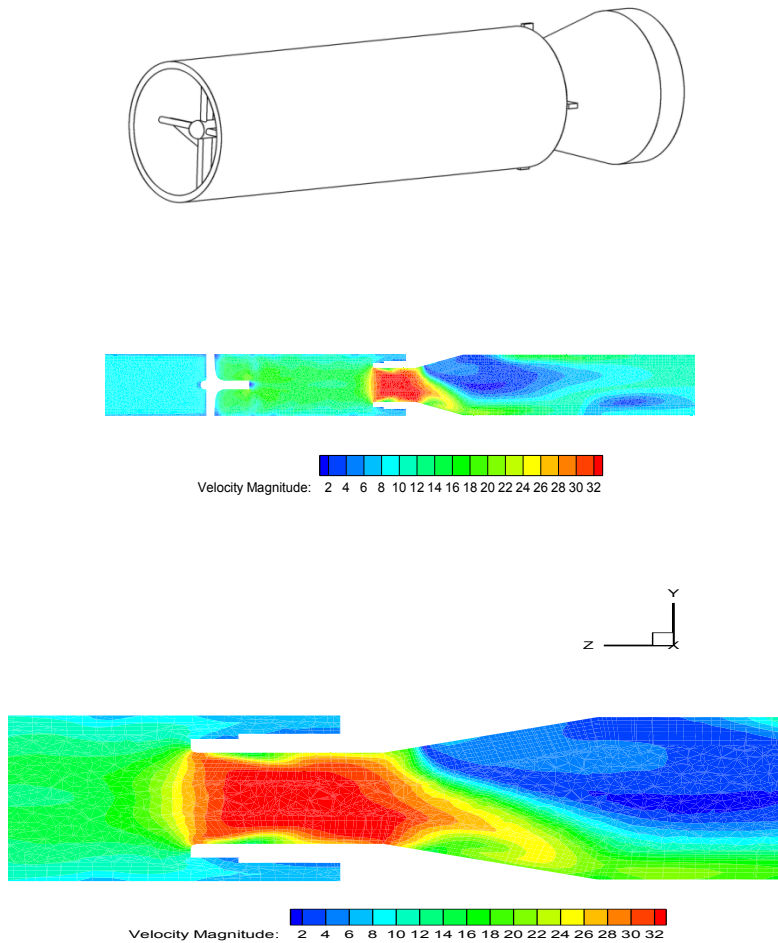


**Figure 15- Contours of velocity magnitude at  $x=0$  plane obtained from standard WF method illustrating a large separation zone**

**Table 3- Comparison of the results of FIRST order and SECOND order solutions at 20cfm**

---

Discretization Approach	Total Pressure (Pa)	Error (%)
Experimental data	231.73	-
First Order Upwinding	304.11	+31.2
Second Order Upwinding	220.77	-4.7

---

Following the above discussions, in the next chapters the analysis of the original design of the inertial gas-solid separator will be presented.

## Chapter 4

In this chapter the validation analysis of the inertial gas-solid separator nominal model is presented. Geometry of the nominal model, grid independency analysis and final CFD results are presented. The results of CFD simulations are achieved by imposing the models and algorithms discussed in the previous chapters and then compared with the available experimental data. The geometry parameters which are more influential on the inertial gas-solid separator performance have been identified and the effect of their change on the flow pressure loss was evaluated. At the end, the best configuration to achieve the minimum pressure loss will be introduced.

Figure 16 and 17 show overall geometry of the inertial gas-solid separator as well as a focused picture showing the configuration of vanes, clean air flow path and the dust particle's path.

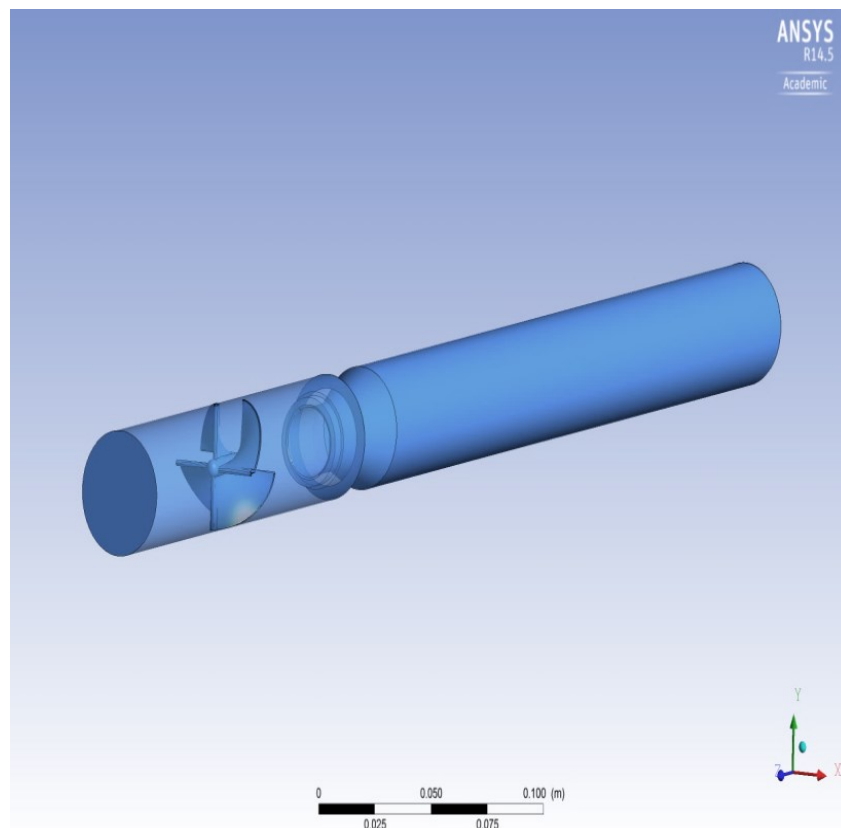


**Figure 16- Schematic of CFD domain of the Mnoclone**

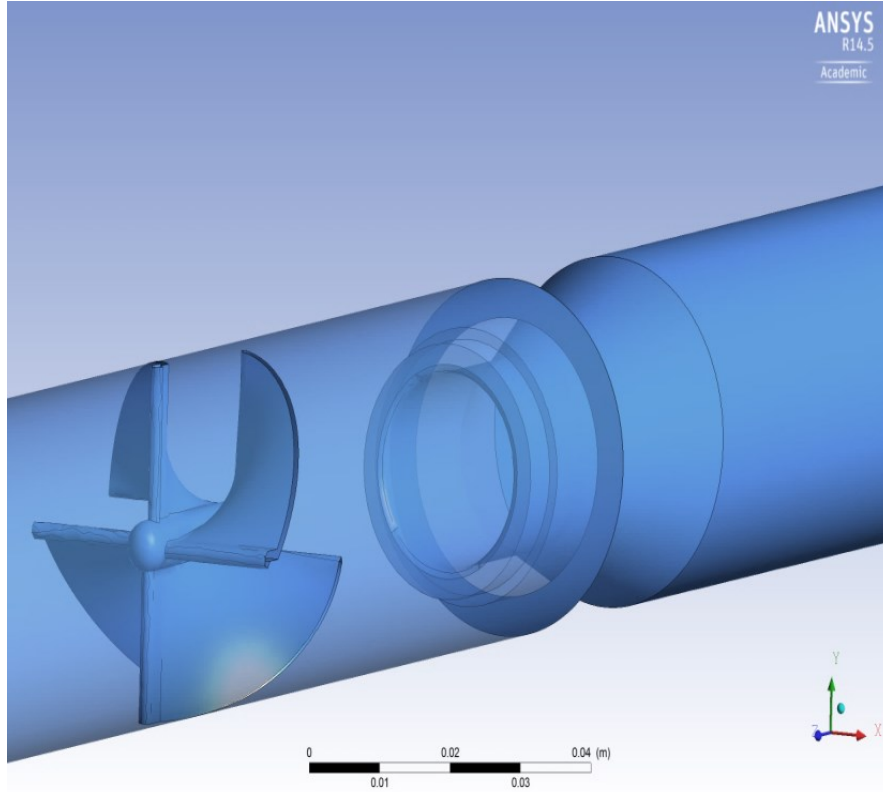


**Figure 17- Schematic of inertial gas-solid separator static vanes and outlets configuration**

## **4.1. Geometry and model dimensions**

The geometry parameters of inertial gas-solid separator were measured and the detailed CAD model is created using CATIA V5R20<sup>®</sup> software. Generative shape design module in CATIA is highly capable of creating curvy and complex parts of the inertial gas-solid separator structure such as vanes. Also modifying the geometry using this software is more convenient and less time consuming therefore it was employed for parametric studies and optimization analysis.

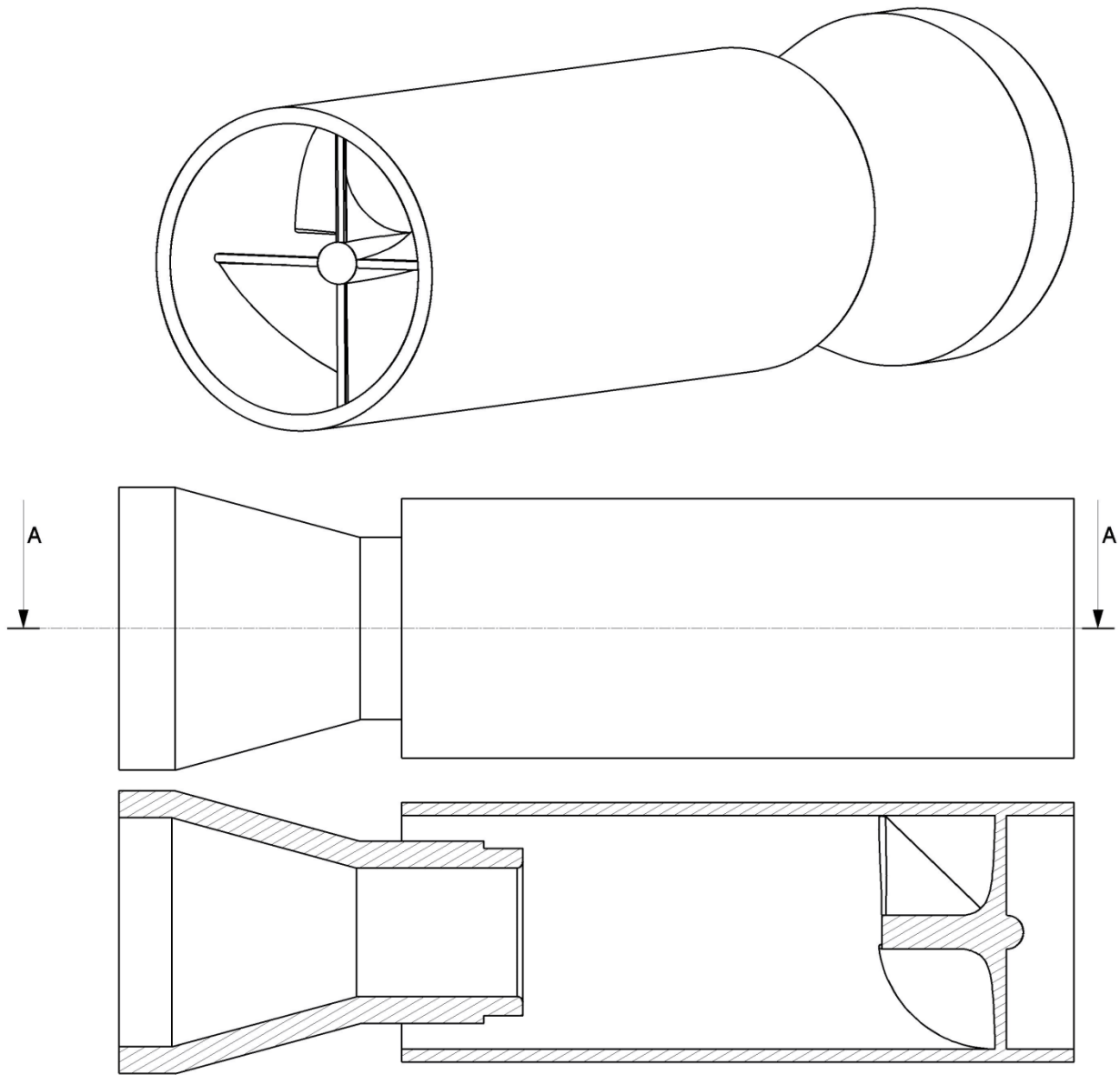


**Figure 18- 2D drawing of the original configuration of inertial gas-solid separator**

#### **4.1.1. Extension tubes**

In order to meet the requirements of the outflow boundary condition and also to match the experimental conditions, two extension tubes are added to the inlet and outlet of the model.

These two additional tubes also exist in the experimental setup of the inertial gas-solid separator in order to impose the suction and get the required flow rate portions. The measurement of pressure in the experiment is performed at one point located 6 inches downstream of the diffuser outlet.

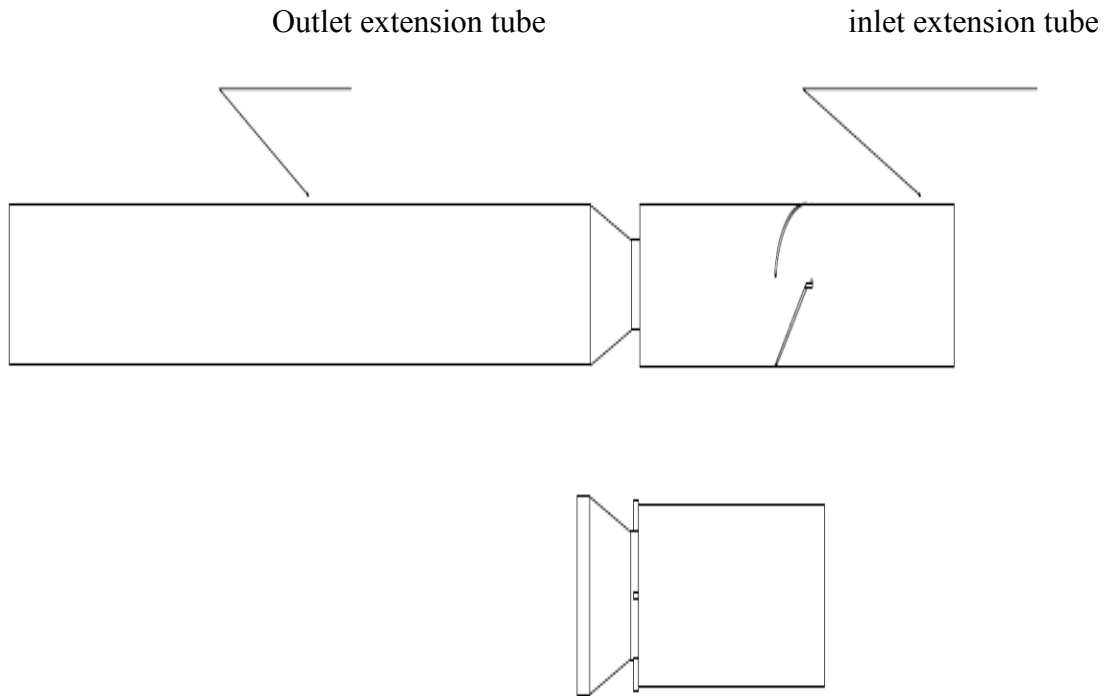


**Figure 19- Configuration of extension tubes**

Table 4 and Figure 19 show the dimensions of added extension tubes as well as the configuration of their installation on the inertial gas-solid separator.

**Table 4- Extension tubes lengths (L=overall length of the original model)**

<b>Extension Tube</b>	<b>Length</b>
Inlet	0.6 L
Outlet	2.0 L

## **4.2. CFD analysis of inertial gas-solid separator**

The following paragraphs will present the CFD analysis of the nominal model of the inertial gas-solid separator

### **4.2.1. Available experimental data and considerations**

Here the CFD results will be compared by the low restriction model data. Figure 20 shows the experimental data which is used in order to validate the numerical model. This experimental chart is obtained at 10% bleed (10% of inlet flow is extracted from dust outlet using a suction pump). The experiments for the pressure loss are performed with pure air without dust particles. The value of the outlet pressure is measured in a distance of 6 inches downstream of the diffuser outlet. The range of tested flow rates lies between 20 and 40 cfm where the values of pressure loss at three flow rates (20, 30 and 40 cfm) are obtained and using the log scaling the experimental graph is achieved.

In order to minimize the errors and to get the closest results to the experimental data, the values of the static and total pressure are measured at the same distance (6 inches) downstream of the diffuser outlet. Also since the exact location of measurement devices was not available, the mass weighted average of the results is obtained at a surface located at 6 inches downstream of the diffuser outlet.

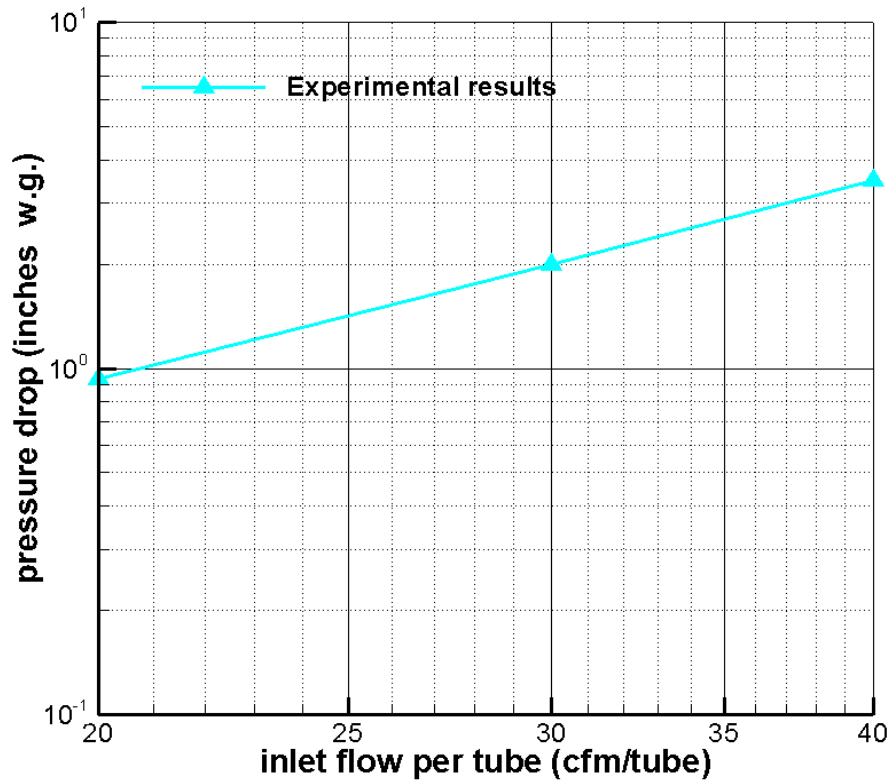
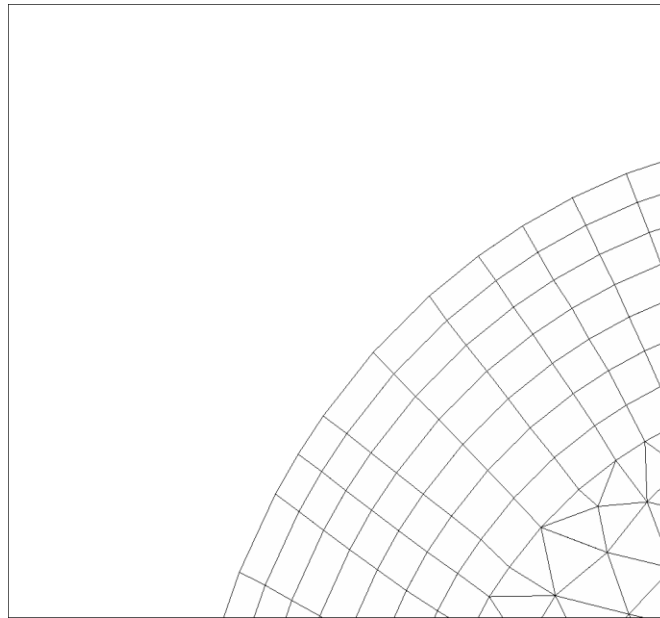


Figure 20- Experimental data of inlet to Outlet total pressure drop at 10% bleed [54]

#### 4.2.2. Boundary layer resolution & time independency

In order to verify that the flow inside the inertial gas-solid separator is accurately resolved and all of the turbulent phenomena such as vortices and separations are precisely captured, the flow was solved with different boundary layer resolutions. As it was discussed in the previous chapters the first layer of the computational grid (adjacent to the wall) has to meet the requirements of the employed turbulence model as well as near wall model. This matter is examined by using a non-dimensional value called wall  $y^+$ . The near wall flow can be resolved with each and every cell from the wall adjacent cell all along the boundary layer which requires much more number of computational grids near the wall. In this case the value of the wall  $Y_{plus}$  has to be less than one ( $y^+ < 1$ ) and the flow will be resolved using enhanced wall treatment. The other approach is the wall function approach which requires the  $y^+$  to be more than 11.225 ( $y^+ > 11.225$ ). In case of inertial gas-solid separator the non-equilibrium wall functions found to

be more reliable and accurate in comparison with other wall functions and consequently were chosen for the coarse boundary layer mesh simulations. These two cases (wall function and enhance wall treatment) are examined in order to verify the sufficiency of boundary layer mesh resolution and to achieve confidence on the results. At the same time the sufficiency of the steady state solutions for both cases have been examined. For this purposes both cases have been solved initially with steady-state solver at 20 cfm flow rate. After reaching the convergence (for steady state), the solver was changed to time-dependent. Both cases were solved for a total flow time of 0.2s which required 2,000 time steps. The convergence of both cases was monitored until the scaled residuals reached to order of  $10e-7$ . The transient data has been evaluated and time variation of pressure values at a specified probe was obtained. It was observed that the steady-state solution was good enough to solve the flow inside the inertial gas-solid separator. On the other hand, the results of two different boundary layer mesh resolutions were found to be consistent with acceptable deviation. Figure 21 and 22 show the boundary layer mesh resolution for both cases and table 6-8 show the simulation details such as distance of first node from the wall, number of cells and time-dependent solver settings for each case.



**Figure 21- Boundary layer mesh compatible with wall functions ( $y^+ > 11.225$ )**

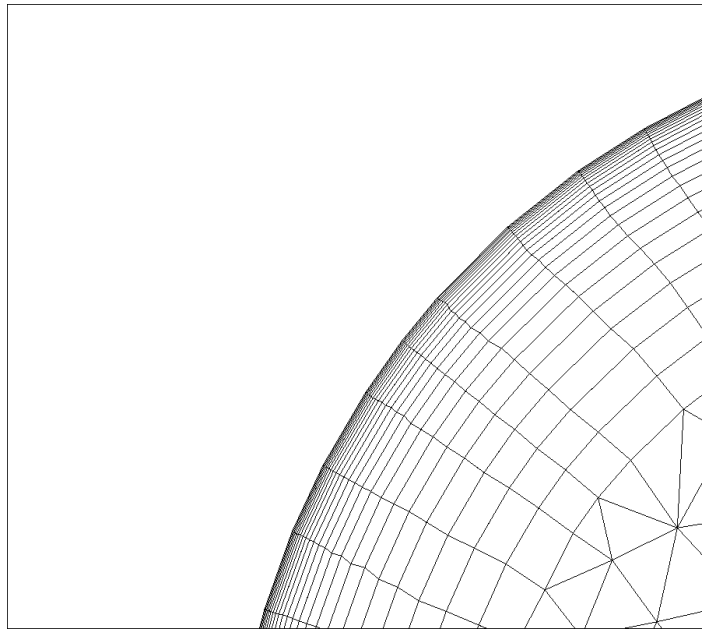


**Figure 22- Boundary layer compatible with enhanced wall treatment ( $y^+ < 1$ )**

**Table 5- Thickness of first grid layer , EWT vs. WF**

<b>Case</b>	<b>thickness (mm)</b>
Fine mesh (EWT)	0.01
Coarse mesh (Non-Eq WF)	0.37

**Table 6- Total number of grids, EWT vs. WF**

<b>Case</b>	<b>Number of grids</b>
Fine mesh (EWT)	1,935,843
Coarse mesh (Non-Eq WF)	672,093

**Table 7- Initial setting of solver, steady state and time-dependant calculations**

---

Flow Rate	20 cfm
No. of steady-state iterations	5000
Time Step size for transient solver	0.0001s
Number of time steps	2,000
Number of iterations per time step	15
Flow Time	0.2s

---

Figure 23 shows the variation of static pressure vs. the solution time until the flow time reached 0.2 seconds (The values are brought in Pa in order to make the variations more visible). Tables 9 and 10 contain the results of the both transient and steady-steady state solutions for both the enhanced wall treatment and wall function models. In order to prevent any inaccuracy caused by placement of the probe inside instability and also to match the experimental setup, the values of static pressure are extracted from a point located 6 inches downstream of the inertial gas-solid separator outlet.

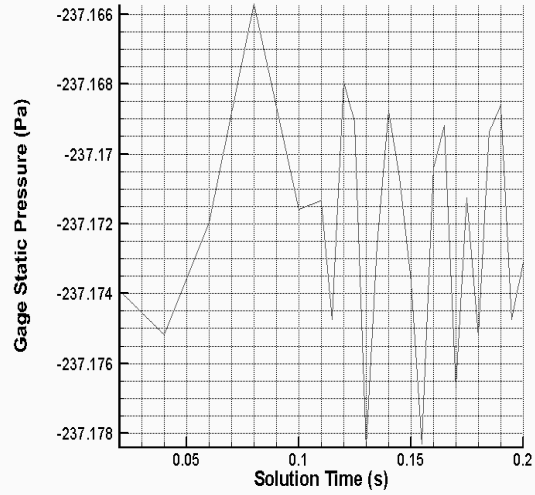
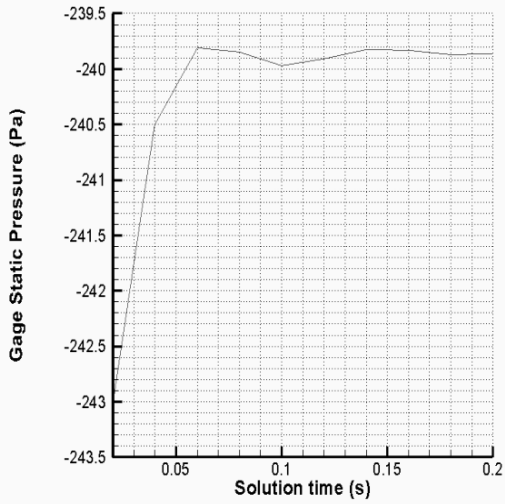


**Figure 23- Static pressure value vs. time- right: enhanced wall treatment left: wall function**

**Table 8- Comparison between static pressures obtained from steady-state calculations, EWT vs. WF**

Parameter	Gage Static Pressure (Pa)
Enhanced Wall treatment ( $y^+ < 1$ )	-251.51
Wall function non-equilibrium ( $y^+ > 15$ )	-237.16

**Table 9- Comparison between static pressures obtained from time-dependent calculations at 0.2 seconds, EWT vs. WF**

Parameter	Gage Static Pressure (Pa)
Enhanced Wall treatment ( $y^+ < 1$ )	-240.01
Wall function non-equilibrium ( $y^+ > 15$ )	-237.13

It was observed that the enhanced wall treatment model gives approximately no variation for the static pressure after certain time steps while the wall function model gives a periodic variation. However the values achieved by both models are in good agreement with each other. The results show that the non-equilibrium wall functions (with steady state solver) are sufficient to solve the flow field inside the inertial gas-solid separator and they are also as accurate as enhanced wall treatment. In conclusion, in order to prevent excessive computational time the model for the inertial gas-solid separator is built using a coarse grid and wall function method.

### 4.3. Inertial gas-solid separator finalized model validation

#### 4.3.1. Solution initialization and convergence procedure

The model for the original configuration of inertial gas-solid separator is solved using FLUENT commercial software with the finalized settings which were discussed earlier. The result of CFD analysis compared with the available experimental data. Mesh independency analysis was performed in order to verify that the results are independent of mesh resolution in the core region.

The working fluid of the inertial gas-solid separator is considered as incompressible air as for the most of cyclone analysis. Since the flow Mach number is well below the value of 0.3 the incompressibility assumption would be reasonable. Flow inside the inertial gas-solid separator does not experience heat transfer and temperature change therefore the assumption of isothermal flow is also reasonable. Hence, the air viscosity will be considered constant. Table no.9 shows the working fluid properties.

**Table 10- Properties of working fluid**

<b>Working fluid</b>	<b>Density (kg/m<sup>3</sup>)</b>	<b>Viscosity(kg/m-s)</b>
Air	1.225	1.7894e-05

The finalized computational grid used to solve the flow inside the original configuration of the inertial gas-solid separator consists of 672,709 computational cells and 231,296 nodes. Mesh independency analysis will prove the sufficiency of this mesh resolution.

The values of total pressure are measured at a distance of 1.8 inches upstream of the inlet for inlet total pressure and 6 inches downstream of the diffuser outlet for outlet total pressure. The total pressure loss in the inertial gas-solid separator is then computed subtracting the inlet value from the outlet. All the measured values are gage values (the reference pressure is 406.64 inches of water (atmospheric pressure)). The results of pressure loss were measured for 3 different flow rates consecutively from 20cfm (cubic feet per minute) to 40 cfm with intervals of 10 cfm. The solutions were initialized (until a convergence of  $10e-07$ ) with using the "hybrid initialization" in FLUENT. It is recommended to start the simulation by first order discretization approaches (particularly for the complex flows) in order to get better convergence and in some cases to prevent the divergence [38]. Therefore each case has been solved with first order approach for the first 750 iterations. The solution then continued with second order discretization approach. The second order solver then solved the flow for minimum of 3000 iterations and the residuals of solution were monitored until the convergence occurred. In addition to the solution residuals the contours of flow variables such as static pressure were checked and compared with the predictions and the experimental data. The computational time required for each case lies between 1 or 2 hours with an 8 cores processor.

Figure 24 shows a sample of accepted scaled residuals of the solution at 20 cfm for the inertial gas-solid separator's original model. The visible discontinuity in the residuals happens when the solution approach changes from the first to second order after 750 iterations. As it can be seen in the Figure 24, the final values of the scaled residuals are achieved at 2,000 iterations and they were stable for the next 1,750 iterations.

Table 11 contains the values of the  $y^+$  obtained by area averaging over the wall boundaries of the domain. They meet the minimum value criterion for the wall functions which is  $y^+=11.225$

**Table 11- Wall  $y^+$  values of the original model at 20cfm**

<b>body</b>	<b>Blades</b>	<b>Diffuser</b>	<b>Outlet duct</b>
17.17	32.03	31.10	16.73

### 4.3.2. Contours of flow properties

After the solution has reached to an acceptable and stable level of convergence, the contours of static pressure and velocity components have been evaluated. These contours are obtained from the original configuration of the inertial gas-solid separator operating at flow rate of 20 CFM. The contours are plotted on the symmetry cut-plane of the inertial gas-solid separator ( $x=0$ )

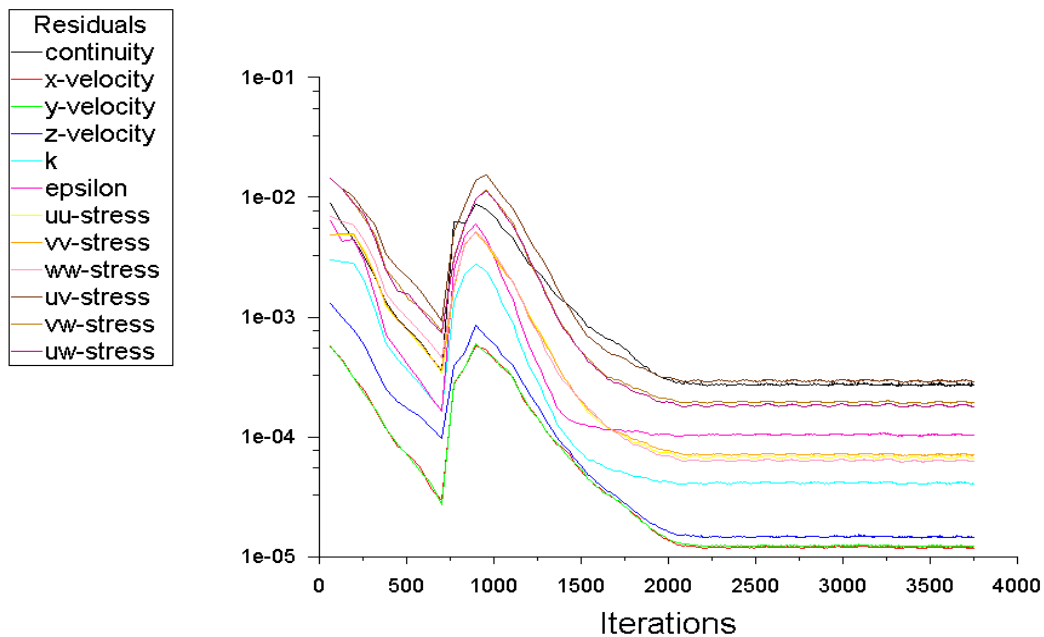
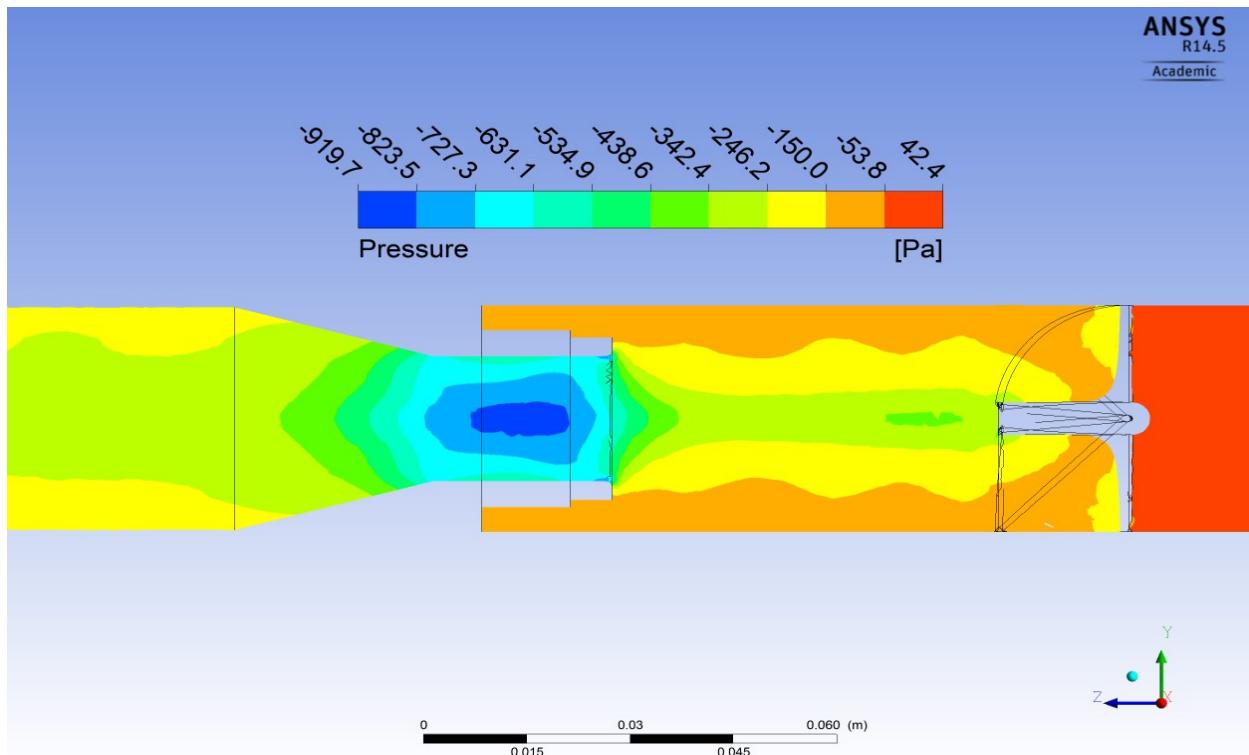


Figure 24- Scaled residuals for steady state solution of original model at 20cfm

Figure 25 illustrates the contours of static pressure. The wire-frames of static vanes and other parts of inertial gas-solid separator are also shown in order to illustrate the working procedure. The direction of flow is from left to right of the figure and the low pressure contours are located in the diffuser part right before the diverging path. Ahead the vanes, the gage static pressure is approximately zero as it is expected. Downstream the static vanes variation of static pressure in different directions can be observed. The pressure field inside the inertial gas-solid separator shows consistency with similar cyclonic flows [53]. The static pressure has its maximum value in vicinity of wall and it decreases by moving towards the core region.



**Figure 25- Contours of static pressure for original model at symmetry cut-plane (x=0), 20 cfm flow rate**

The red colored contours demonstrate the high- pressure and low-velocity regions. The green and yellow contours show moderate levels of pressure and velocity and the blue contours demonstrate the minimum pressure levels in the flow field which implies the maximum velocity regions. The reduction of area at the inlet of diffuser is the reason for such increase in the velocity which is one of the major contributors of the total pressure loss generation in the inertial gas-solid separator. The matter is clearer in the contours of total pressure shown in Figure 26. The considerable lower levels of total pressure can be seen in the diffuser part implying the contribution of this region in generation of total pressure loss in the flow field. After the diffuser, flow starts to decelerate and the pressure levels increase accordingly until the duct becomes straight.

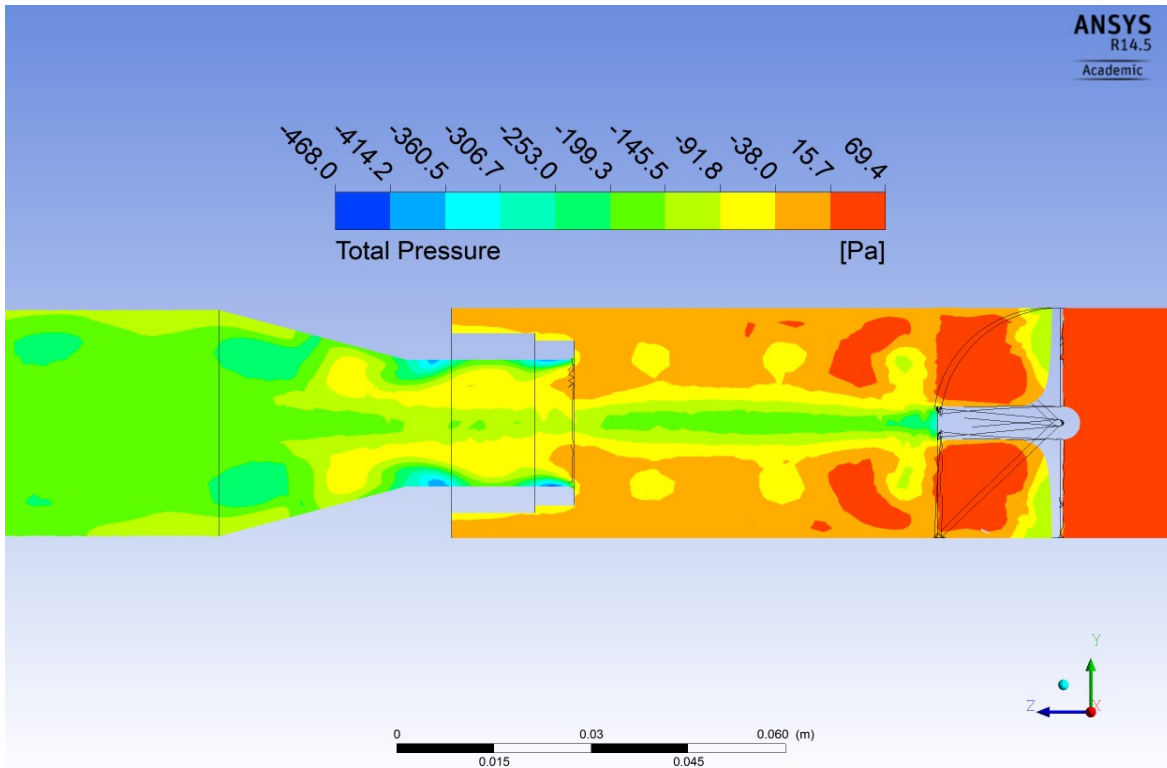


Figure 26-Contours of total pressure for original model at symmetry cut plane ( $x=0$ ), 20 cfm flow rate

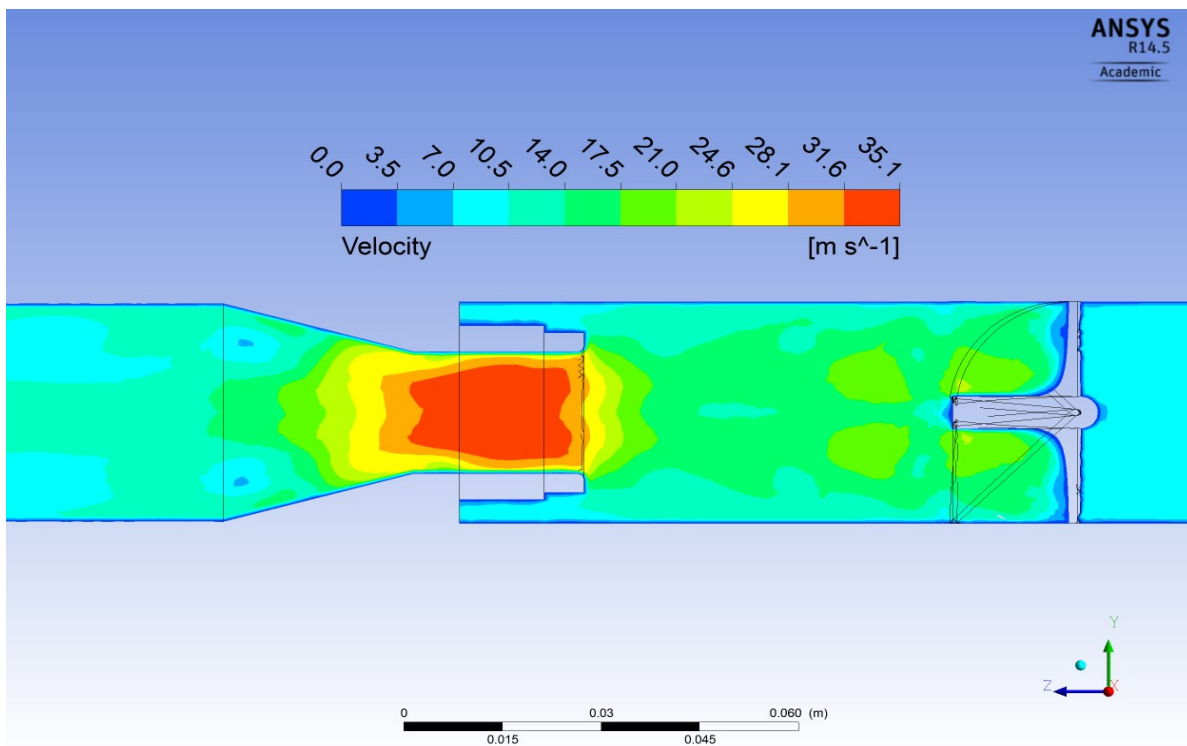
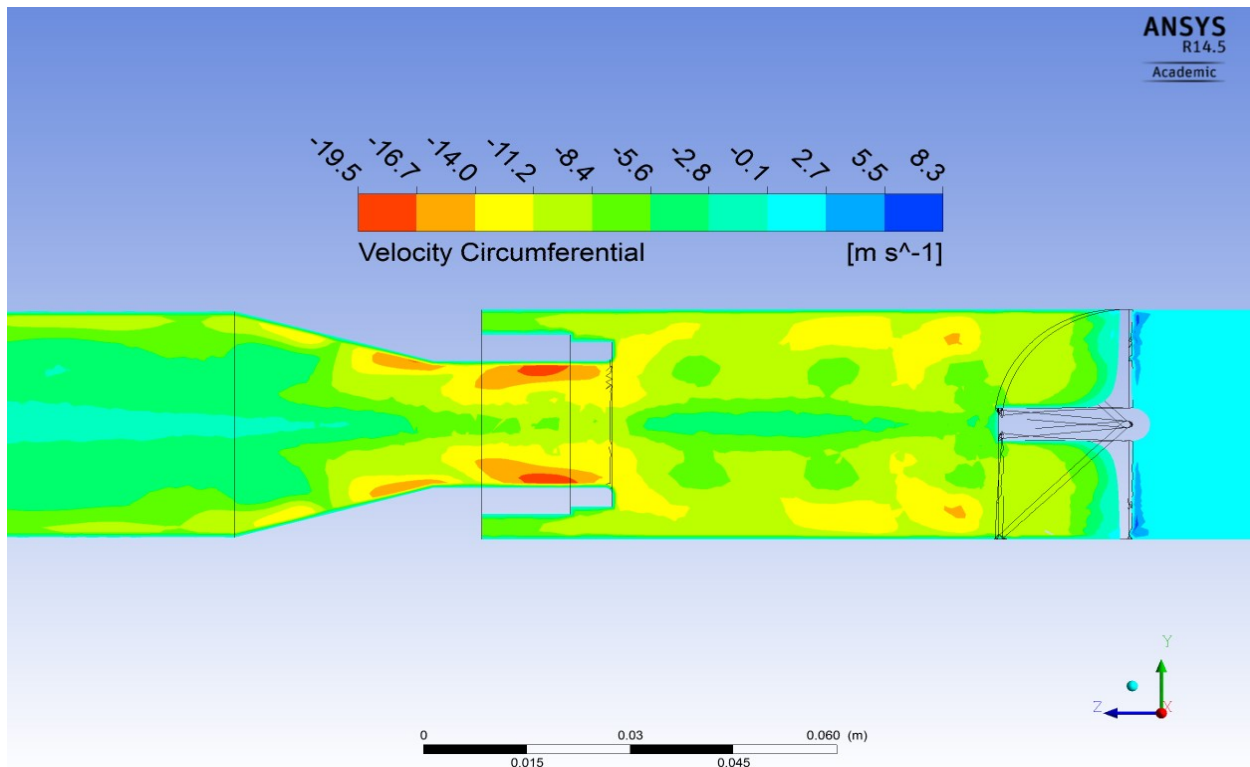


Figure 27-Contours of velocity magnitude for original model at symmetry cut-plane ( $x=0$ ) at 20 cfm flow rate

Figure 27 shows the contours of velocity magnitude. It can be seen that maximum velocity levels up to 35 m/s occur in the diffuser which is considerably fast relative to the rest of flow field. In the diverging part of the diffuser separation regions (small blue colored regions) can be observed close to the upper and lower walls. The reason for these separations is that the fast moving rotational flow experiences a highly divergent pattern (15.2° divergence angle) and cannot stay attached to the walls. These separations and the associated vortices and non-stabilities can also result in total pressure loss production in the flow domain.



**Figure 28-Contours of tangential velocity for original model at symmetry cut-plane ( $x=0$ ) at 20cfm flow rate**

Contours of tangential velocity (circumferential velocity) in Figure 28 show consistency with similar cyclonic flows where the maximum rotation strength can be seen near the walls and then decreases towards the core region. This velocity component is of main interest in deriving mathematical models for flow inside the cyclones especially for collection efficiency. Since the centrifugal force is directly related to tangential velocity, it can be inferred that higher tangential velocities in the flow field will result in higher collection efficiency. Upstream of the static vanes there is no tangential velocity since the flow is perfectly axial. By passing over the static vanes,

tangential velocity is produced in the flow field. By entering the diffuser we can see the maximum values of tangential velocity in the flow field. The radial variation of tangential velocity is verified to be consistent with similar cyclonic flows and expectations. Tangential velocity component starts to vanish after passing the diffuser but rotation of the flow lasts until the outlets.

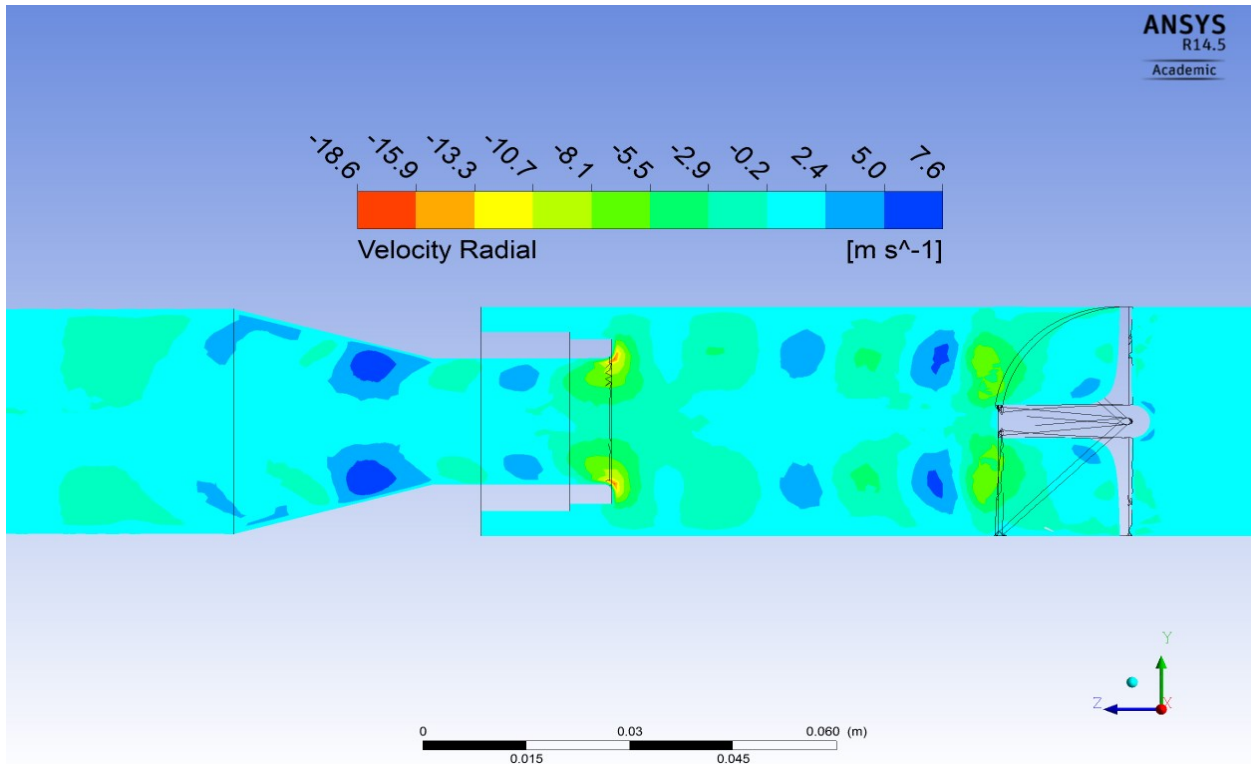


**Figure 29- Contours of radial velocity for original model at symmetry cut-plane ( $x=0$ ) at 20 cfm**

Figure 29 shows the radial velocity distribution in the inertial gas-solid separator. After the static vanes the tendency of flow to move towards the walls can be observed in these contours. The results of numerical simulations are presented in table 12 and followed by a chart (Figure 30) showing the accuracy of the numerical model in predicting the pressure loss in inertial gas-solid separator.

Table 12- Comparison between numerical vs. exp results of total pressure loss for original model  
(units: inches w.g.)

Flow Rate (CFM)	Experiment	Numerical	Error (%)
20	0.93	0.929	-0.1
30	2	2.005	+0.5
40	3.5	3.521	+0.6

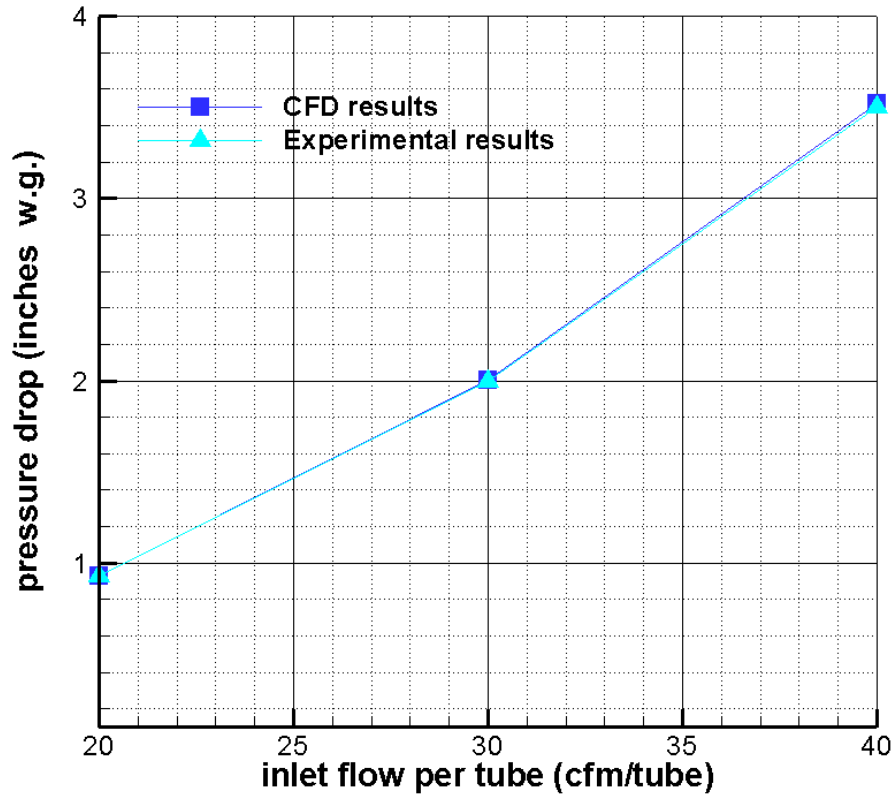


Figure 30- Comparison between numerical and experimental results of total pressure loss, original model

### 4.3.3. Core mesh refinement and mesh independency analysis

In addition to boundary layer mesh refinement, a core mesh refinement has been carried out for the same boundary layer mesh resolution in order to verify the mesh independency of the simulations. A coarse mesh case with 550,000 cells and a fine mesh with 915,000 cells have

been generated for the same geometry. The refinement was done in flow core region only and all along the flows domain. The simulation has been performed at mass flow rates between 20 to 40 cfm with interval of 10 and the convergence of the solution was monitored. The area averaged values of the  $y^+$  was checked in order to verify the consistency of boundary layer mesh for all the cases. The results of this analysis are tabulated and plotted below.

**Table 13- Comparison between experimental and numerical total pressure loss at 20 cfm (units: inches w.g.)**

<b>Number of cells</b>	<b>Pressure Loss Numerical</b>	<b>Pressure loss Experimental</b>	<b>Error (%)</b>
550k	0.917	0.93	-1.4
672k	0.929	0.93	-0.1
915k	0.908	0.93	-2.3

In the above range of cell numbers the maximum difference between the results is only 2.3% which is an acceptable deviation [35]. The comparison charts obtained from all the flow rates and all three mesh cases are plotted in Figure 31.

**Table 14- Comparison between results of total pressure loss obtained from different mesh resolutions at all operating flow rates (units: inches w.g.)**

<b>Flow Rate (cfm)</b>	<b>20</b>	<b>30</b>	<b>40</b>
550,000 cells	0.917	2.008	3.522
672,000 cells	0.929	2.005	3.521
915,000 cells	0.908	1.963	3.417

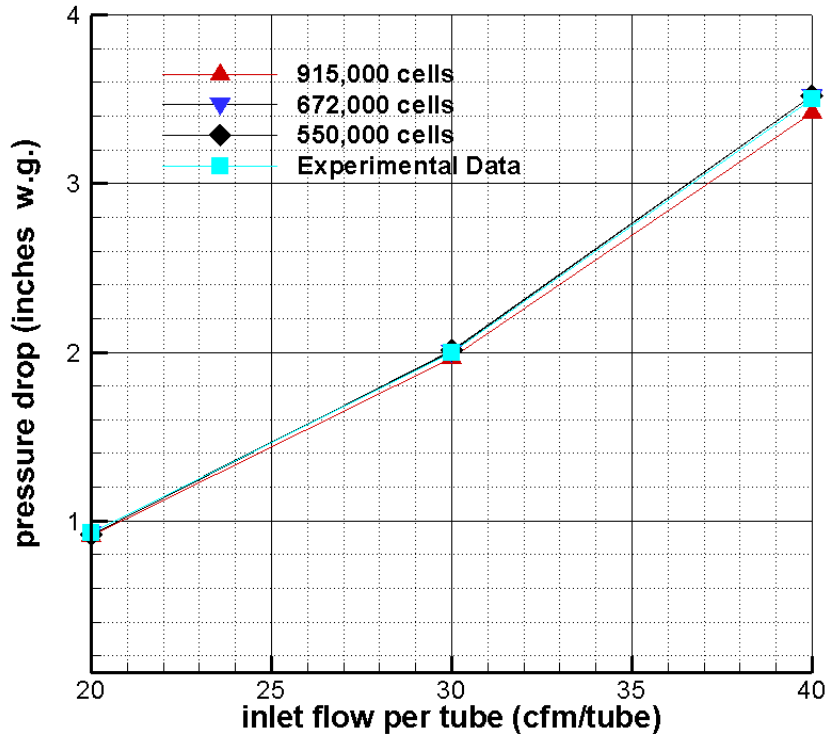


Figure 31- Comparison between results of different core mesh resolutions

## 4.4. Parametric study of the inertial gas-solid separator

In this section the results of parametric study of inertial gas-solid separator will be presented. According to the application of the inertial gas-solid separator, the pressure loss is more focused in this research. The mostly important and effective geometrical parameters of the inertial gas-solid separator were selected and the parametric study was done in order to enhance the performance of inertial gas-solid separator by reducing the amount of pressure loss. All the modified geometries have been solved numerically using ANSYS-FLUENT commercial software and the comparison charts are presented.

### 4.4.1. Selection of geometrical parameters

In cyclonic flows, pressure loss and collection efficiency are the main objectives of the optimizations and the geometrical parameters are the main decision variables in these researches. Various researchers have performed parametric studies and optimization in order to obtain less

pressure loss and high collection efficiency. As it was briefly discussed in the second chapter the mostly investigated geometrical parameters for parametric studies of cyclonic flows are, see Figure 6[10]:

- Cyclone body diameter (D),
- Dust outlet diameter (B),
- Gas outlet diameter ( $D_e$ )
- Total cyclone height (H)
- Cyclone gas outlet duct length (S)

Despite all the parametric studies and optimizations done for different types of the cyclones, straight-through swirl tubes are not sufficiently investigated. However due to conceptual similarity of the cyclones and inertial gas-solid separator, the above mentioned parameters can be related to the inertial gas-solid separator dimensions. The flow field inside the inertial gas-solid separator was evaluated, the sources of losses and non-stabilities were recognized and accordingly some geometrical parameters were initially considered to be modified. In selecting the important geometrical parameters, it was desired to select the ones which has minimal negative influence on the collection efficiency of the inertial gas-solid separator therefore if there is any improvement in pressure loss that would be accompanied by same or higher collection efficiency. For each simulation only one geometrical parameter was changed in order to achieve a distinction between the effects of each parameter. Table 15 shows the final chosen parameters to be modified as well as the modification ranges.

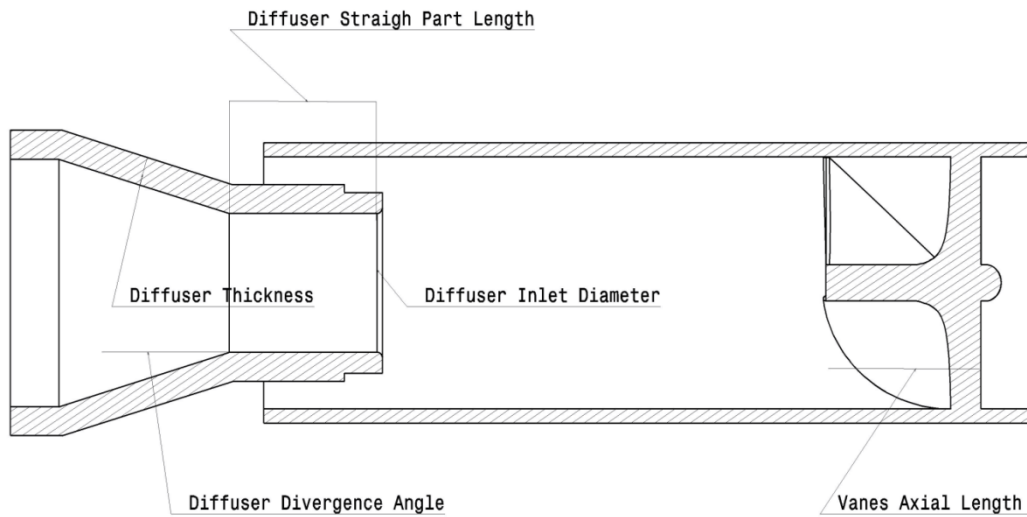


**Figure 32- Illustration of name of geometrical dimesnions**

**Table 15-Selected parameters and range of modification (org=original)**

<b>Diffuser divergence angle &amp; straight part length</b>	Org-5°	Org-2.5°	Org	Org+1°
<b>Diffuser inlet diameter</b>	Org-10%	Org	Org+10%	Org+20%
<b>Vaness axial length</b>	Org-20%	Org	Org+20%	

#### **4.4.2. Results of parametric studies**

The required CAD models for each modification were made and the computational grid was generated for each case with same resolution as the original model. The boundary conditions in parametric studies simulations were set identical to the original model and the comparison charts have been derived for same range of flow rates. The simulations were performed until the convergence of second order discretization approach was achieved. In order to verify the mesh

resolution sufficiency the value of the wall  $y^+$  was checked for each case after the convergence and the contours of different flow parameters were obtained and analyzed.

#### 4.4.2.1. Diffuser straight tube length & divergence angle

This modification is a combination of diffuser straight part's length and the diffuser angle. Since overall length of the inertial gas-solid separator had to be constant, decreasing the length of straight part of the diffuser was accompanied by decrease in divergence angle of the diffuser which was also believed to have positive effects on the flow field. The original divergence angle of the diffuser is rather large for the high speed rotational flow in that region which can cause boundary layer separation and consequently non stable vortices in the flow field. One of the factors which have considerable contribution in flow disturbances and consequently pressure loss is the flow path variations. The reason for this modification was first to decrease the length of the region with reduced area in the diffuser and second to decrease the flow separation by smoothing the flow path (divergence angle). Since the particle collection happens before flow reaches to the diffuser, these two parameters will have minimal influence on the collection efficiency of the inertial gas-solid separator. In order to verify the improvements of this modification two diffuser parts with smaller divergence angles as well as one with larger angle were considered and the results were evaluated. The contours of velocity and pressure were evaluated in order to visualize the improvements in the flow field and finally the values of pressure loss for different diffuser angles have been compared. Figures 33 to 35 show the contours of different flow parameters for each step of the modification. Table 18 contains the simulations details for each case.

**Table 16-Initial solver settings for modification of diffuser divergence angle**

<b>Case</b>	<b>Org-5°</b>	<b>Org-2.5°</b>	<b>Original</b>	<b>Org+1°</b>
<b>Flow rate (cfm)</b>	20	20	20	20
<b>Number of grids</b>	681K	675K	672K	666K

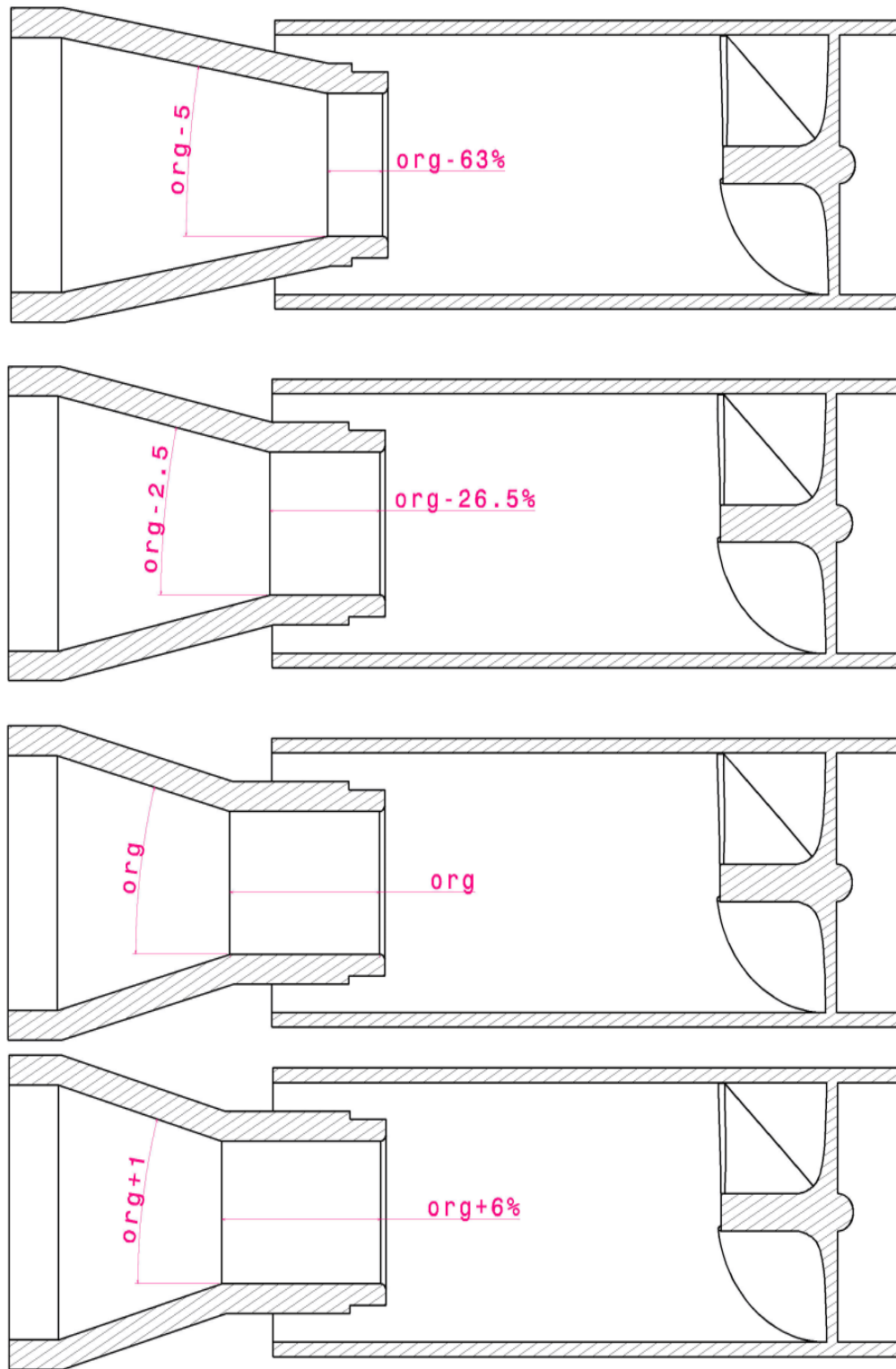
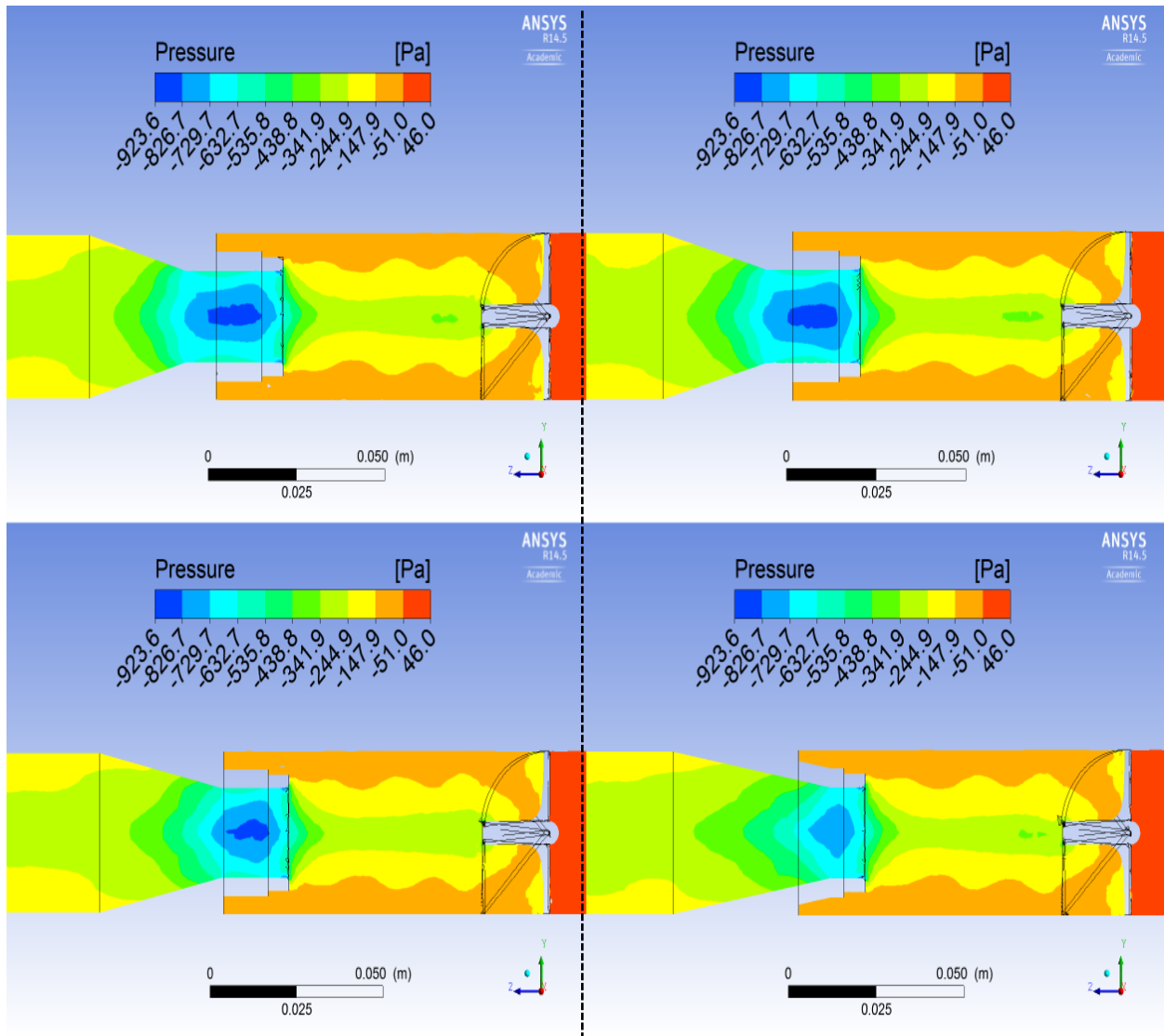


Figure 33- Graphical illustration of diffuser straight length and divergence angle variation



**Figure 34-Comparison of pressure contours for different diffuser angles, top left: (org+1°); right : original; bottom left: (org-2.5°) ; right : (org-5°)**

The effects of these modifications were mostly seen in the diffuser part itself while the flow field upstream of the diffuser inlet does not experience considerable changes. Therefore it was concluded that the collection efficiency of the filter would not be affected by changing the straight part of the diffuser and the diffuser angle. Since the straight tube became shorter as the angle decreases, the low pressure regions (blue) get smaller by decreasing the angle. This results in obstruction reduction and would be an additional reason for the reduced total pressure loss.

The second reason for the improvement is the reduction of separations due to smoother diverging path.

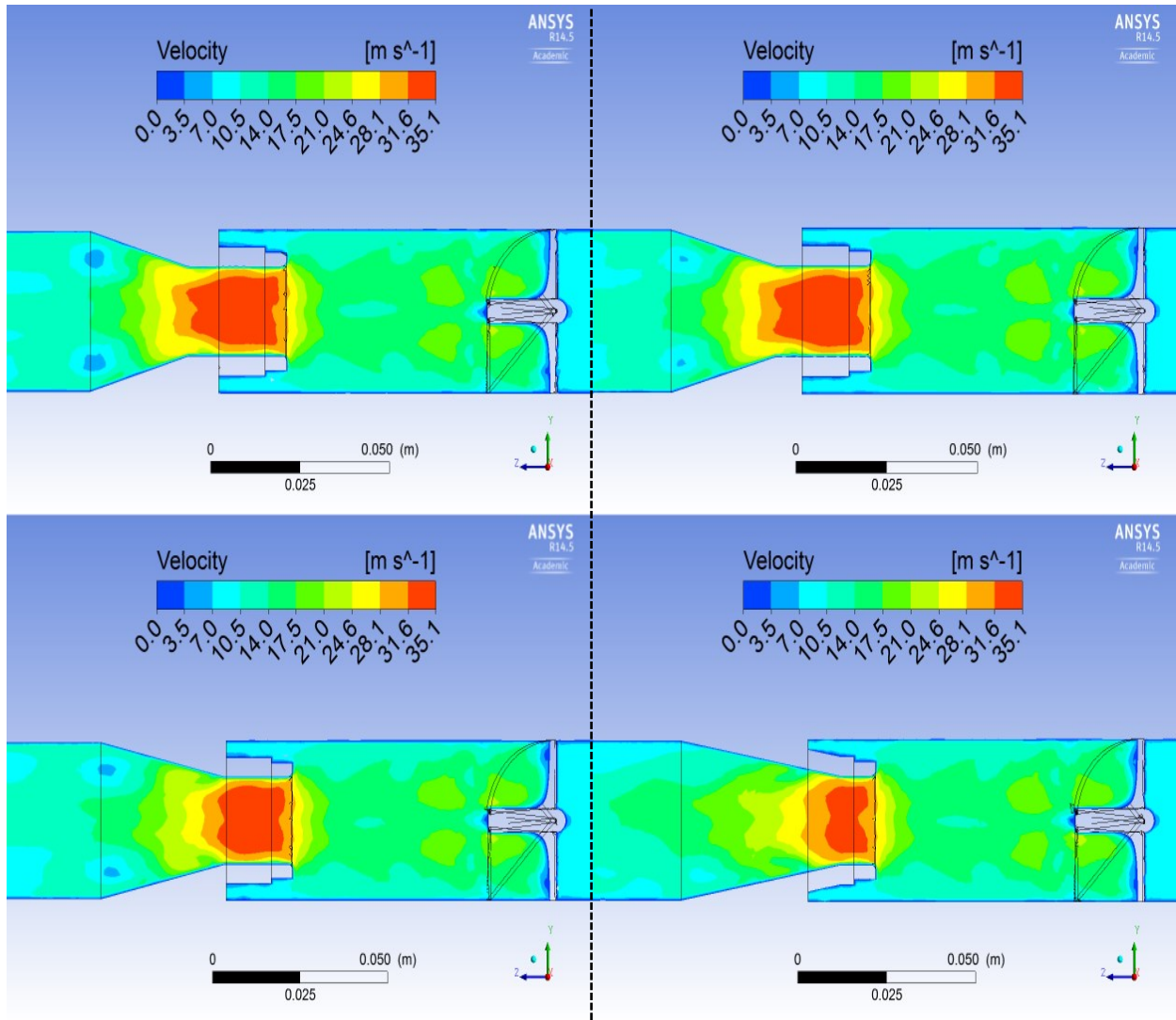


Figure 35- Comparison of velocity magnitude contours for different diffuser angles, top left: (org+1°); right : original; bottom left: (org-2.5°) ; right : (org-5°)

Contours of velocity are also demonstrative in this case. The rotational flow inside the inertial gas-solid separator tube will experience more losses if its velocity levels are higher. The red contours which represent high velocity region are getting smaller by shortening the straight part of the diffuser and therefore lower pressure loss is expected. This improvement can also be related to the reduction of obstruction in the flow path. In addition, the separations which were present in the diverging part of the diffuser become smaller by decreasing the diffuser angle and

they start to vanish in smaller angles. It is desired to prevent the boundary layer separations in the flow field and it was observed that reducing the angle of divergence in the diffuser will have positive effects in this regard. The conclusion of above mentioned improvements in the flow field is reduction of the total pressure loss.

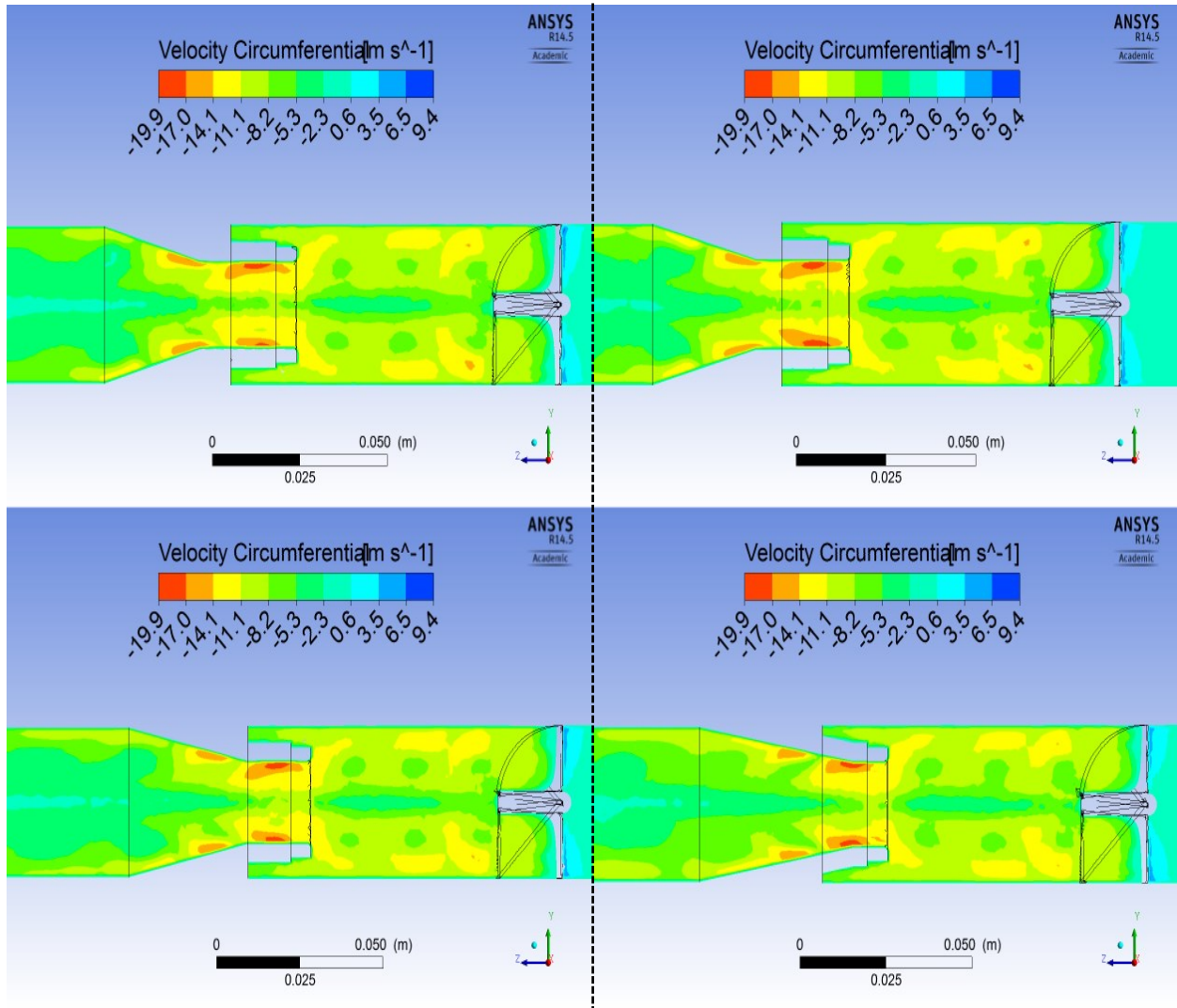


Figure 36- Comparison of tangential velocity contours for different diffuser angles, top left: (org+1°); right : original; bottom left: (org-2.5°) ; right : (org-5°)

Contours of tangential velocity prove identical flow behavior before the diffuser entrance implying the same collection efficiency. In case of high divergence angles lower tangential velocities can be observed in the diverging portion of the diffuser which shows the flow separations and stationary flow in that region.

Due to manufacturing considerations it was not possible to decrease the diffuser divergence angle more than a certain value but it is evident that pressure loss will keep decreasing by further reducing the diffuser divergence angle where its effects become more visible at diffuser angles around 5 degrees. Tables 17 and 18 show the final results achieved by modifying the straight part and divergence angle of the diffuser and Figure 37 is the comparison chart for different diffuser angles.

**Table 17- Comparison between the results of total pressure loss for different diffuser divergence angles  
(units: inches w.g.)**

<b>Flow Rate (cfm)</b>	<b>Org+1°</b>	<b>Original</b>	<b>Org-2.5°</b>	<b>Org-5°</b>
<b>20</b>	0.920	0.929	0.906	0.896
<b>30</b>	1.989	2.005	1.974	1.953
<b>40</b>	3.501	3.521	3.434	3.331

**Table 18-Percentage of pressure loss change relative to original model for different diffuser divergence angles**

<b>Flow Rate (cfm)</b>	<b>Org+1°</b>	<b>Org-2.5°</b>	<b>Org-5°</b>
<b>20</b>	-0.9%	-2.5%	-3.5%
<b>30</b>	-0.8%	-1.6%	-2.6%
<b>40</b>	-0.5%	-2.5%	-5.4%

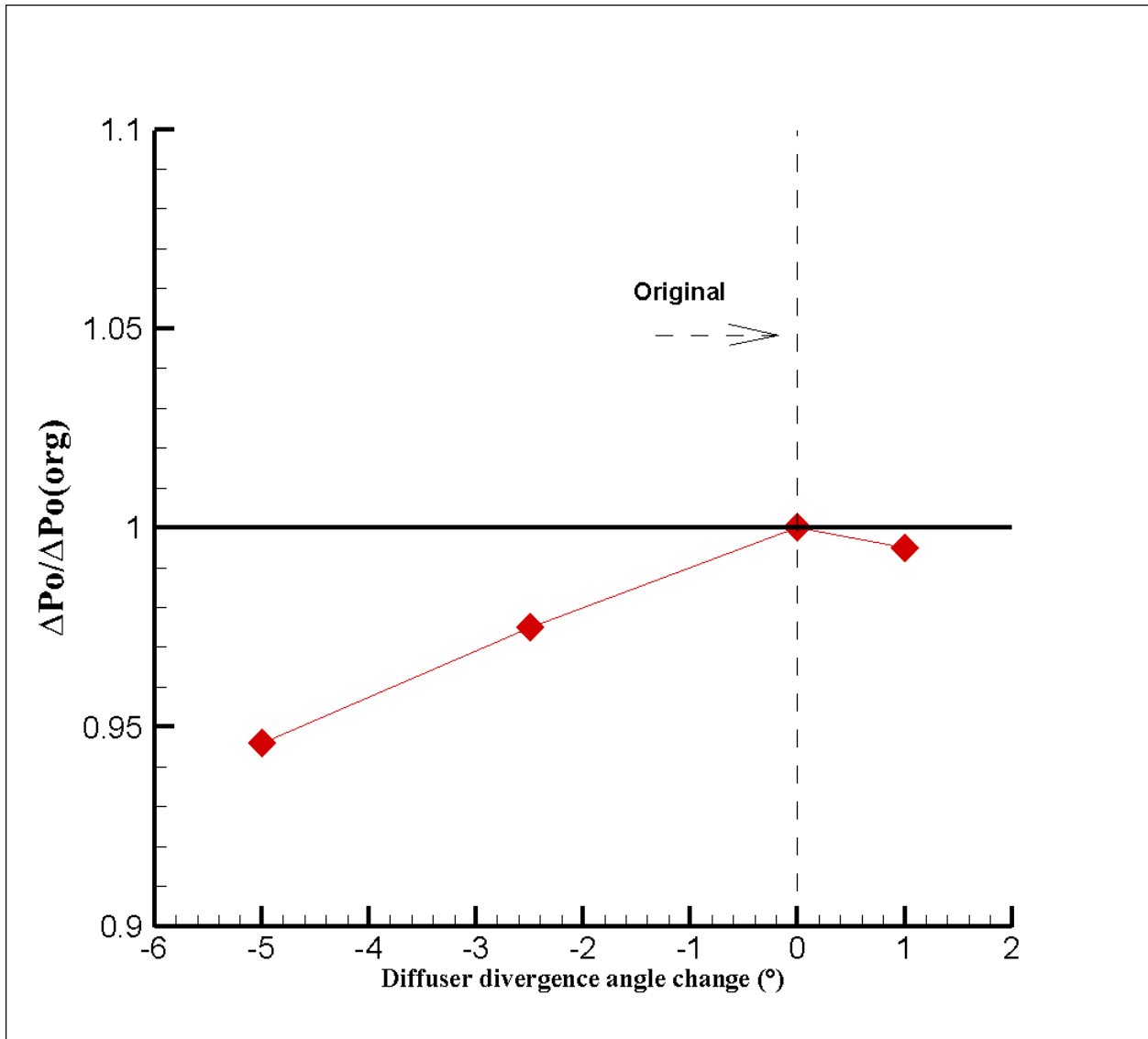


Figure 37-Comparison between results of total pressure loss for different diffuser modifications at 40cfm flow rate

#### 4.4.2.2. Diffuser inlet diameter (achieved by reducing the thickness)

The flow inside the inertial gas-solid separator is a complex rotational flow due to different geometry variations along its way. At the inlet of the diffuser part, the highly rotating flow has to enter a duct which has smaller diameter. The reduction of the flow area acts like a convergent nozzle which accelerates the flow and at the same time acts like an obstruction in the flow field. These matters were found to have considerable contribution in generation of pressure

loss in the inertial gas-solid separator. It is concluded that decreasing the changes in the flow path and smoothing it in any possible way will result in pressure loss reduction. In order to analyze the effects of diffuser inlet dimensions on the flow and consequently pressure loss, the diameter of the diffuser inlet increased to provide the rotating flow with more space at this section. This reduction in diffuser diameter could be done in two ways; either decreasing the thickness of the diffuser part or maintaining the same dust outlet area or maintaining the same thickness and increasing the diameter of the diffuser inlet which results in lower dust outlet area. The later will have negative effects on the collection efficiency due to reduction of dust outlet area while the first will have minor effects on the efficiency. Therefore the increase of diffuser inlet diameter was performed by decreasing the material thickness with two intervals each 10% of the original value. The resulted diffuser inlet diameters are shown in table no 20. The minimum tested thickness verified to be manufacturable.

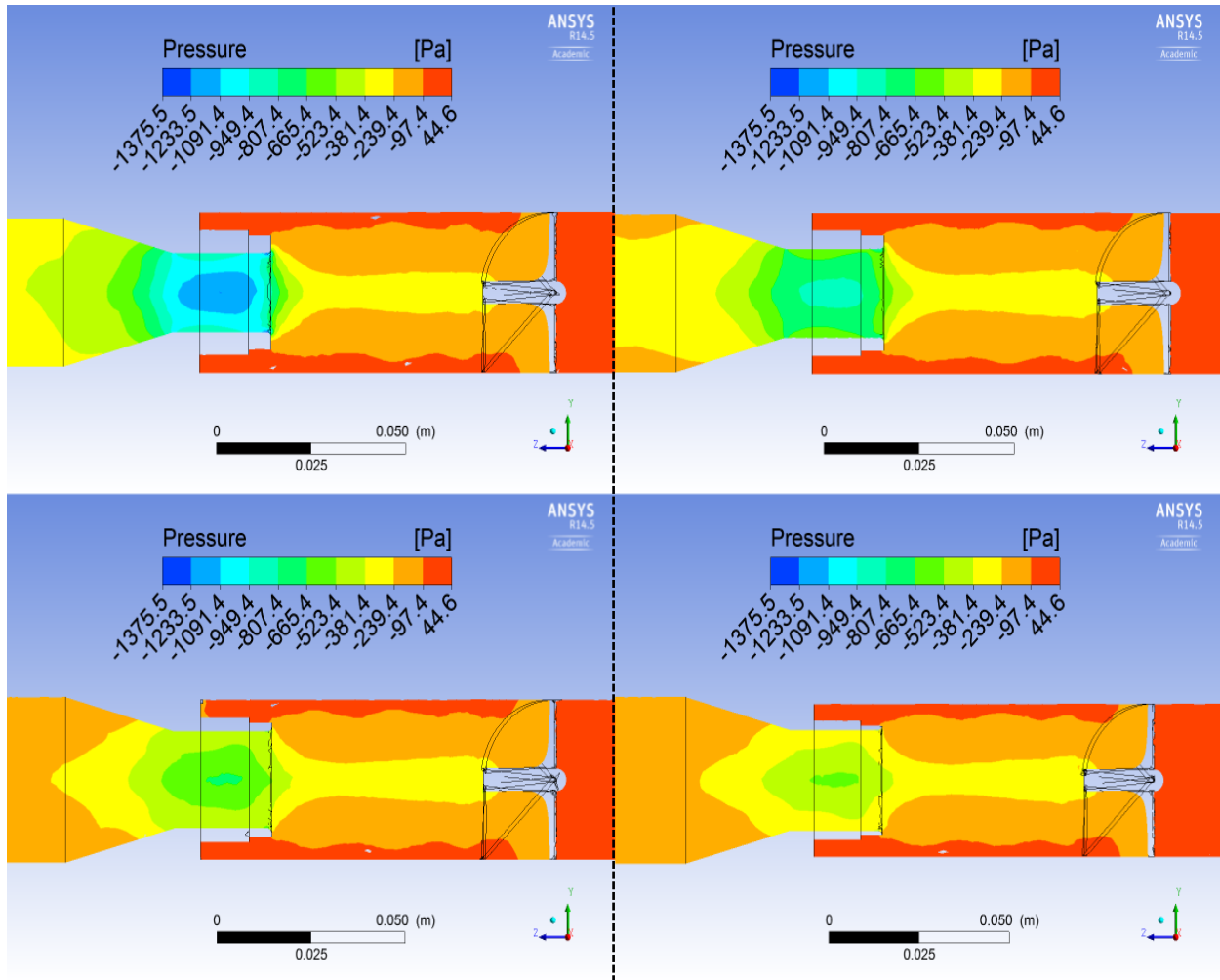
Table 19 contains the details of the CFD simulations from which the following contours (Figures 39-41) are achieved. Due to larger area and consequently larger flow path the number of computational grids varies by this modification but the boundary layer mesh has the same resolution and configuration.

**Table 19- Initial solver settings for cases of diffuser inlet diameter modification**

<b>Case</b>	<b>Org-10%</b>	<b>Org</b>	<b>Org+10%</b>	<b>Org+20%</b>
<b>Flow rate (cfm)</b>	20	20	20	20
<b>Number of grids</b>	626K	672K	711K	758K

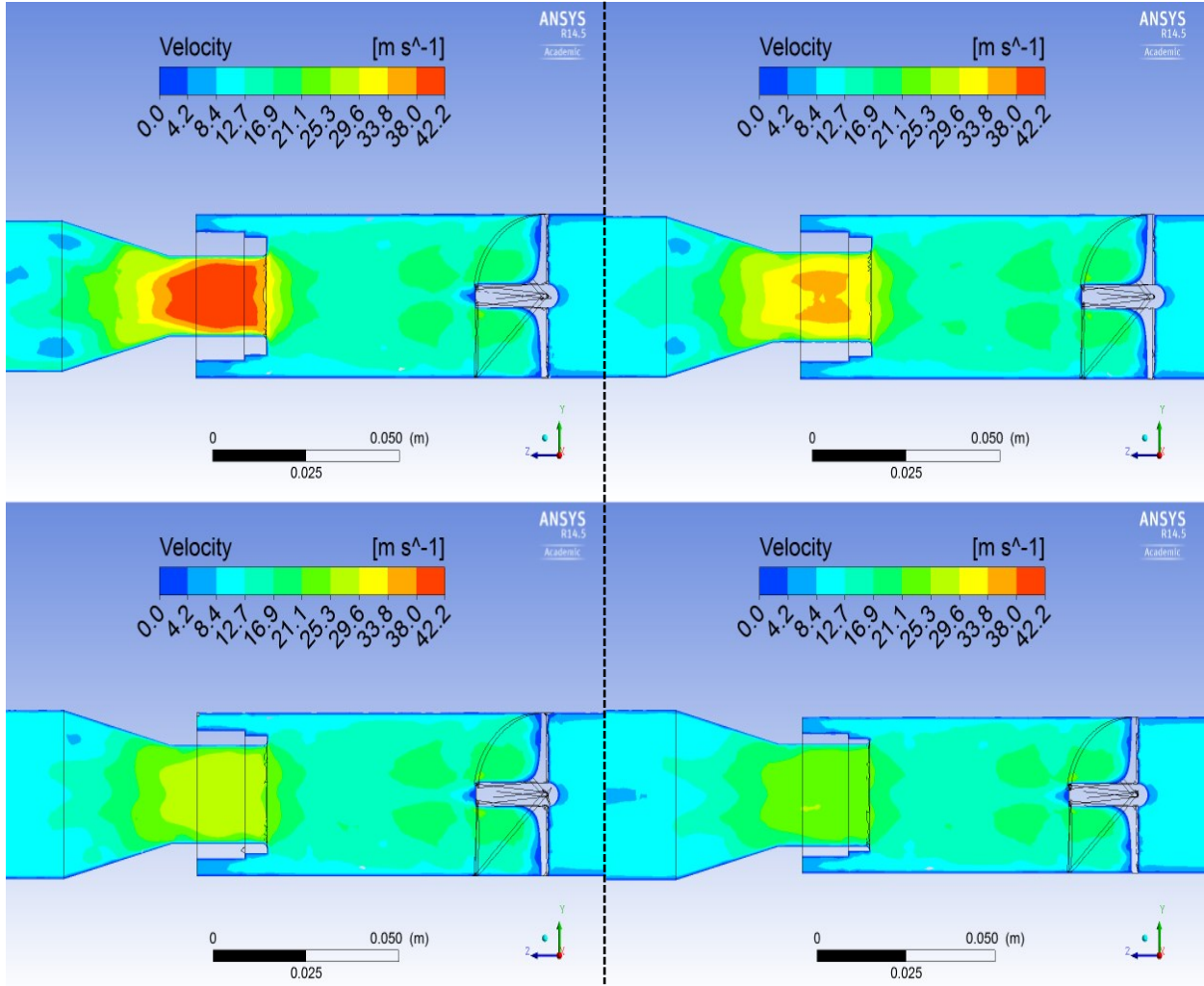


Figure 38- Graphical illustration of diffuser inlet diameter (thickness) variation



**Figure 39-Comparison of pressure contours for different diffuser diameters, top left: org+10% ; right : original; bottom left: org+10% ; right : org+20%**

In the above contours, the blue colored regions demonstrate the lowest pressure and highest velocity levels. The improvements in the contours of pressures are considerable by this modification. The minimum pressure levels in the flow field are increased (changed from blue to green) from -1300 pa gage up to -500 pa gage. As in case of diffuser divergence angle, the flow field upstream of the diffuser inlet is not affected by this modification therefore the same collection efficiency is expected. The main idea for this modification is to reduce the geometry variations as well as the obstruction in the flow path.



**Figure 40- Comparison of velocity magnitude contours for different diffuser diameters, top left: org-10% ; right : original; bottom left: org+10% ; right : org+20%**

The contours of velocity magnitude are clear demonstrators of velocity field improvement. The highly accelerating flow in the diffuser part is decelerated which causes the flow to pass the divergent part of the diffuser smoothly. Reduction in the flow separations and non-stabilities can be also observed due to lower velocity levels.

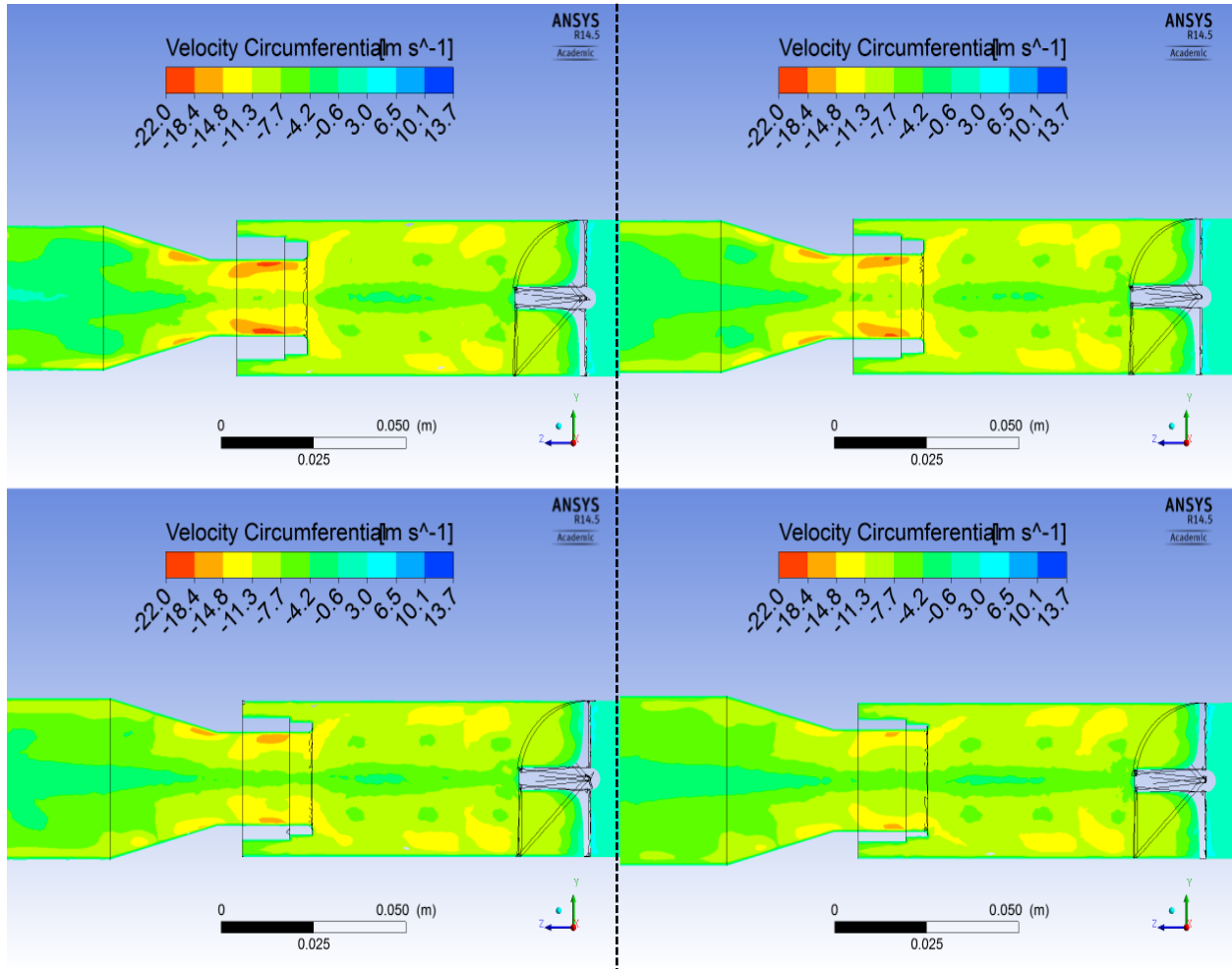


Figure 41-Comparison of tangential velocity contours for different diffuser diameters, top left: org-10% ; right : original; bottom left: org+10% ; right : org+20%

Tangential velocity contours upstream of the diffuser inlet demonstrate acceptable similarities in all cases and therefore minimal collection efficiency change is concluded. The purpose of diffuser part is to decelerate the flow and deliver it to the engines therefore more smooth and stable flow is desired in this part. The current modification was found to be highly effective in improving the flow field disturbances and reducing the pressure loss. The results of total pressure loss reductions are presented in the following tables and charts.

**Table 20-Comparison between the results of total pressure loss for different diffuser inlet diameters  
(units: inches water)**

<b>Flow Rate</b>	<b>Org-10%</b>	<b>Org</b>	<b>Org+10%</b>	<b>Org+20%</b>
<b>20</b>	1.333	0.929	0.730	0.622
<b>30</b>	3.960	2.005	1.607	1.368
<b>40</b>	6.931	3.521	2.768	2.408

**Table 21-Percentage of total pressure loss change relative to original model for different modifications of  
diffuser inlet diameters**

<b>Flow Rate</b>	<b>Org-10%</b>	<b>Org+10%</b>	<b>Org+20%</b>
<b>20</b>	+43.5	-21.4%	-33.0%
<b>30</b>	+97.5	-19.8%	-31.7%
<b>40</b>	+96.8	-21.4%	-31.6%

The results shown in tables 20 and 21 demonstrate considerable improvement in the pressure loss value while due to the nature of modification the collection efficiency of the device will have

minimal changes. As it was mentioned before, reducing the thickness is one way to have higher inlet diameter for the diffuser. In addition to thickness modification, increasing the diameter without changing the thickness was also modeled and simulated. The total pressure loss values in that case were up to 5% less than the thickness modifications which means even better performance but due to reduction of dust outlet area the negative effects on the efficiency have to be considered in that case.

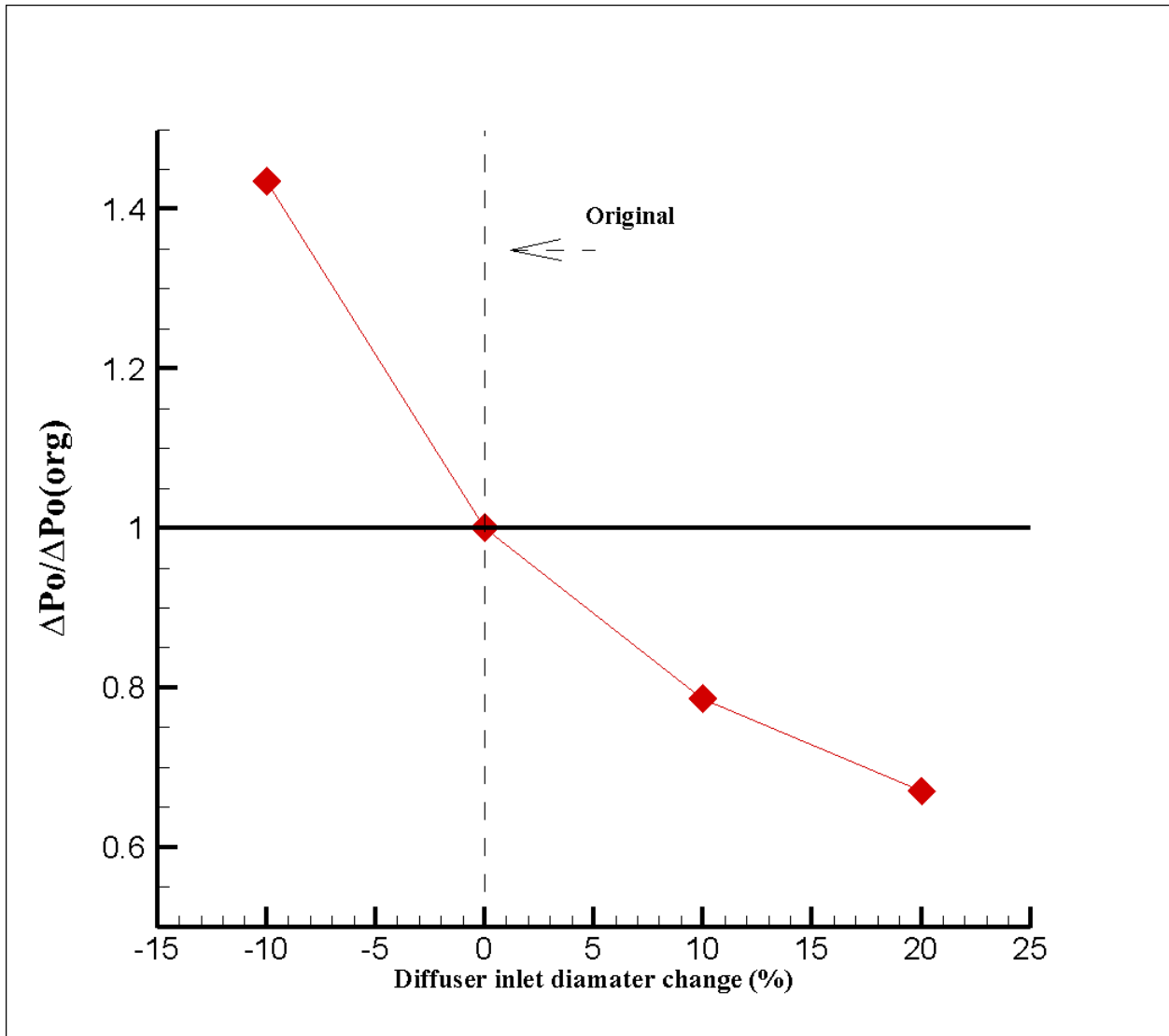


Figure 42-Comparison of pressure loss for diffuser diameter modifications at 20 cfm flow rate

#### **4.4.2.3. Vanes axial length (axial chord)**

This parameter also was considered to have some impacts on the flow pattern and consequently the flow properties along the domain. In case of higher axial length the distance between the vanes trailing edge and diffuser decreases therefore it was believed that this parameter would not affect the collection efficiency considerably. The flow field changes resulted from variation of this parameter was investigated for shorter and longer values. Figure 44-46 show the contours of the pressure, axial velocity and tangential velocities achieved by the modifications of this parameter.

Due to change in the vanes' trailing edges, the angle at which flow leaves the vanes decreases and it causes less rotation in the flow field. On the other hand, the vanes will provide more space for the flow to pass and consequently the blockage of the vanes would be reduced. This matter was observed as expected in the contours of flow field obtained at symmetry cut-plane. One can see the weaker rotation of the flow right after the vanes. Also due to more space between the vanes the overall velocity levels of the flow field are decreased which can be considered as an improvement. However it is difficult to have an estimation of the collection efficiency since at the same time the distance between the vanes and the diffuser is reduced and consequently rotating particles will not have enough space to move toward the flow core and escape the dust outlet. Therefore, despite the previous parameters, in this case a discrete phase flow analysis and particle injection would be necessary in order to precisely judge the collection efficiency. However, reduction in the amount of pressure loss by increasing the axial length of the blades was observed. This improvement in the pressure loss is mostly due to reduction of overall velocity in the flow field. As it was mentioned before, the higher the velocity of the rotating flow is, the more pressure loss it will experience by passing through a complex geometrical path due to stronger vortices and non-stabilities. It has to be mentioned that this modification creates a new flow pattern in the inertial gas-solid separator which has to be evaluated carefully. Table 22 shows the simulation details from which the following contours are obtained.

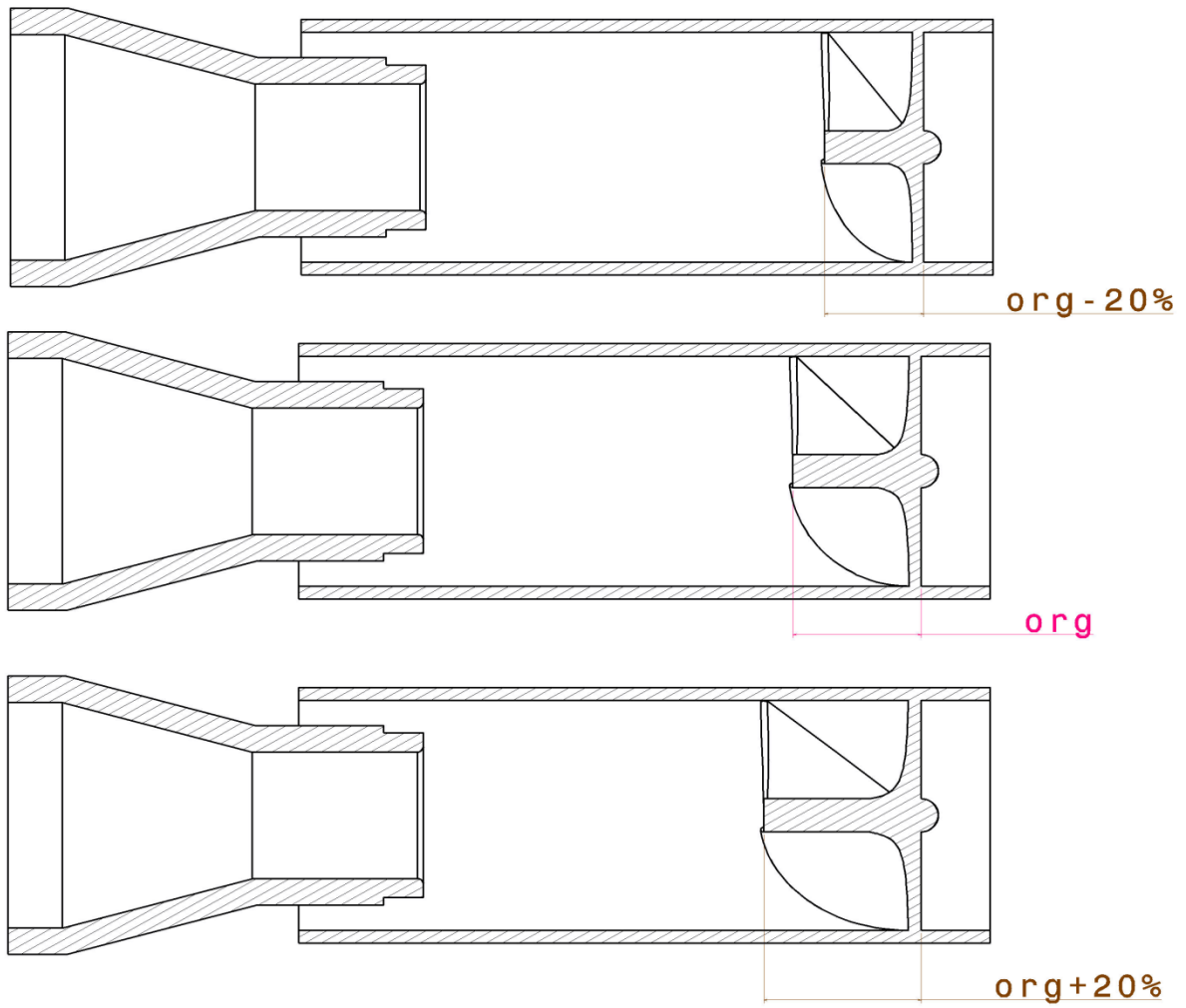
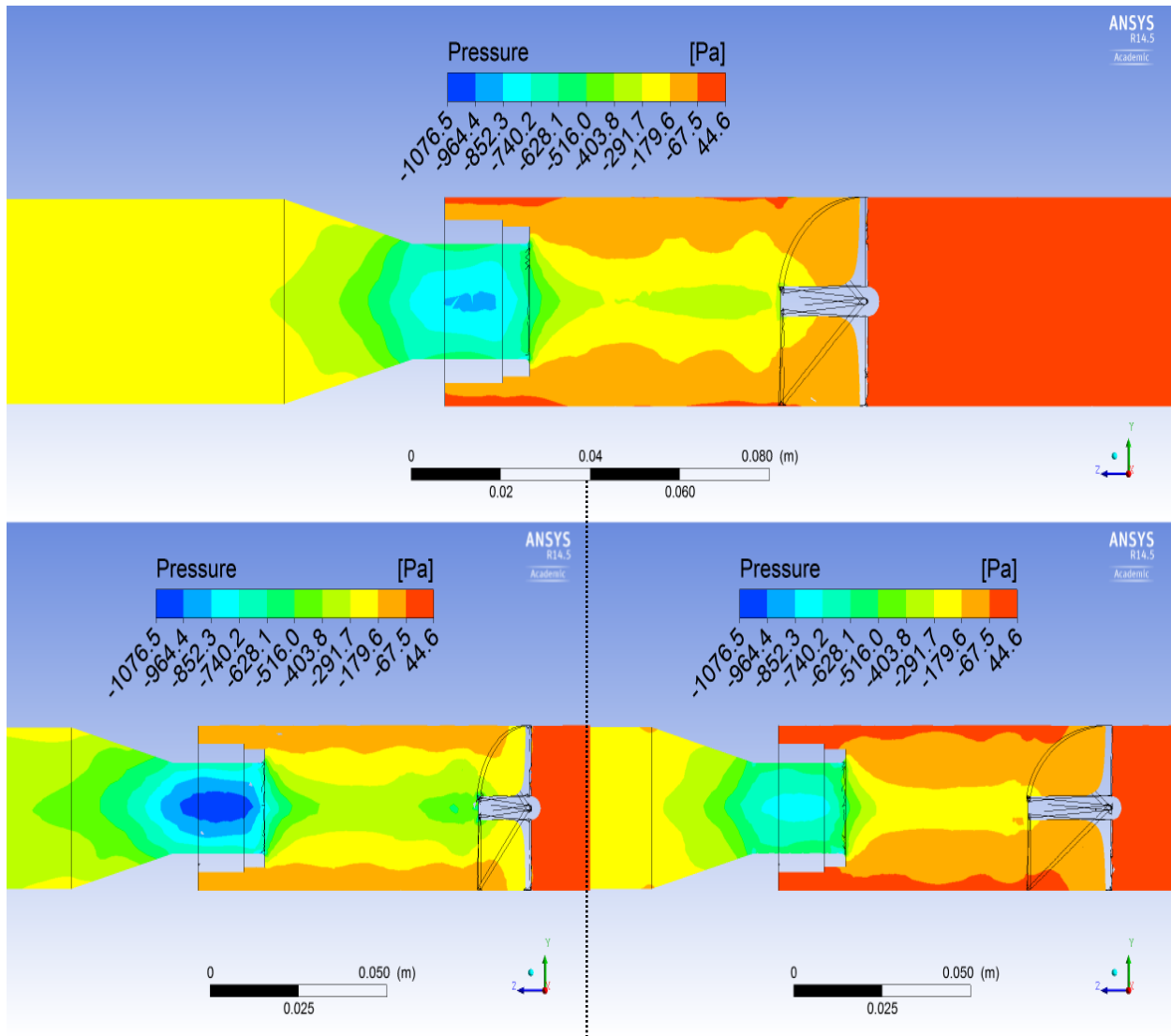


Figure 43- Graphical illustration of vanes axial length modifications

Table 22- Initial settings of solver for cases of vane length modification

Case	Org-20%	Org	Org+20%
Flow rate (cfm)	20	20	20
Number of grids	657K	672K	679K



**Figure 44-Comparison of pressure contours for different vanes lengths, top: original ; bottom left : org-20% vanes ; right: org+20%**

Contours of static pressure demonstrate the changes in the pressure field inside the inertial gas-solid separator. Basically as the vanes become longer the pressure levels in the flow field will increase. This increase is more visible in the diffuser part showing lower levels of velocity. In addition to the overall assessment of the contours it was observed that as the vanes become longer their trailing edge angles are reduced and pressure levels increase in the region close to the periphery indicating less rotational velocity in these regions. The flow in the diffuser part experiences its lowest pressure (highest velocity) in case of shortest vane length.

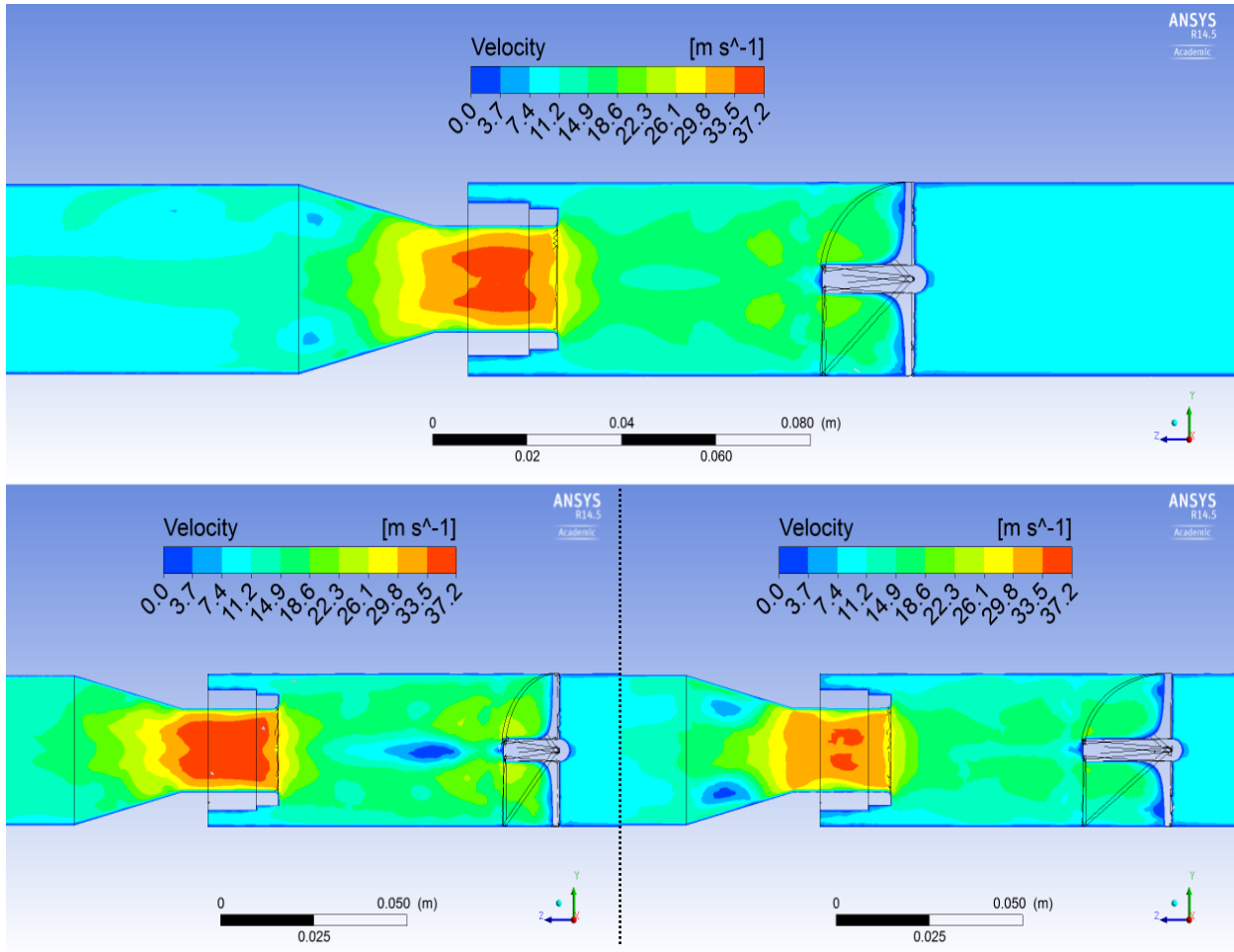


**Figure 45- Comparison of velocity magnitude contours for different vanes lengths, top: original ; bottom left : org-20% vanes ; right: org+20%**

Contours of velocity magnitude show consistency with the conclusions from the pressure contours. Higher levels of velocity are found to be main cause of having higher total pressure loss in the flow field. In case of longest vane length, there are two separation regions detected. This kind of flow behavior is due to diverging path of the diffuser where the possibilities of separation always exist. However despite having these separations still the flow has less total pressure drop since the effects of the separations in lower velocities are not dominant.

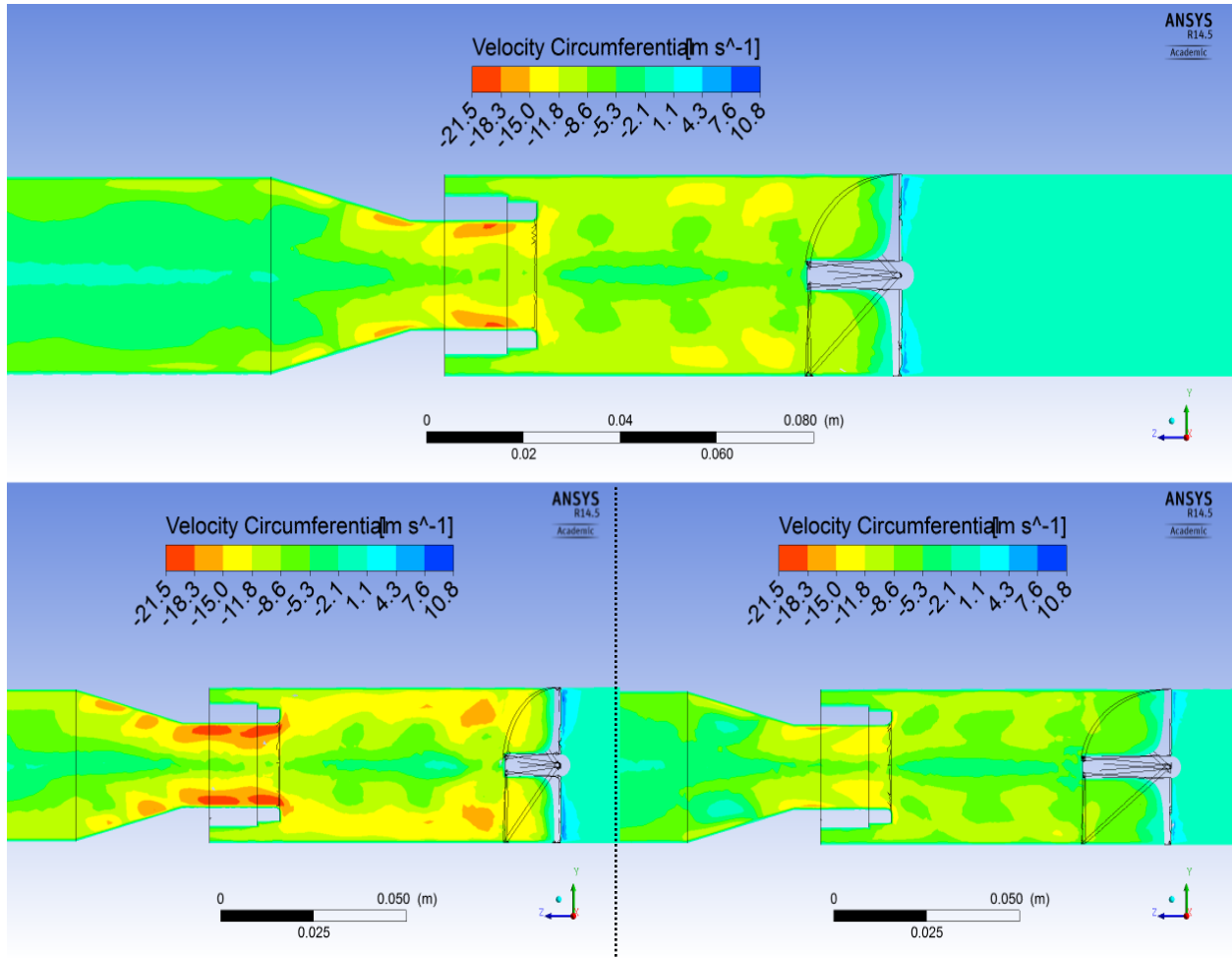


**Figure 46-Comparison of tangential velocity contours for different vane lengths, top: original ; bottom left : org-20% vanes ; right: org+20%**

The effect of this modification is clearer in the contours of tangential velocity. More rotation strength after the vanes can be observed. The strongly swirled flow for all cases accelerates by reaching to the diffuser. Again the maximum levels of velocity can be seen in case of shortest vane length.

The results of pressure loss at different flow rates for each modification have been obtained with same procedure as the original model (mass weighted average in the plane located 6 inches downstream of the diffuser outlet). Each case has been simulated for three flow rates and results can be seen in tables 23 and 24.

**Table 23- Comparison between results of total pressure loss for different vane lengths (units: inches water)**

---

<b>Flow Rate</b>	<b>Org-20%</b>	<b>Org</b>	<b>Org+20%</b>
<b>20</b>	1.224	0.929	0.848
<b>30</b>	2.703	2.005	1.837
<b>40</b>	4.743	3.521	3.191

---

**Table 24- Comparison between total pressure loss changes for vane length modifications relative to original model**

---

<b>Flow Rate</b>	<b>Org-20%</b>	<b>Org+20%</b>
<b>20</b>	+31.7%	-8.7%
<b>30</b>	+34.8%	-8.4%
<b>40</b>	+34.7%	-9.4%

---

The negative percentage values show the improvement in the amount of pressure loss. The 8.4% improvement in the pressure loss at 30cfm (which is mostly expected operational flow rate) would be a considerable improvement. It should be noticed that the modification of vanes axial length shows its effects more clearly at higher flow rates. Figure 47 presents the variation of pressure loss relative to the original values for the different vanes lengths.

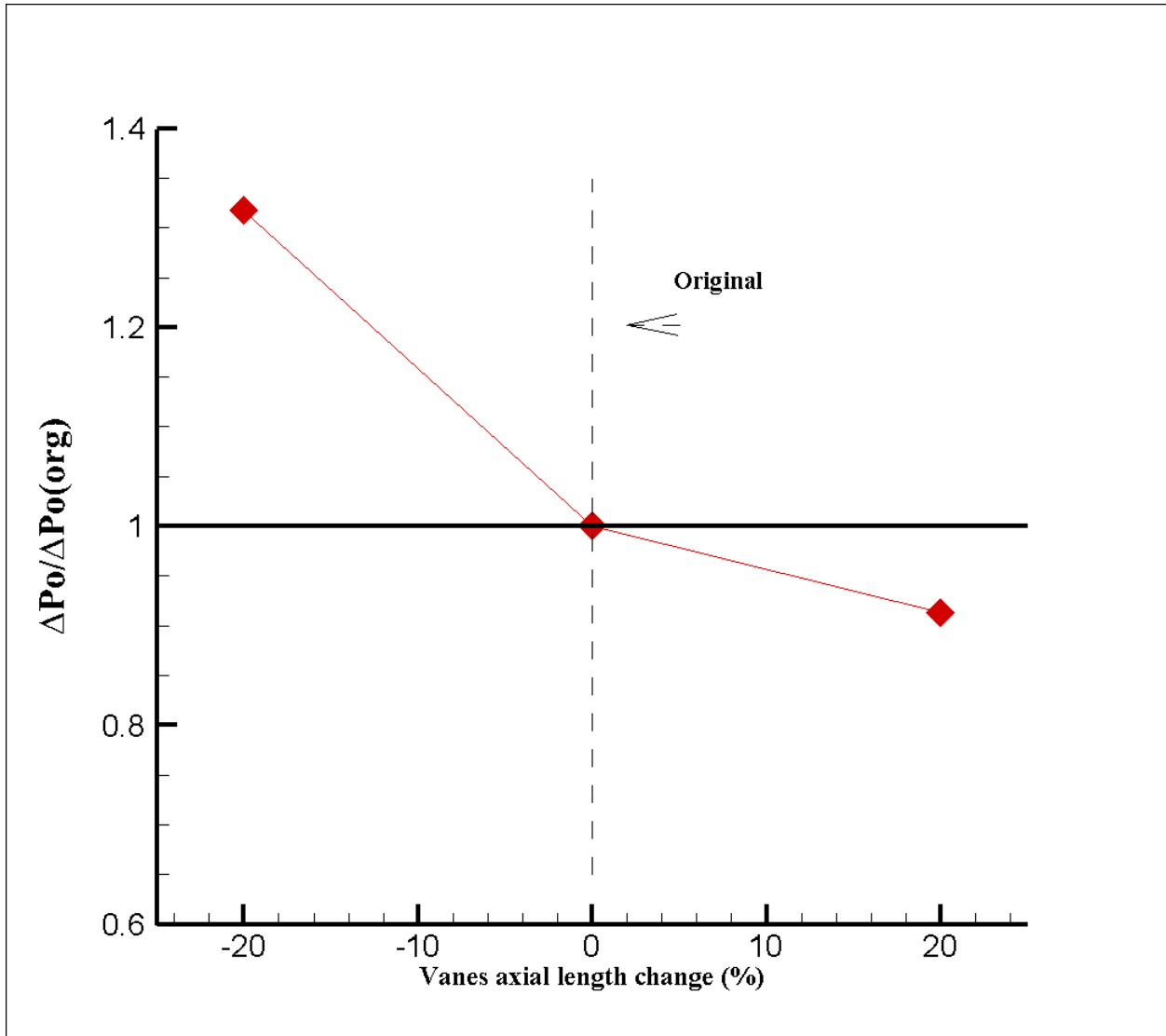


Figure 47- Comparison of total pressure loss changes for different vane lengths at 20cfm flow rate

#### 4.4.3. Conclusion of the findings in parametric studies

In the analysis of the original model the complex geometry of the air-filter found to be highly contributing in creating a complex flow field and its consequences. Three different geometrical parameters have been varied and the results of the modifications showed consistency with the prediction from initial flow analysis. In choosing the parameters there were some restrictions from manufacturing point of view such as overall length of the device as well as its overall diameter. Therefore the analysis and geometrical modifications were limited to diffuser

divergence angle accompanied by the length of the straight part in diffuser, diffuser diameter and the axial length of the static vanes. It was desired to perform the modifications such that they will have minimal effects on the collection efficiency of the filter. The findings of these parametric studies were conclusive and the most effective one was found to be the diffuser diameter. By choosing the appropriate value for this parameters the pressure loss value was reduced up to 33% while since the dust outlet passage was not changed, it is expected that changing the diffuser inlet diameter would not affect the collection efficiency. This matter was also verified by evaluating the contours of the tangential velocity in the inertial gas-solid separator flow field. The next effective parameter was found to be the axial length of the vanes where a pressure loss reduction up 9.4% was achieved. Modifying this parameter has some effects on the distribution of the tangential velocity in the flow field. Hence, it is expected that the collection efficiency would be affected changing this parameter. The diffuser divergence angle and the length of the straight part of the diffuser have also positive effects on the pressure loss with minimal influence on the collection efficiency. Up to 5.4% decrease in the pressure loss has been achieved by modifying this parameter.

# Chapter 5

In this chapter using the results achieved in the parametric studies, a finalized model for the air-filter is introduced and analyzed. The simulation details are reported and the contours of different flow parameters have been obtained and compared with the original model.

## 5.1. Geometry of the optimized model

Figure 48 show the geometry of the final optimized model. The dimensions of this model are modified in order to attain lower pressure loss maintaining the same collection efficiency. The final modified geometrical parameters are:

- Diffuser inlet diameter increased 20 %
- Diffuser straight part length and divergence angle decreased by 2.5°

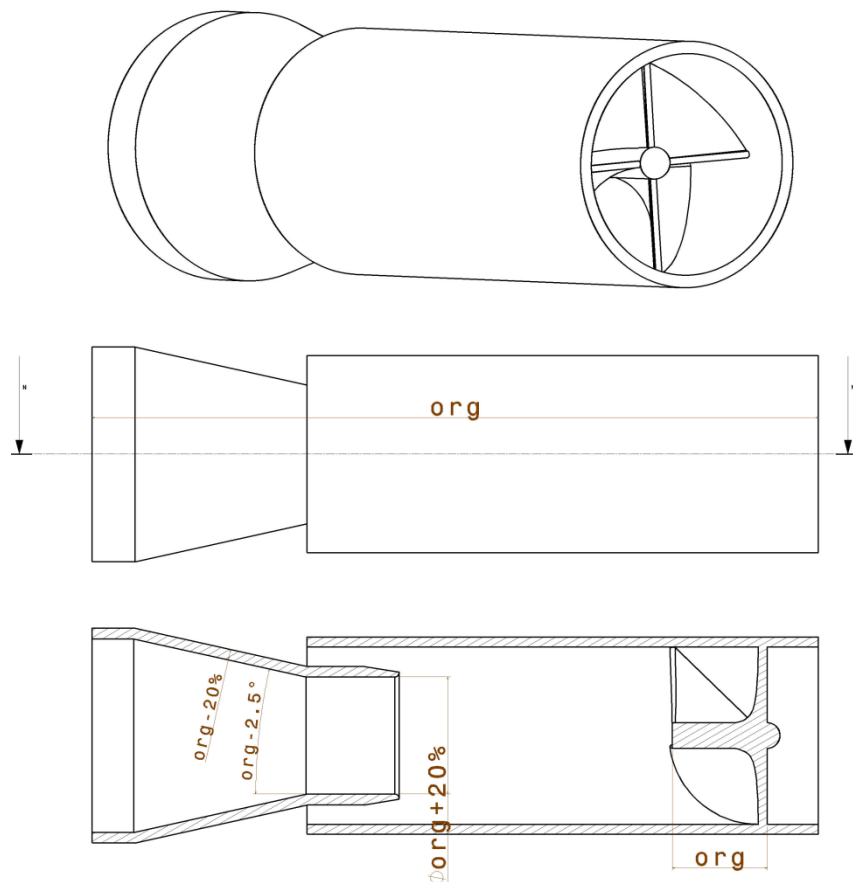


Figure 48- Geometry of the proposed inertial gas-solid separator model (units: inches)

## 5.2. Simulation settings and results

Different solution algorithms as well as computational grid considerations were investigated and tested in order to obtain a reliable and precise model for the original configuration of the inertial gas-solid separator. The final proposed geometry was also simulated with the same considerations and settings in order to compare and understand the changes and improvements of the flow field. It was expected that the flow field would be less disturbed by performing the aforementioned geometrical modifications. In that case a coarser computational grid would be also adequate, however in order to maintain the consistency of the two models the resolution of computational grid as well as the distance of the first node to the wall was kept identical to the original model. The Reynolds stress turbulence model was found to be sufficiently accurate to capture the turbulent features inside the inertial gas-solid separator. The use of non-equilibrium wall functions showed better convergence and solution stability as well as more accurate results while comparing with the available experimental data. Standard wall functions which are popularly used for tangential cyclones showed weak convergence and non-reliable predictions for the case of inertial gas-solid separator (straight-through swirl tube). The boundary conditions and discretization algorithms are also identical for both models and the solutions were initialized using same method provided in ANSYS-FLUENT with 20 initial iterations (hybrid initialization). The finalized model was solved for three consecutive flow rates starting from 20 cfm with interval of 10 cfm (this is the main operating range of the inertial gas-solid separator). The solution was monitored until the scaled residuals stabilized at acceptable levels. The computational time for each case of the final proposed model is around 3 hours with an 8 cores processor. Table 25 shows the simulation information for the final model.

**Table 25-Initial settings of solver for calculations of optimized model vs. original model**

---

<b>Model</b>	<b>Original Model</b>	<b>Optimized model</b>
<b>Flow rate (cfm)</b>	20-30-40	20-30-40
<b>Number of grids</b>	672K	750K
<b>First node distance to wall (mm)</b>	0.37	0.37

---

Values of wall  $y^+$  have been checked in order to verify that they meet the requirements of turbulence model and wall functions. It was observed that the wall  $y^+$  values are slightly less than the ones for the original model showing slower and less disturbed flow in the diffuser part. Therefore it is possible to increase the distance of the first computational node from the wall and generate coarser meshes.

**Table 26- Wall Yplus values obtained from simulations of optimized model**

---

<b>Body</b>	<b>Blades</b>	<b>Divergence</b>	<b>Outlet duct</b>
16.98	31.77	24.10	13.79

---

After the convergence, contours of static pressure, axial velocity and tangential velocities were obtained for both cases and compared. The presented contours are obtained at flow rate of 20 cfm.

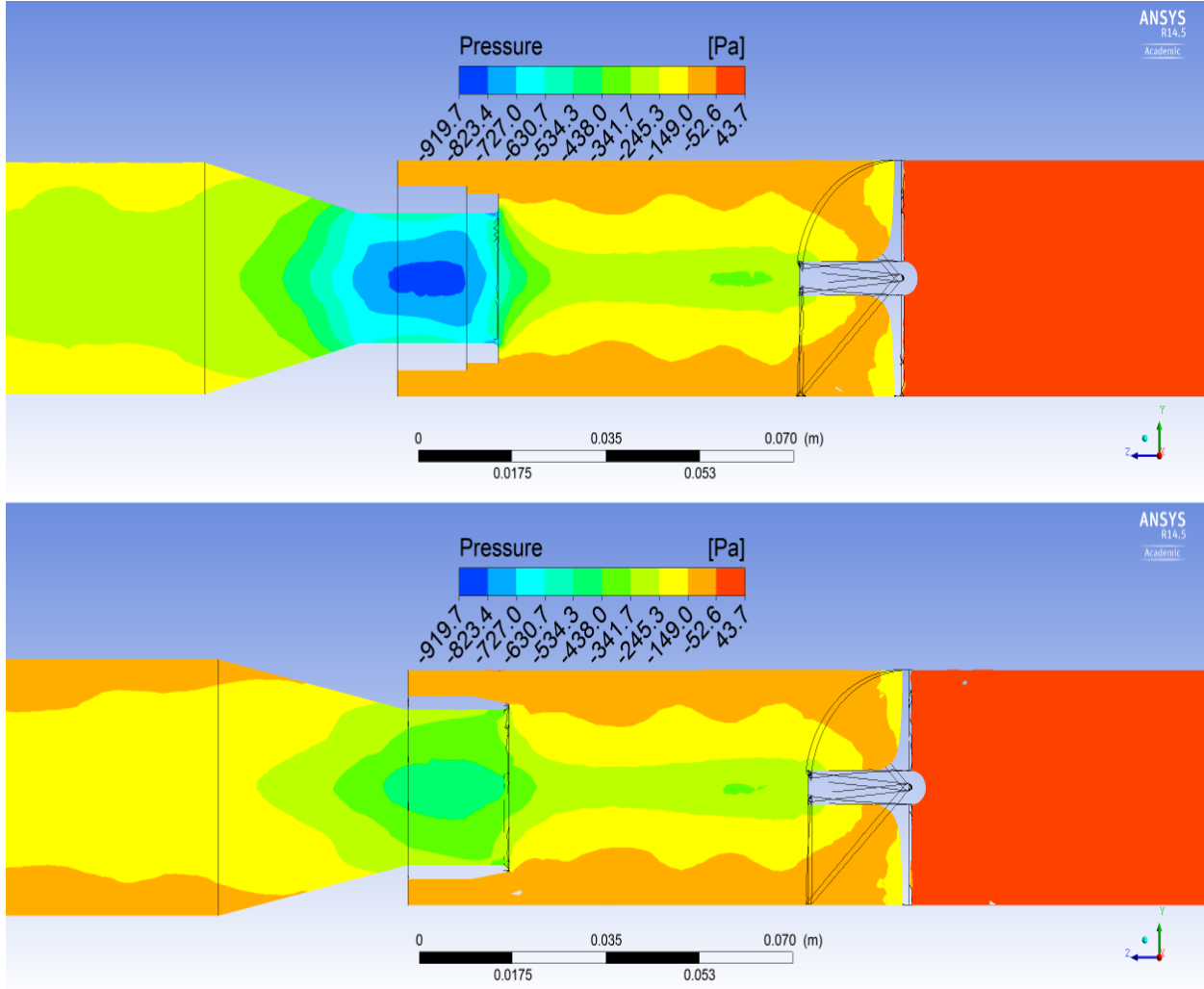


**Figure 49-Comparisin between static ressure contours of original and optimized model , top: original model ; bottom: optimized model**

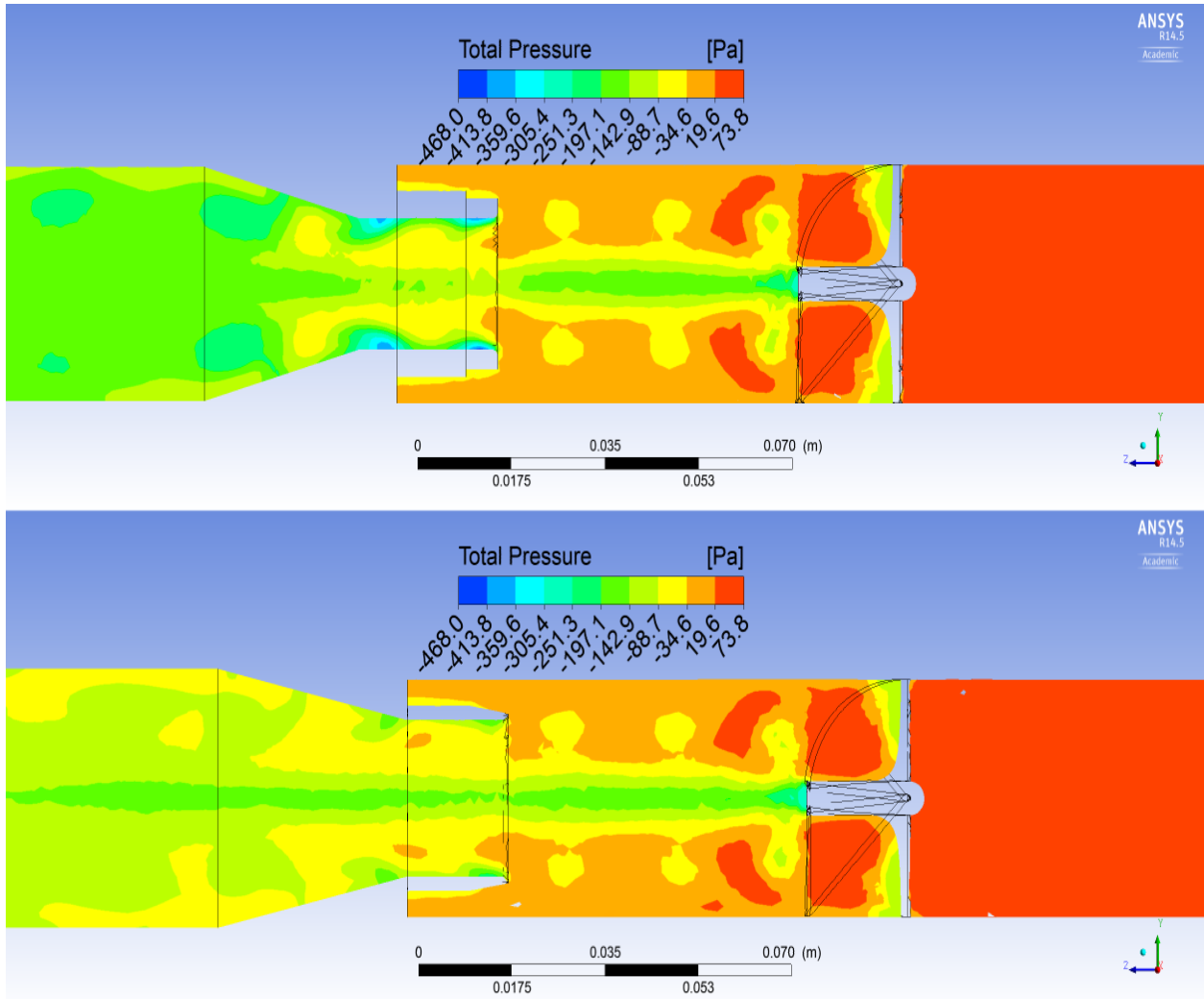


**Figure 50-Comparisin between total pressure contours of original and optimized model, top: original model ; bottom: optimized model**

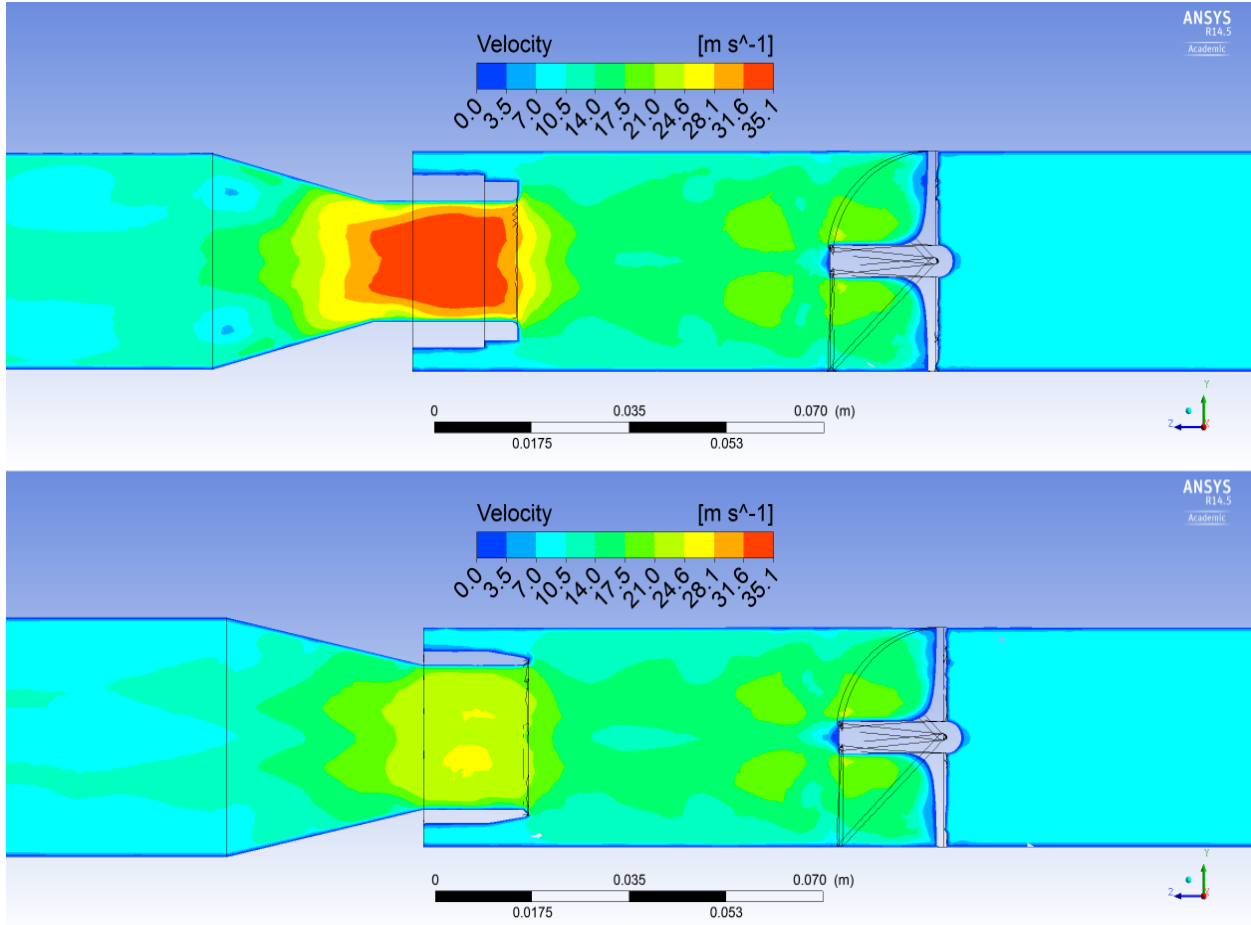


**Figure 51-Comparison velocity magnitude contours of original and optimized model, top: original model ; bottom: optimized model**

Figure 49 and 50 show the contours of the static pressure and total pressure. The overall pressure level in the flow field of diffuser part is increased due to overall velocity reduction. The complex vortices in the diffuser part are reduced considerably resulting in reduction of total pressure loss in the flow field. According to the fact that the optimized model has the same flow rate capacity as the original model, decreasing the overall level of the velocity and preventing the extreme changes in the flow path will result in reduction of the pressure loss. Figure 50 shows that the overall levels of total pressure contours are increased in the flow field. Contours of velocity (see Figure 48) demonstrate more smooth and stable flow inside the diffuser which has considerable positive effects on the amount of pressure loss. It can be seen that by modifying the geometry, the large high velocity region (red contours) inside the diffuser is vanished while the

collection efficiency of the air-filter will not be considerably affected. Contours of tangential velocity in Figure 52 show same rotational behavior of the flow before the diffuser entrance. Since the tangential velocity determines the amount centrifugal force in the flow field, similar tangential velocities in the flow field imply minimal changes in the collection efficiency.

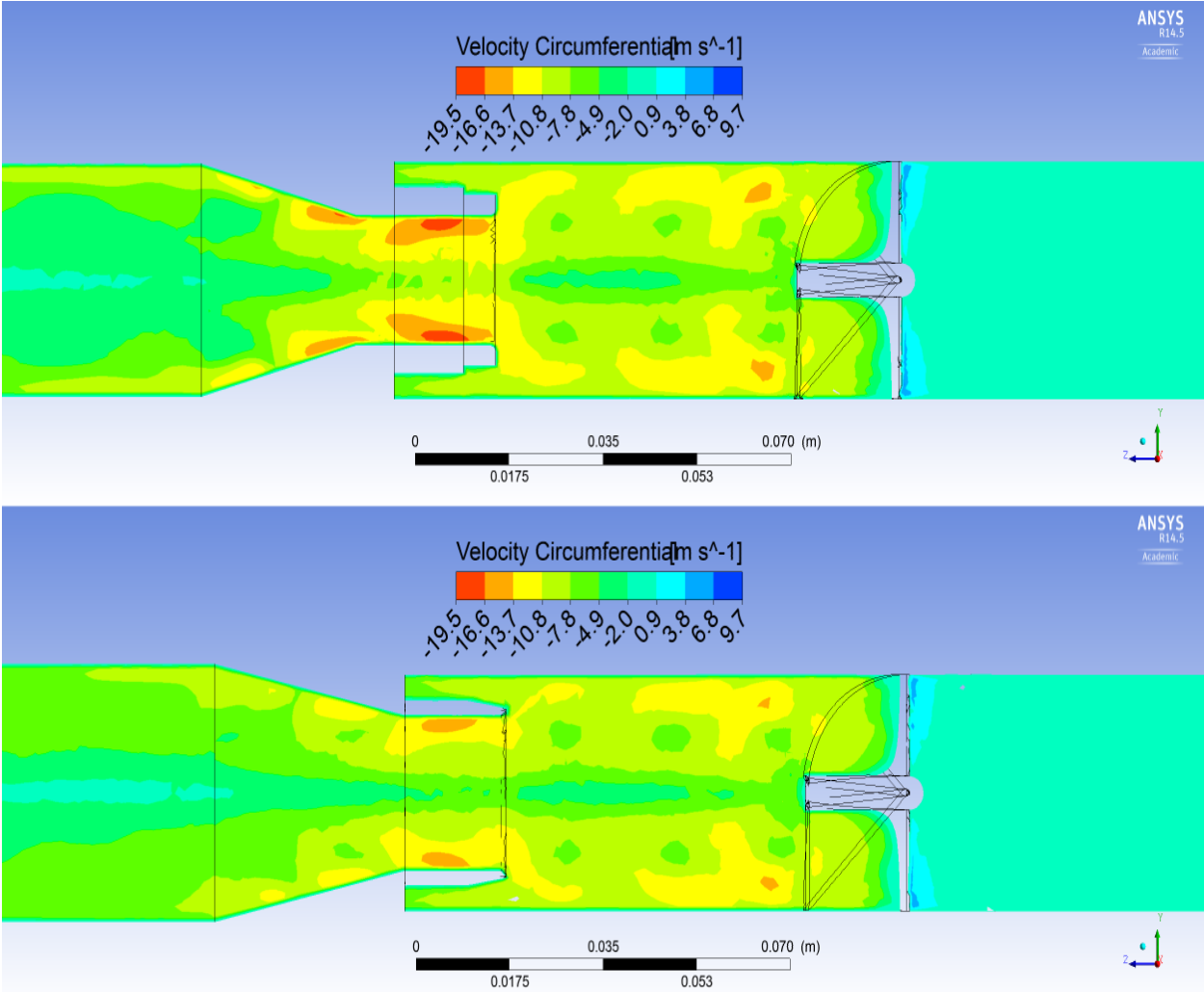


**Figure 52-Comparison of tangential velocity contours of original and optimized model, top: original model; bottom: optimized model**

In order to further verifying the effect of final modifications on the collection efficiency, the radial distributions of tangential velocity for original and optimized models are compared at two different locations shown in the following figure.

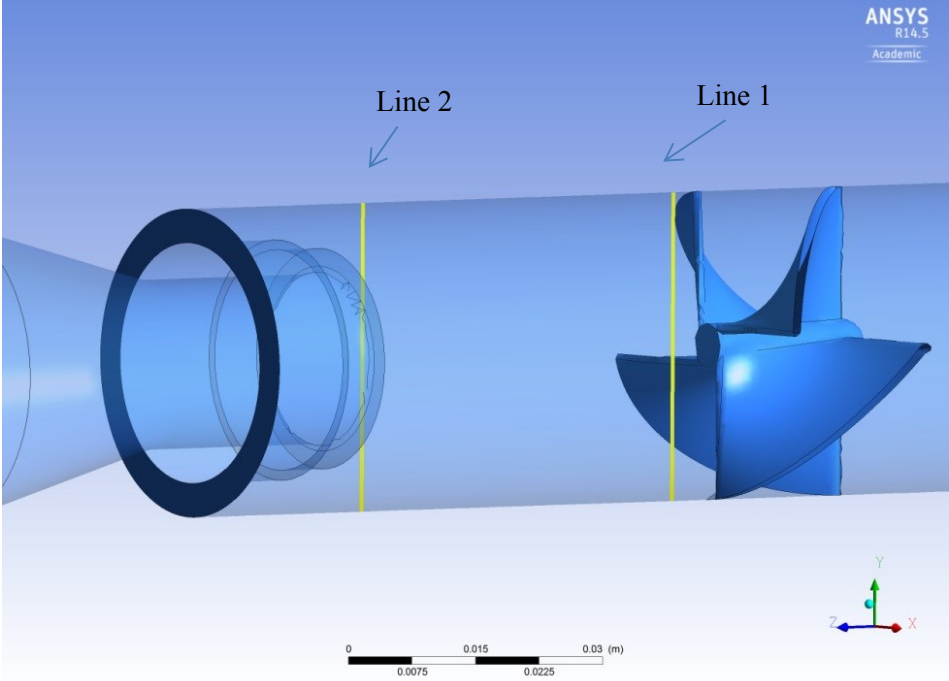


**Figure 53- locations of extracting the radial distribution of tangential velocity**

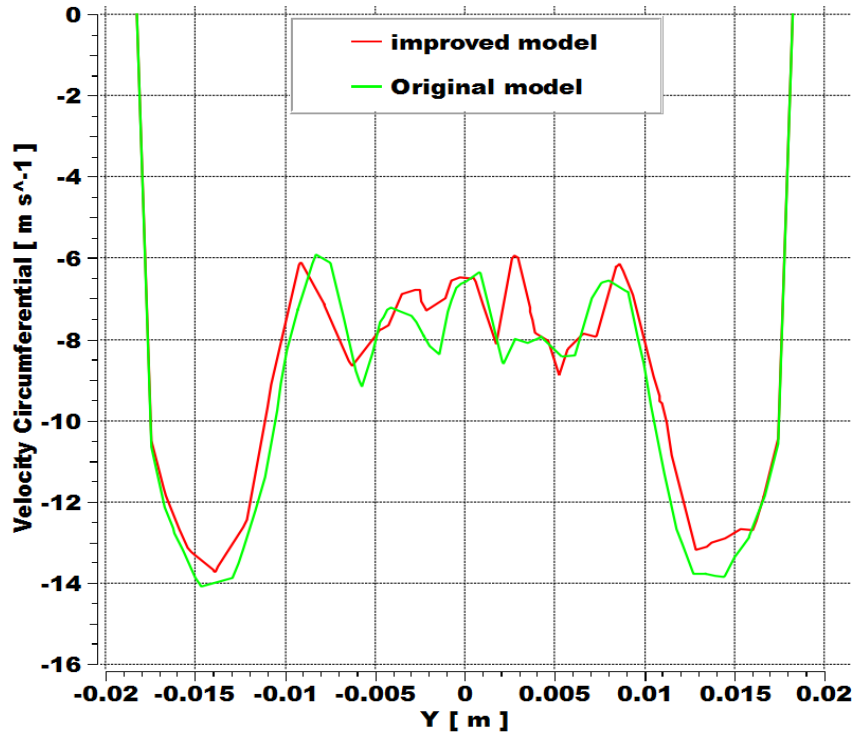


Figure 54- Comparison between radial distributions of tangential velocity at line 1

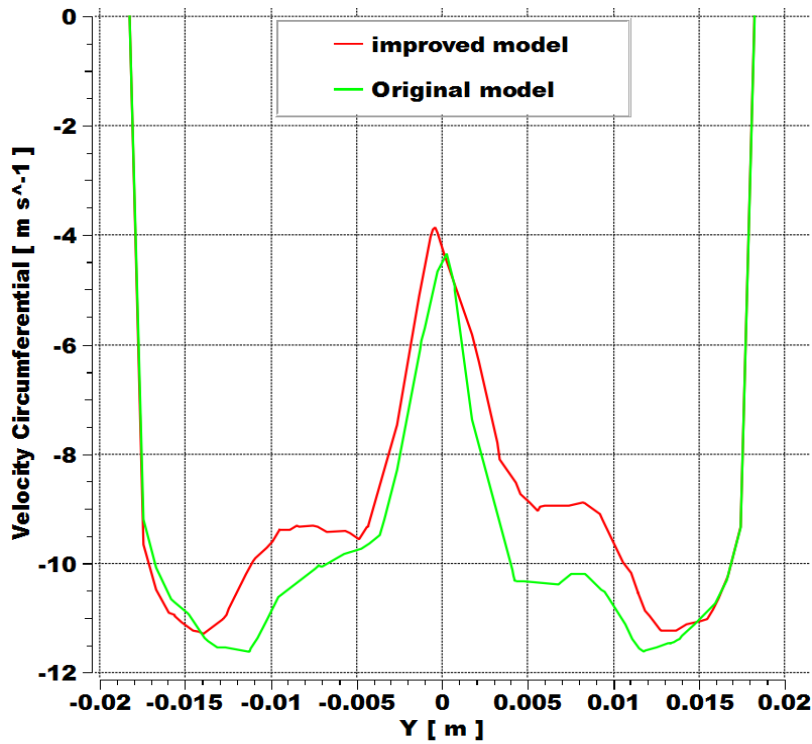


Figure 55- Comparison between radial distribution of tangential velocity at line 2

As it can be seen in the above figures the flow rotation pattern is identical in both original and improved models. Since the centrifugal forces are proportional to the tangential velocity this matters implies identical collection efficiencies for both models. The distribution on line 2 shows lower levels of tangential velocity in the core region before the diffuser entrance which illustrates the effects of diffuser modifications where more space for the flow is provided. The matter would not considerably affect the collection efficiency since the flow behavior close to the walls is still similar.

**Table 27-Comparison between the results of total pressure loss for original and optimized model  
(units: inches w.g.)**

<b>Flow rate</b>	<b>Original (Experiment)</b>	<b>Original (CFD)</b>	<b>Optimized model</b>
<b>20</b>	0.93	0.929	0.620
<b>30</b>	2	2.005	1.373
<b>40</b>	3.5	3.521	2.405

**Table 28-Percentage of total pressure loss change of optimized model relative to original model**

<b>Flow rate</b>	<b>Optimized Model</b>
<b>20</b>	-33.3%
<b>30</b>	-31.5%
<b>40</b>	-31.7%

The results of the optimized model show acceptable consistency with the expectations. The amount of pressure loss reduction is maintained when all the modifications are grouped in a unique geometry. Comparing the results of final model with the original model shows up to

33.3% reduction in the amount of total pressure loss. As it was mentioned before and according to analysis of the flow inside optimized model, it is expected that the current final geometry will have approximately same collection efficiency as the distributions of tangential velocity before the diffuser are identical. Therefore the final model can extremely improve the overall performance of its cycle. Considering the fact that there would be lots of similar tubes installed in the system the accumulated amount of pressure loss reduction would be significant. Figure 56 shows the comparison between the available experimental data, original model and the final proposed modified model which is considerably improved.

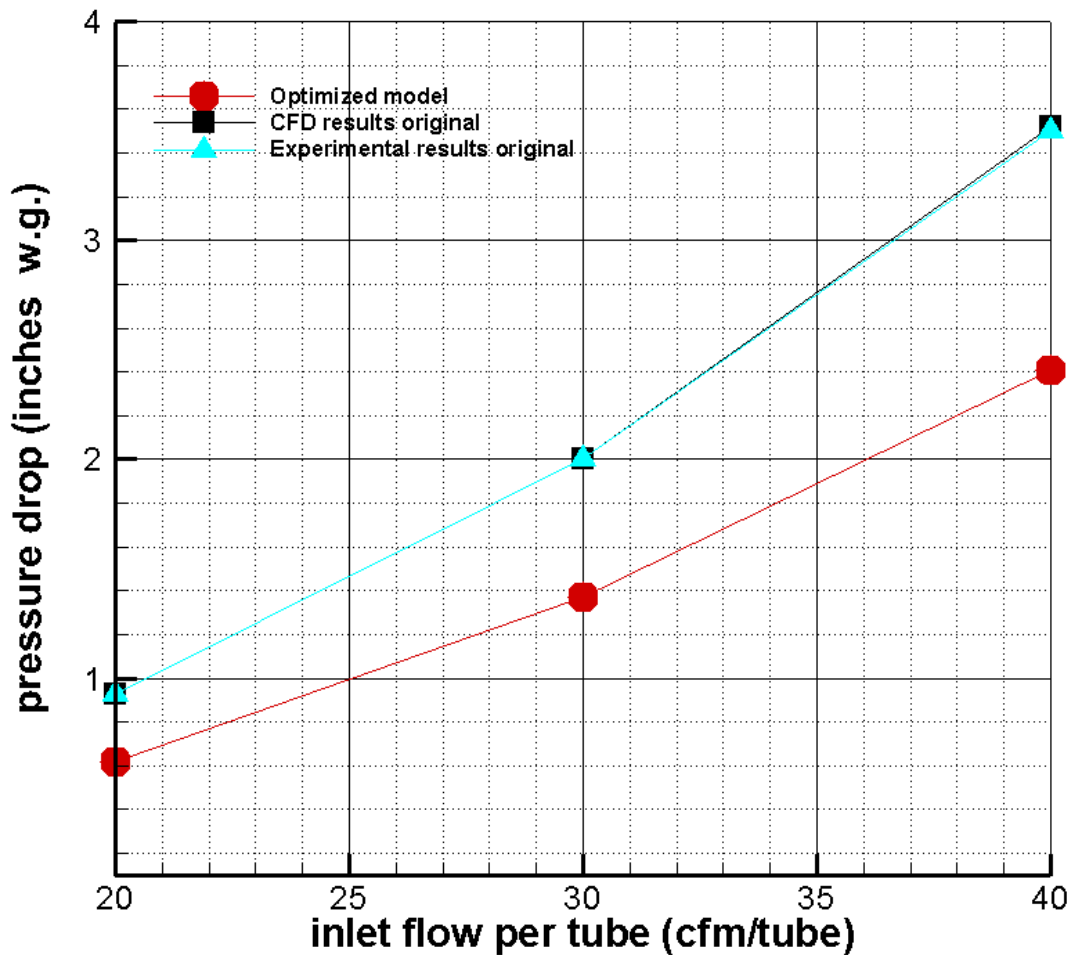


Figure 56-Comparison of pressure loss between experiment, original model and optimized model

# Chapter 6

## Conclusion

### 6.1. Summary

A comprehensive numerical 3-D model has been created for a straight-through swirl tube inertial gas-solid separator, where both the clean air outlet and dust outlets are aligned along the axial direction and the direction of the inlet flow does not reverse in the structure. A CAD model was created in CATIA V5R20 for the original design of the air-filter and unstructured computational grid has been generated. Different mesh resolutions, turbulence models and solution algorithms have been tested in order to verify their applicability for the case of inertial gas-solid separator. The Reynolds stress turbulence model along with non-equilibrium wall function, with coarse mesh adjacent to the wall was found to be applicable for the gas-solid separator subject of present research. The results of time-dependent solutions were verified to show either no variation or periodic oscillations by the time with values close to the steady-state solution. These solver settings have shown fast, stable and accurate solutions in comparison to conventional models used for tangential flow cyclones.

The results of inlet to outlet pressure loss for the original model were obtained and the created model was initially validated with the available experimental data. The flow field inside the air-filter has been evaluated by means of analyzing different flow variable contours. The overall velocity level of the flow field was found dominantly determining in pressure loss. It is concluded that with the same flow rates, having a converging part in the flow field results firstly in an obstruction and secondly in a high velocity turbulent flow which will experience considerable increase in the pressure loss as it proceeds through the tube. The decreased area passage at the entrance of the diffuser acts like an obstruction which generates pressure losses. In addition to these factors, boundary layer separations as well as non-symmetrical vortices have been observed in the divergent part of the diffuser. This is due to highly divergent angle (for the original model  $15.2^\circ$ ) that the rotating flow experiences.

By having the knowledge of the pressure loss sources in the original model, different cases of modified geometry have been created in order to test and verify their improvements. The

aim was to modify the geometry in a way which the collection efficiency of the inertial gas-solid separator experience minimal changes. In addition to the collection efficiency there were certain manufacturing limitations which had to be considered such as overall length and diameters. Three geometrical parameters have been chosen (one for the static vanes and two for diffuser) and the modifications have been performed in order to decrease the total amount of pressure loss.

- Length of the diffuser straight part and divergence angle
- Diffuser inlet diameter (by decreasing the thickness)
- Axial length of the vanes

For the first parameter, the angle of divergence in the diffuser part has been modified in order to verify its effects. It was concluded that higher divergence angles will result in more separations and non-symmetrical phenomena while decreasing this angle would have positive effects on the flow field. More importantly decrease of the diffuser straight part length has positive effect on the flow field and the pressure loss because it reduces the obstruction in the flow path and the high velocity region in the diffuser becomes smoother. With this modification, up to 5.4% decrease in the pressure loss was achieved when diffuser angle was decreased by 5 degrees.

Second modification was performed on the diffuser inlet diameter in order to reduce the area change in the flow pattern as it was discussed earlier. This modification was performed in a way which does not affect the collection efficiency by decreasing the thickness of the diffuser part. In this case the dust outlet passage would not be changed; therefore the same collection efficiency would be expected. The minimum thickness was verified to be manufacturable. This modification was found to have maximum positive effect on the amount of pressure loss. Having increased the inlet diameter by 20% of its original value resulted in up to 33% reduction in the amount of pressure loss.

The last geometrical parameter to change was the axial length of the vanes. The effect of this parameter in the collection efficiency was not completely predictable but the results of pressure loss were found to be satisfactory. Up to 9.4% of reduction in amount pressure loss was achieved by modifying this parameter. This reduction of pressure loss is resulted from overall reduction in the velocity levels in the flow field as it was expected to be one of the effective parameters. The tangential velocity distribution was found to be changed by this geometry modification therefore

changes in the collection efficiency is expected. On the other hand decreasing the length of the vanes will result in higher tangential velocity in the flow field. Hence, higher collection efficiency would be expected by decreasing the vanes axial length but the results of pressure loss shows up to 30% increase in pressure loss associated with this modification.

The modified geometrical parameters which resulted in lower pressure loss were combined and the results were evaluated. The results of pressure loss were satisfactory and up to 33.4% of pressure loss reduction has been achieved while the minimum changes of collection efficiency is predicted according to the comparisons made between the velocity fields of original and optimized models.

In the process of parametric studies where variety of geometrical modifications were tested, the initial models and algorithms including the characteristics and resolution of computational grid, turbulence model and near wall treatment as well as the solver settings shown to be capable of producing fast, stable and accurate results. Besides the CFD settings, the created CAD model using the CATIA® software found to be satisfactory and useful for future works.

## **6.2. Future work**

- Since there is a few previously done researches in the field of swirl tubes the future work in this field could be enormous. Modification of different geometrical parameters such as the overall diameter and length of the air-filter which would be possible by having the allowance to vary the overall length of the filter.
- The current model for the flow can be extended by adding the dust. The particle phase can be added to the flow inside the air-filter and the amount of collection efficiency can be numerically calculated. This collection efficiency can be expressed in terms of cut-off size of the air- filter or percentage of absorption of different particle sizes at different flow rates.
- Parametric study in order to achieve better efficiency can be the next major step since in some applications the collection efficiency is of high interest relative to the pressure loss.

# Bibliography

1. Anderson JD. Computational fluid dynamics. Springer; 1995.
2. Bernardo S, Peres A, Mori M. Computational study of cyclone flow fluid dynamics using a different inlet section angle. *Revista de Engenharia Térmica*. 2005;4(1).
3. Bhasker C. Flow simulation in industrial cyclone separator. *Adv Eng Software*. 2010;41(2):220-8.
4. Boysan F, Ayers W, Swithenbank J. A fundamental mathematical modelling approach to cyclone design. *Transactions of the Institution of Chemical Engineers*. 1982;60(4):222-30.
5. Boysan F, Weber R, Swithenbank J, Lawn C. Modeling coal-fired cyclone combustors. *Combust Flame*. 1986;63(1):73-86.
6. Casal J, Martinez-Benet JM. Better way to calculate cyclone pressure drop. *Chemical engineering*. 1983;90(2):99-100.
7. Chen Z, Przekwas A. A coupled pressure-based computational method for incompressible/compressible flows. *Journal of Computational Physics*. 2010;229(24):9150-65.
8. Cooper CD, Alley F. *Air pollution control: A design approach*. Waveland Press Prospect Heights, IL; 1994.
9. Cortes C, Gil A. Modeling the gas and particle flow inside cyclone separators. *Progress in Energy and Combustion Science*. 2007;33(5):409-52.
10. de Vasconcelos Salvo R, de Souza FJ, de Moro Martins, Diego Alves. Assessment of numerical integration schemes applied to inertial particle tracking in cyclone separators.
11. Dietz P. Collection efficiency of cyclone separators. *AICHE J*. 1981;27(6):888-92.
12. Dirgo JA. Relationships between cyclone dimensions and performance. ; 1988.

13. Elsayed K, Lacor C. Modeling and pareto optimization of gas cyclone separator performance using RBF type artificial neural networks and genetic algorithms. *Powder Technol.* 2012;217:84-99.
14. Elsayed K, Lacor C. The effect of cyclone inlet dimensions on the flow pattern and performance. *Appl Math Model.* 2011;35(4):1952-68.
15. Elsayed K, Lacor C. Optimization of the cyclone separator geometry for minimum pressure drop using mathematical models and CFD simulations. *Chemical engineering science.* 2010;65(22):6048-58.
16. Ferziger JH, Perić M. *Computational methods for fluid dynamics.* Springer Berlin; 1996.
17. Fluent R. 6.3. 26, help system, ANSYS.
18. Frank T, Schade K, Petrak D. Numerical simulation and experimental investigation of a gas-solid two-phase flow in a horizontal channel. *Int J Multiphase Flow.* 1993;19(1):187-98.
19. Gim bun J, Chuah T, Fakhru'l-Razi A, Choong TS. The influence of temperature and inlet velocity on cyclone pressure drop: A CFD study. *Chemical Engineering and Processing: Process Intensification.* 2005;44(1):7-12.
20. Gomez L, Mohan R, Shoham O, Kouba G. Enhanced mechanistic model and field-application design of gas/liquid cylindrical cyclone separators. *Spe Journal.* 2000;5(02):190-8.
21. Gong G, Yang Z, Zhu S. Numerical investigation of the effect of helix angle and leaf margin on the flow pattern and the performance of the axial flow cyclone separator. *Appl Math Model.* 2012;36(8):3916-30.
22. Griffiths W, Boysan F. Computational fluid dynamics (CFD) and empirical modelling of the performance of a number of cyclone samplers. *J Aerosol Sci.* 1996;27(2):281-304.
23. Hoekstra A, Derksen J, Van Den Akker H. An experimental and numerical study of turbulent swirling flow in gas cyclones. *Chemical Engineering Science.* 1999;54(13):2055-65.

24. Hoffmann AC, Stein LE. Gas cyclones and swirl tubes. Springer; 2002.
25. Kaya F, Karagoz I. Performance analysis of numerical schemes in highly swirling turbulent flows in cyclones. *Curr Sci.* 2008;94(10):1273-8.
26. Kim J, Ghajar AJ, Tang C, Foutch GL. Comparison of near-wall treatment methods for high reynolds number backward-facing step flow. *International Journal of Computational Fluid Dynamics.* 2005;19(7):493-500.
27. Kim S, Choudhury D, Patel B. Computations of complex turbulent flows using the commercial code FLUENT. In: *Modeling complex turbulent flows.* Springer; 1999. p. 259-76.
28. Launder BE, Spalding D. The numerical computation of turbulent flows. *Comput Methods Appl Mech Eng.* 1974;3(2):269-89.
29. Martignoni W, Bernardo S, Quintani C. Evaluation of cyclone geometry and its influence on performance parameters by computational fluid dynamics (CFD). *Brazil J Chem Eng.* 2007;24(1):83-94.
30. Meier HF, Mori M. Anisotropic behavior of the reynolds stress in gas and gas–solid flows in cyclones. *Powder Technol.* 1999;101(2):108-19.
31. Oesterle B, Petitjean A. Simulation of particle-to-particle interactions in gas solid flows. *Int J Multiphase Flow.* 1993;19(1):199-211.
32. Okedere O, Sonibare J, Fakinle B, Jimoda L. Usefulness of particulate cyclone in air pollution control. *Management of Environmental Quality: An International Journal.* 2013;24(6):771-81.
33. Ould-Rouiss M, Dries A, Mazouz A. Numerical predictions of turbulent heat transfer for air flow in rotating pipe. *Int J Heat Fluid Flow.* 2010;31(4):507-17.

34. Papageorgakis G, Assanis DN. Comparison of linear and nonlinear RNG-based k-epsilon models for incompressible turbulent flows. *Numerical Heat Transfer: Part B: Fundamentals*. 1999;35(1):1-22.
35. Patankar SV, Spalding DB. *Heat and mass transfer in boundary layers*. Morgan-Grampian; 1968.
36. Peng W, Boot P, Udding A, Hoffmann A, Dries H, Ekker A, et al. Determining the best modelling assumptions for cyclones and swirl tubes by CFD and LDA. *PARTEC (international congress for particle technology)*; Citeseer; 2001.
37. Peng W, Hoffmann AC, Dries H. Separation characteristics of swirl-tube dust separators. *AICHE J*. 2004;50(1):87-96.
38. Pishbin SI, Moghiman M. Optimization of cyclone separators using genetic algorithm. *International Review of Chemical Engineering-Rapid Communications*. 2010;2(6).
39. Raoufi A, Shams M, Farzaneh M, Ebrahimi R. Numerical simulation and optimization of fluid flow in cyclone vortex finder. *Chemical Engineering and Processing: Process Intensification*. 2008;47(1):128-37.
40. Raoufi A, Shams M, Kanani H. CFD analysis of flow field in square cyclones. *Powder Technol*. 2009;191(3):349-57.
41. Ravi G, Gupta SK, Ray M. Multiobjective optimization of cyclone separators using genetic algorithm. *Ind Eng Chem Res*. 2000;39(11):4272-86.
42. Safikhani H, Akhavan-Behabadi M, Shams M, Rahimyan M. Numerical simulation of flow field in three types of standard cyclone separators. *Advanced Powder Technology*. 2010;21(4):435-42.
43. Safikhani H, Hajiloo A, Ranjbar M. Modeling and multi-objective optimization of cyclone separators using CFD and genetic algorithms. *Comput Chem Eng*. 2011;35(6):1064-71.

44. Salim SM, Cheah S. Wall Y strategy for dealing with wall-bounded turbulent flows. Proceedings of the international MultiConference of engineers and computer scientists; ; 2009.
45. Shah KB, Ferziger JH. A fluid mechanics view of wind engineering: Large eddy simulation of flow past a cubic obstacle. *J Wind Eng Ind Aerodyn*. 1997;67:211-24.
46. Shepherd C, Lapple C. Flow pattern and pressure drop in cyclone dust collectors. *Industrial & Engineering Chemistry*. 1939;31(8):972-84.
47. Slack M, Prasad R, Bakker A, Boysan F. Advances in cyclone modelling using unstructured grids. *Chem Eng Res Design*. 2000;78(8):1098-104.
48. Tsai C, Chen D, Chein H, Chen S, Roth J, Hsu Y, et al. Theoretical and experimental study of an axial flow cyclone for fine particle removal in vacuum conditions. *J Aerosol Sci*. 2004;35(9):1105-18.
49. Van Doormaal J, Raithby G. Enhancements of the SIMPLE method for predicting incompressible fluid flows. *Numerical heat transfer*. 1984;7(2):147-63.
50. Wolfshtein M. The velocity and temperature distribution in one-dimensional flow with turbulence augmentation and pressure gradient. *Int J Heat Mass Transfer*. 1969;12(3):301-18.
51. Yakhot V, Orszag SA. Renormalization-group analysis of turbulence. *Phys Rev Lett*. 1986;57(14):1722.
52. Yang J, Sun G, Gao C. Effect of the inlet dimensions on the maximum-efficiency cyclone height. *Separation and Purification Technology*. 2013;105:15-23.
53. Zhao B, Su Y, Zhang J. Simulation of gas flow pattern and separation efficiency in cyclone with conventional single and spiral double inlet configuration. *Chem Eng Res Design*. 2006;84(12):1158-65.
54. Camfil Farr . inertial gas-solid separator inertial air filters. Product sheet RPM1011-06-04:Performance